NASA CONTRACTOR REPORT

NASA CR-1381

NASA CR-1381

CHARACTERISTICS OF A THERMIONIC CONVERTER WITH A FLUORIDE VAPOR DEPOSITED TUNGSTEN EMITTER ETCHED TO PREFERENTIALLY EXPOSE THE 110 CRYSTAL PLANES

by V. C. Wilson and J. Lawrence

Prepared by
GENERAL ELECTRIC COMPANY
Schenectady, N. Y.
for Lewis Research Center

NATIONAL AERONAUTICS AND SPACE ADMINISTRATION • WASHINGTON, D. C. • AUGUST 1969

NASA CR-1381

CHARACTERISTICS OF A THERMIONIC CONVERTER WITH A FLUORIDE VAPOR DEPOSITED TUNGSTEN EMITTER ETCHED TO PREFERENTIALLY EXPOSE THE 110 CRYSTAL PLANES

By V. C. Wilson and J. Lawrence

Prepared under Contract No. NAS 3-8511 by
GENERAL ELECTRIC COMPANY
Schenectady, N.Y.

for Lewis Research Center

NATIONAL AERONAUTICS AND SPACE ADMINISTRATION

For sale by the Clearinghouse for Federal Scientific and Technical Information
Springfield, Virginia 22151 – CFSTI price $3.00

ABSTRACT

A variable spaced planar thermionic converter was built with a tungsten emitter, a niobium collector and a niobium guard ring. The tungsten emitting surface was a 0.020-inch-thick layer of fluoride vapor deposited tungsten. X-ray analysis and etch pit studies showed this surface was oriented with a (100) plane parallel to the bulk surface. The surface was etched to expose the (110) planes which are inclined 45 degrees to the (100) planes. The surface was then a mass of peaks, ridges and valleys several microns in depth, and had an exposed area about 40 percent greater than the plane surface.

The initial output performance of this surface at low cesium pressures and also at large spacings was better than unetched (100) tungsten. The most output was obtained at 10 mils spacing or more for emitter temperatures from 1700°K to 2000°K. Operation for 21.8 hours at 2155°K reduced the sharpness of the points and ridges and the output performance decreased, particularly at larger spacings.

FOREWORD

The research described herein was conducted by the General Electric Research and Development Center under NASA Contract NAS 3-8511. The NASA Project Manager was Mr. J. F. Mondt, Direct Energy Conversion Division, Lewis Research Center. The report was originally assigned General Electric document No. GEST-2107.

Page Intentionally Left Blank

CONTENTS

	Page
SUMMARY	1
INTRODUCTION	3
TEST VEHICLE	5
Preparation of the Emitter Surface	5
Converter Characteristics	16
Aging the Emitter	26
CONCLUSIONS	39
REFERENCES	40
APPENDIX A - FAMILIES OF LOAD LINES	41

SUMMARY

This topical report represents one of a series of reports to be prepared under Contract NAS 3-8511, Task III, Investigation of the Effect of Electrode Materials, Surface Treatments, and Electrode Spacing on Thermionic Converter Performance. NASA CR-1033 gives a complete description of the converter construction, the method of varying the spacing, the processing procedures and the measuring techniques. For the work reported here, a guard ring surrounded the collector. The collector and guard could be held at the same temperature and electrical potential.

The tungsten emitter surface was a 0.020-inch-thick layer of fluoride vapor deposited tungsten. X-ray and etch pit identification showed that this surface was oriented with the (100) planes parallel to the bulk surface. The surface was etched to expose the (110) planes which are inclined 45 degrees to the (100) planes. The resulting etched surface has an abundance of peaks, ridges, and valleys. As a result, the surface area is about 40 percent greater than the geometrical area. More important, the (110) plane of tungsten has the highest vacuum work function and it is believed to be the best tungsten plane for a thermionic converter emitter surface.

Initially the converter had exceptionally high electrical output. For example, at an emitter temperature of 2155°K, a collector temperature of 973°K, and a spacing of 0.005 inches, it developed 30 amperes per square centimeter at over one volt at the electrodes.

Complete families of output characteristics were taken with the emitter temperature varied from 1660°K to 2155°K. Comparing this converter with a similar converter with a polycrystalline tungsten emitter, this converter produced more power at 5 times the spacing. For example, at an emitter temperature of 1960°K, it produced more power at a 10-mil spacing than the converter with the polycrystalline converter produced at a 2-mil spacing.

The most outstanding characteristic of the etched emitter was that it produced the maximum output powers at comparatively low cesium vapor pressures. This is probably the result of a strong adsorption of cesium on the (110) planes which lowers the necessary cesium pressure to obtain the optimum cesium coverage on the emitter. The lower cesium pressure reduces the electron scattering in the plasma and a particular plasma voltage loss is obtained at a much wider spacing. Also, a better cesium coverage on the collector at the lower cesium pressure slightly increases the output voltage. The increased surface area of the etched emitter appears to increase the effective current density.

After 21.8 hours of operation at 2155°K, the output of this converter degraded somewhat; however, it still produced more power than the similar converter with the polycrystalline tungsten emitter. The degradation was caused by thermal etching of the surface which rounded the sharp edges and valleys of the (110) facets. This reduced the surface area slightly, but more importantly, it exposed tungsten crystal planes that had undesirable orientations. In terms of the work function, the final surface was patchy. Patchy work function surfaces are not ideal for thermionic converter emitters because it is impossible to optimize the cesium pressure for optimum cesium coverage of all patches.

INTRODUCTION

This work is part of a continuing program to build and operate thermionic converters with various electrode materials in order to characterize, evaluate, and identify the most promising electrode surfaces for converter operation. The design of the test converter was conceived and standardized in 1963. It permitted an accurate determination of the electrode spacing and used a guard ring to accurately define the converter area. The guard ring could be kept at the same temperature and potential as the collector. The first six lines of Table 1 list the electrode materials and the spacings for six converters built according to the 1963 design. The output power from these converters was consistently high and variations in output power could be explained by variations in electrode surfaces. The emitters of these converters were pre-heated to 2500°C for one-half hour and all other parts of the converter were heated at least 100°C hotter during processing than the operating temperature for each part.

In 1966, under NASA sponsorship, the program was altered in two respects: (1) A more elaborate converter was built so that the electrode spacing of each converter could be varied. (2) A much more intensive program to characterize the emitters was inaugurated. This report gives the emitter preparation and the test results from the second variable spaced converter (item 8, Table 1).

Table 1. CONVERTERS PREVIOUSLY TESTED

	Emitter	Collector	Spacing (inches)	Reference
1.	Poly Xtal W	Ni	0.005	1
2.	Poly Xtal Re	Ni	0.005	1
3.	Poly Xtal Re	Ni	0.002	2, 3, 4
4.	Poly Xtal W	Ni	0.002	4, 5
5.	Poly Xtal W	W	0.002	5
6.	W-25 w/o Re	Ni	0.005	6
7.	Poly Xtal W	Nb	0.001 to 0.020	7, 8
8.	Vap. Dep. (100) W,	Nb	0.001 to 0.020	9

Several investigators[10] have pointed out that cesium diode thermionic converters will operate more efficiently or can be operated with wider spacings if the partial cesium monolayer on the emitter surface may be obtained at a low cesium pressure; therefore, it is important to have a base emitter material which strongly adsorbs cesium. Webster[11] has demonstrated that the (110) planes of tungsten adsorb cesium most strongly. He has also pointed out that the (110) planes are the most densely packed and the most stable surfaces. If a tungsten layer that has a preferred orientation with the (100) planes parallel to the bulk surface is etched using an etch developed by Webster,[12] the (110) planes are exposed. Since these (110) planes are inclined at 45 degrees to the (100) planes, the resulting etched surface has an abundance of peaks, ridges, and valleys. This causes the emitter surface area to be about 40% greater than the geometrical area.

TEST VEHICLE

Figure 1 shows a cross section drawing of the thermionic converter. The electrode spacing is variable and the electrodes are a tungsten emitter and a niobium collector. The construction is quite similar to the thermionic converter reported in NASA CR-1033, except that this converter has a niobium guard ring while the other did not.[13] In operation, the guard ring may be kept at the same temperature and at the same electrical potential as the collector. Figure 2, showing current versus voltage for the guard ring (G) and collector (C), illustrates how similar the potential on the two electrodes could be maintained during a 60-cycle sweep.

PREPARATION OF THE EMITTER SURFACE

A 0.250-inch-thick polycrystalline tungsten emitter disk which was coated with a 0.020-inch-thick layer of (100) oriented tungsten by the fluoride vapor deposition process was selected for surface preparation. This emitter was one of nine purchased from San Fernando Laboratories. After a preliminary polish, a hardness test developed by Festa and Danko[14] indicated that the sample had less than 10 ppm of fluoride in the tungsten. The surface preparation technique included a final mechanical polish, followed by an electropolish. The polishing solution was 90 grams of sodium hydroxide in three liters of water. The emitter disk was placed on a tungsten plate with the coated surface up. A tungsten grid was mounted about 3/8-inch above the emitter surface; the emitter surface and the entire assembly were immersed in the sodium hydroxide solution. For the electropolish, the grid was held 15 volts negative with respect to the emitter. To etch the surface, the potential difference was reduced to 2 volts. An etch exposing the (110) etch facets in a material with a preferred (100) oriented substrate surface parallel to the bulk surface should form small pyramidal holes with the edges of the holes square. This situation is illustrated in the large grain at the lower right of Figure 3. Notice that some of the other grains in this micrograph are not oriented with the (100) planes parallel to the surface; and, therefore, the etch pits are not square in cross section but

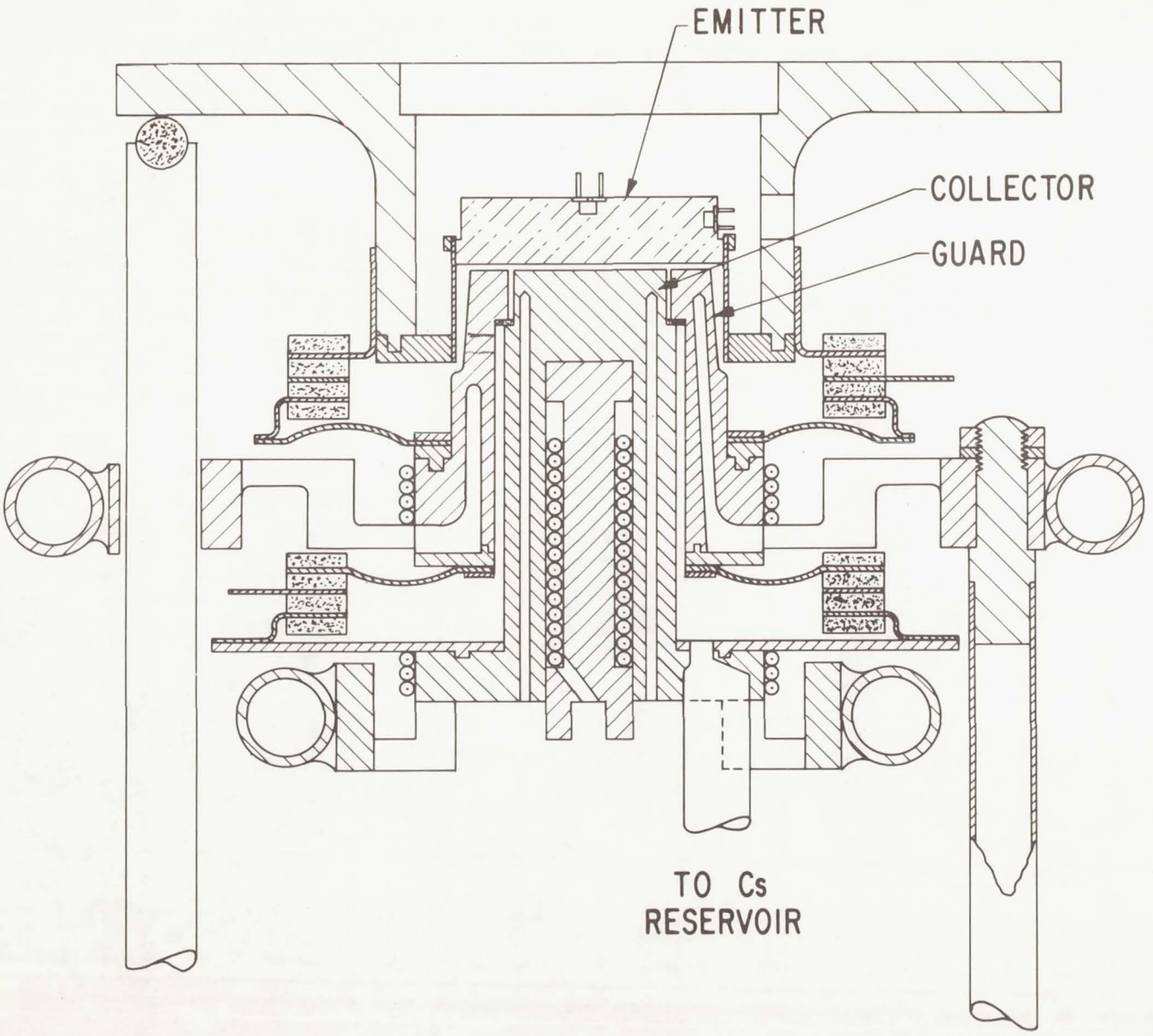

Figure 1. - Variable spaced thermionic converter.

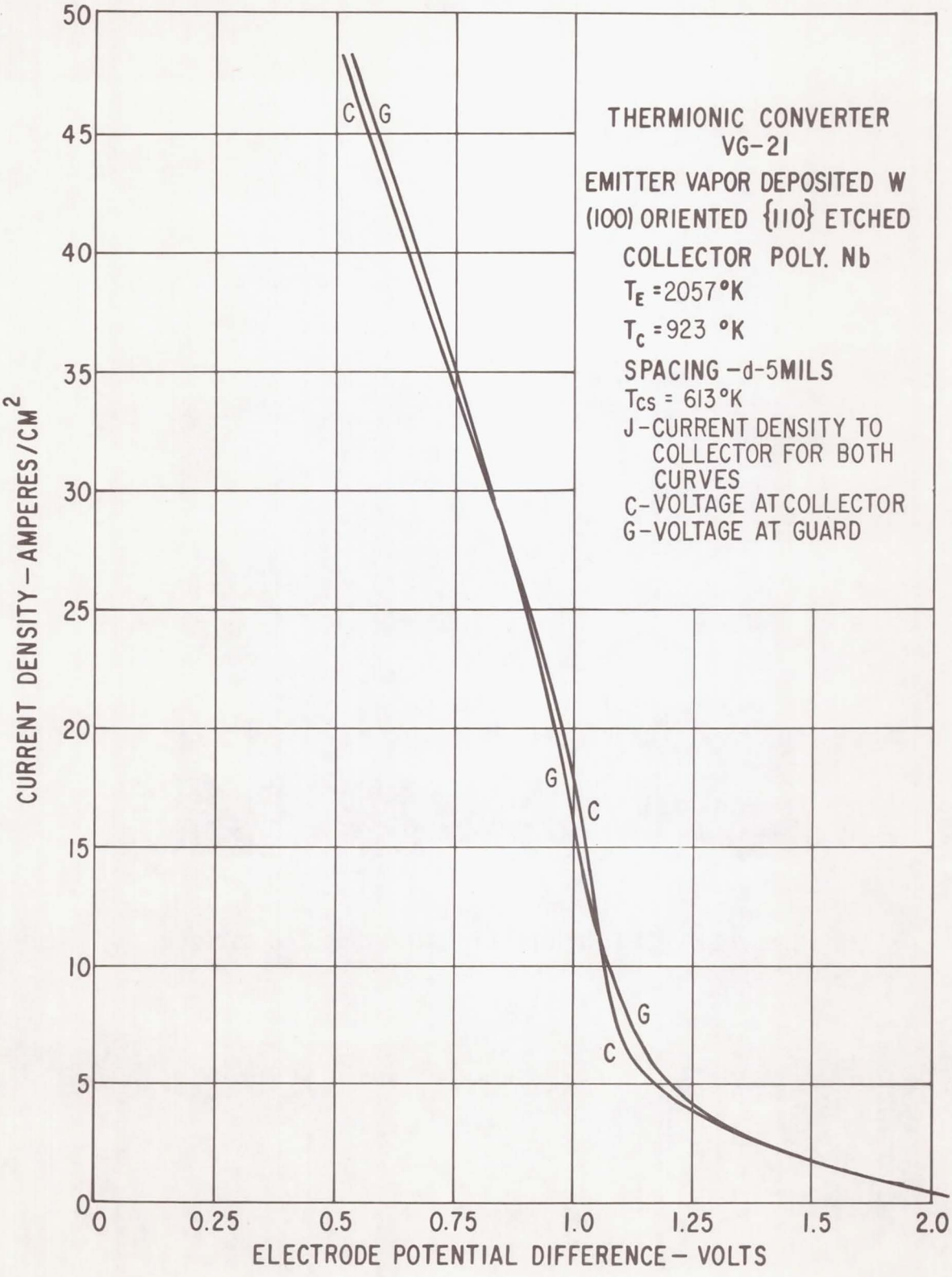

Figure 2. - Electric potential of collector and guard ring.

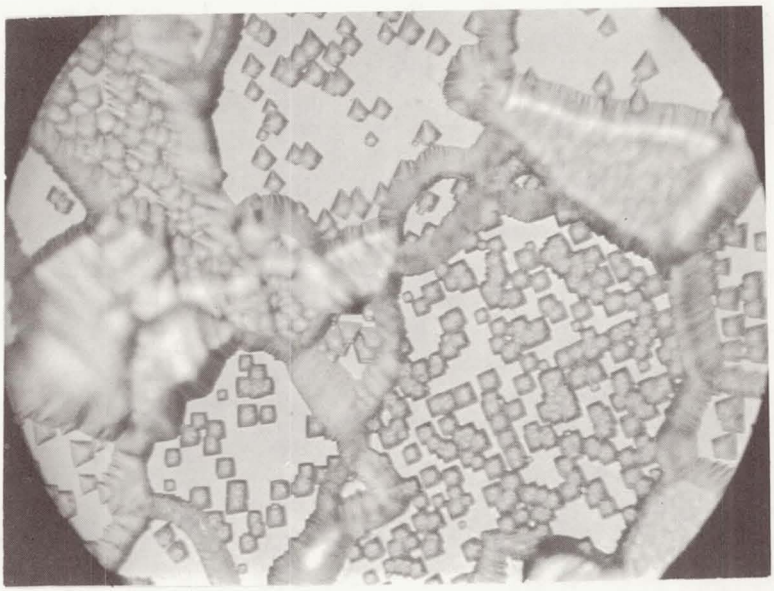

Figure 3. - 110 Etch pits in (100) tungsten surface.

instead are kite shaped. After an electropolish followed by a 2 second etch, the emitter was visually scanned with the microscope and characteristic areas photographed after the surface preparation technique was established. The emitters were electropolished and x-ray diffraction measurements were made to determine the degree of preferred (100) orientation of the surface. Following this step, the emitters were ultrasonically cleaned in alcohol and placed in a vacuum bell jar and heat treated to 2500°C for one-half hour. The surfaces were examined and unusual characteristics photographed. A small amount of thermal etching revealed that the grains were larger after the heat treatment. This was also verified by x-ray diffraction analysis.

On the basis of the x-ray diffraction studies, the nine emitters had essentially the same degree of preferred (100) orientation. On the basis of appearance when etched, the emitter selected for further analysis had no apparent blemishes. This emitter in the hardness test also showed the least amount of fluorine--less than 10 ppm. After an electropolish and a thermal etch at 2500°C for one-half hour, the emitter work function was measured in the temperature range of 1900°K to 2350°K by drawing the saturation electron emission in a vacuum environment.

The emitter was then etched for about 20 minutes at 2 volts with interruptions to study the progression of the etch pits. After the thermal treatment, the grains formed very few etch pits other than those that occurred at the grain boundaries. Etch pits start at imperfections such as screw dislocations. Presumably, the thermal treatment left few imperfections in the individual metal grains. Figure 4 taken after 2 minutes of etching illustrates this. Upon further etching, the etched regions spread throughout the entire surface, and the valleys and pyramidal holes become deeper. Figure 5 shows the final condition of the emitter. The depth of focus of the microscope was not great enough to show the entire surface. The fuzzy areas are merely out of focus. By hand focusing the microscope, one could be convinced that the entire surface was made up of planes oriented at about 45° to the surface of the bulk tungsten.

Figure 4. - After 2500^{O} C for one-half hour heat treatment; etch pits initiate at grain boundaries only.

Figure 5. - After 20 minutes of electroetch.

Figure 6 shows a complete history of the work function measurements for the emitter. The solid circles show the work function measurements before etching but after a 2500°C heat treatment. The open circles are for a polycrystalline tungsten sample used in an earlier converter.[9, 13] The open diamonds indicate the work function after the surface was etched to the physical appearance shown in Figure 5. The final selection of the emitter was made on the basis of the appearance when etched and on the basis of the work function measurements before and after etching. The emitter was then heated to 2500°C for 10 minutes. The open squares indicate the work function immediately after this heat treatment. The solid squares represent data that were taken the following day. This increase in work function could be attributed to a slight contamination from oxygen. Figure 7 shows the condition of the emitter after the 10 minutes heat at 2500°C. Notice that the sharp edges and the sharp grooves forming the valleys have been rounded; this thermal etching would expose many small areas of lower work function than the (110) surface and would easily explain the reduction in the overall work function.

Since the method of assembling the thermionic converter requires a 2450°C braze between the emitter and a tantalum support ring, this braze was made and the surface was subsequently reetched. The solid diamonds shown on Figure 6 represent the work function of the final emitter surface measured just before the cesium was introduced into the converter. A photomicrograph (Figure 8) shows the appearance of the emitter surface just before assembly into the converter. This photomicrograph is at a lower magnification because the tantalum support ring would not permit the use of a larger, higher magnification lens. After a complete family of load lines was taken for the converter including a run for 95 minutes at 2155°K, the work function of the surface was again measured by keeping the cesium reservoir as cold as possible and increasing the emitter temperature rapidly. The two open triangles in Figure 6 give this result. Finally, after 21.8 hours at T_E = 2155°K, the work function of the emitter was again measured. These values are represented by the solid triangles. The two

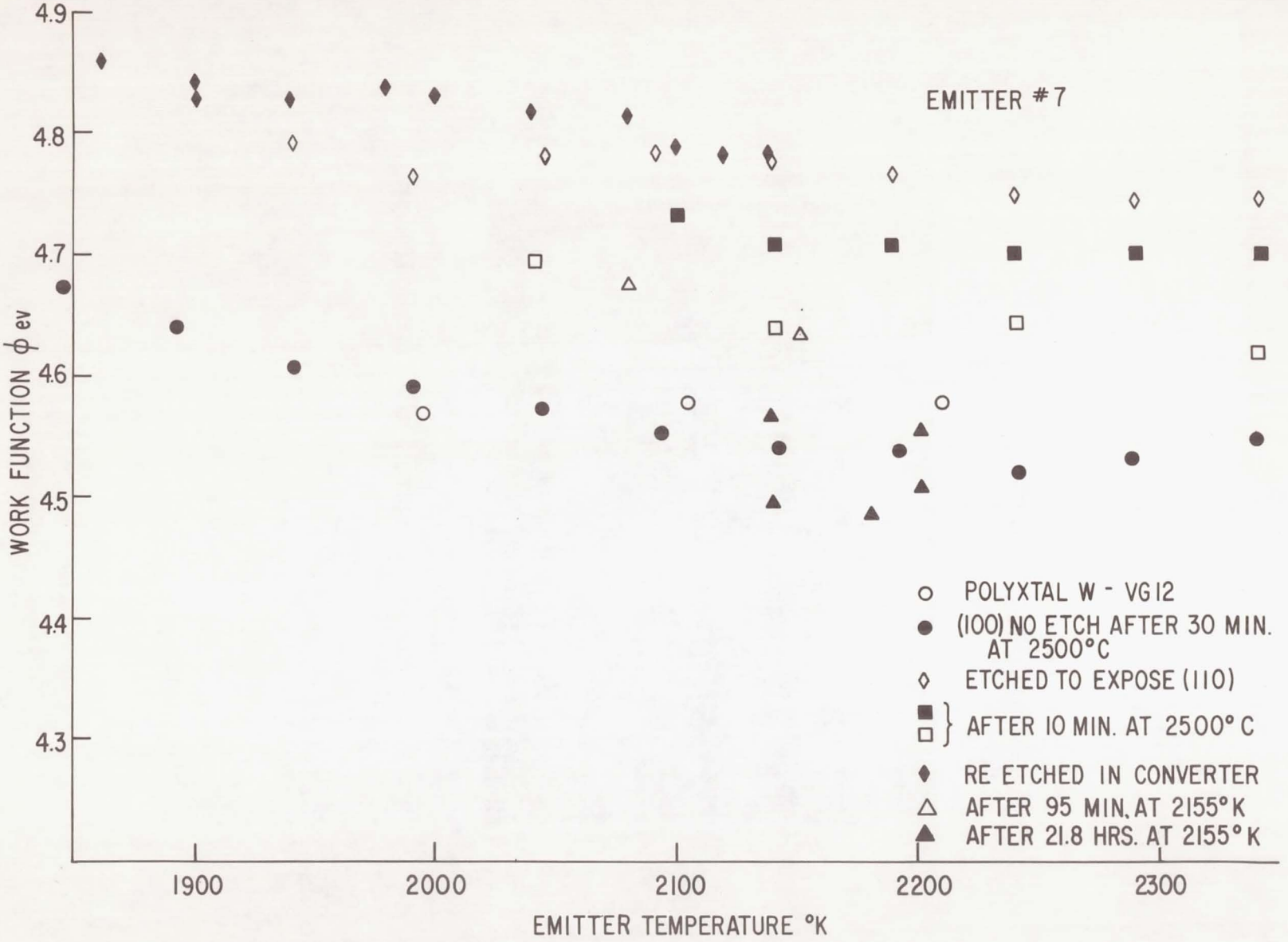

Figure 6. - Work function of emitter 7.

Figure 7. - Similar to figure 5 after one-half hour at 2500° C.

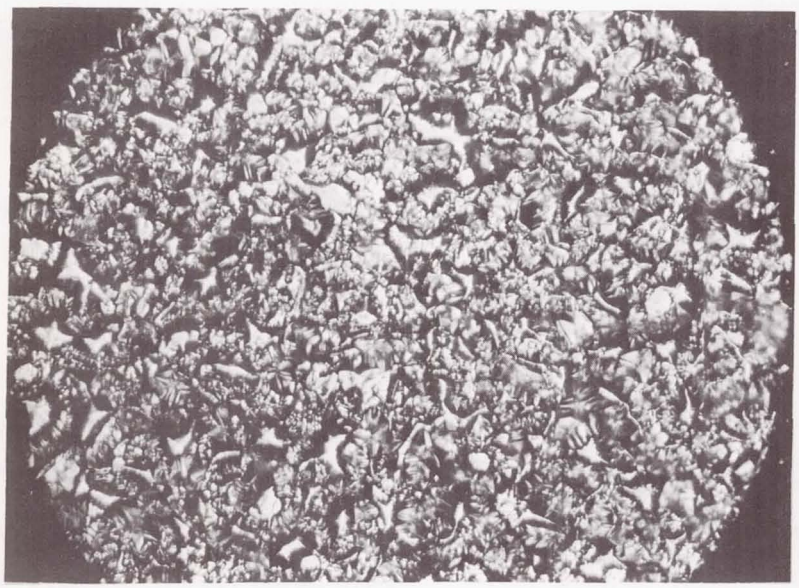

Figure 8. - Emitter surface just before assembly into converter.

upper values were taken with the cesium reservoir at 9°C, the cooling water temperature. The three lower values were taken about two minutes after starting up the emitter and the cesium reservoir had started to warm up; therefore, these three lower values probably are characteristic of a slight contamination from cesium.

Figure 9 shows the condition of the emitter surface after about 70 hours of operation, including 21.8 hours at 2155°K and 20 hours at 2050°K. The average work function was about the same as for a polycrystalline tungsten sample for a (100) crystalline surface. However, it is apparent from the picture that the true surface is not a (100) surface but is a new distribution of surfaces consisting of many crystal surface orientations.

CONVERTER CHARACTERISTICS

As mentioned before, when the emitter was heated to 2500°C for 10 minutes, the sharp edges of the etched surface were rounded considerably. To obtain the characteristics of the converter with the emitter in its initial as-etched state, a complete set of load lines was taken at the lowest emitter temperature, 1650°K. Periodically, after operating the emitter at successively high temperatures, an initial load line was rerun to determine if any change had occurred in the converter characteristics. The first observable change occurred after the converter had been operated for 95 minutes at 2155°K. Figures 10, 11, and 12 show typical families of load lines for the converter in its initial condition.

Similar load lines under closely identical conditions for a converter with a polycrystalline tungsten emitter and a niobium collector are shown on Figures 13, 14, and 15 taken from Figures B-6, B-15 and B-46 of NASA CR-1033. It is most significant that the new converter operates at much lower cesium pressures. It is also significant that at the higher emitter temperatures the oriented and etched emitter develops more power at 5 times the spacing; i.e., 10 mils versus 2 mils at 1960°K and 5 mils versus 1 mil at 2150°K.

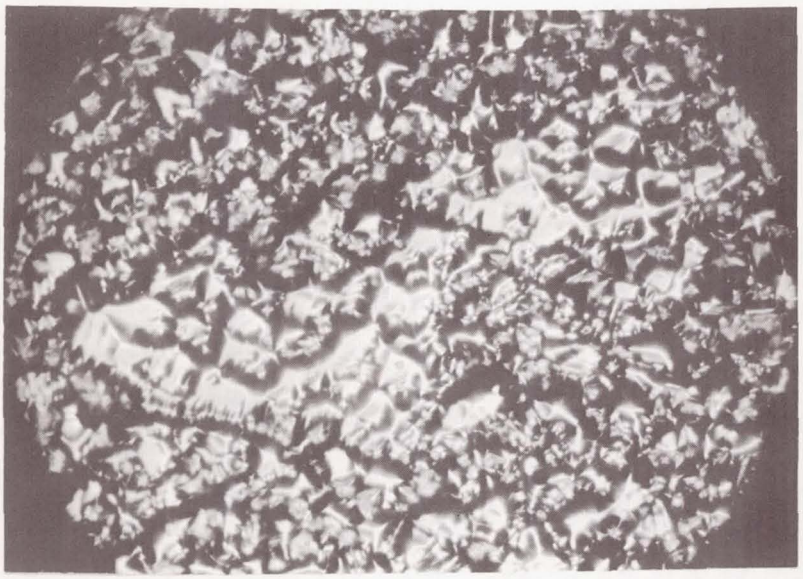

Figure 9. - Emitter surface after operation in converter.

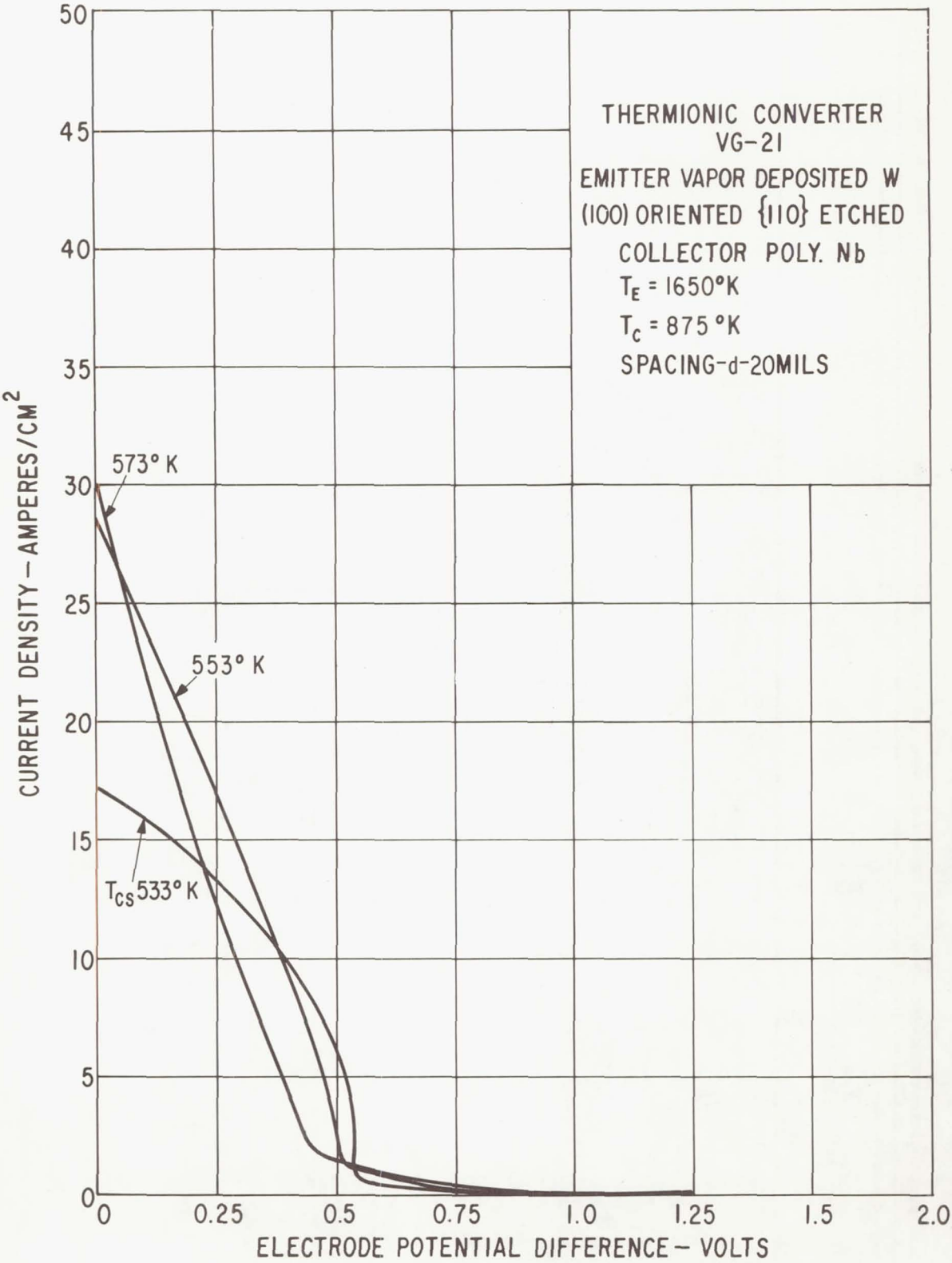

Figure 10. - Load lines for $T_E = 1650^O$ K.

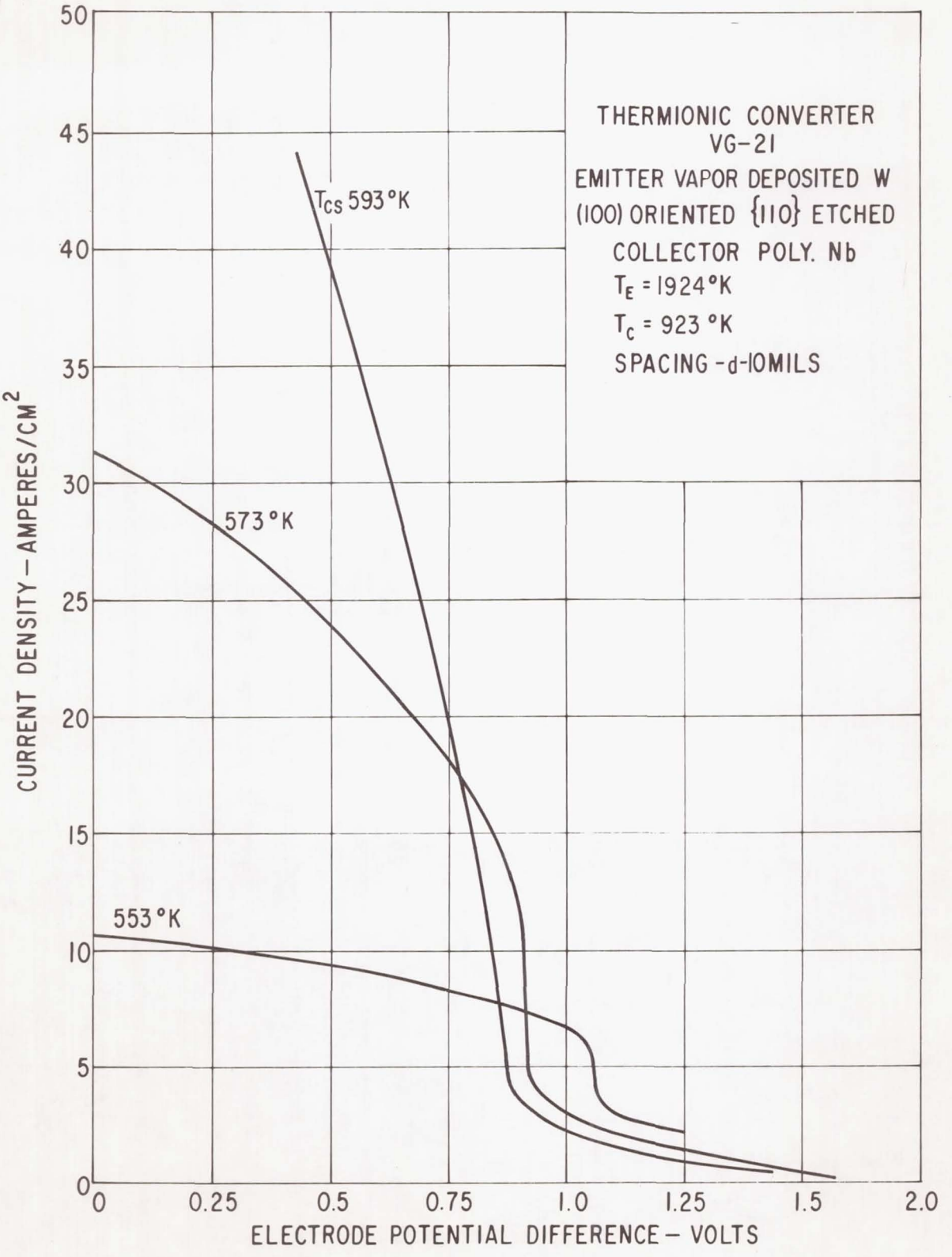

Figure 11. - Load lines for $T_E = 1924^O$ K.

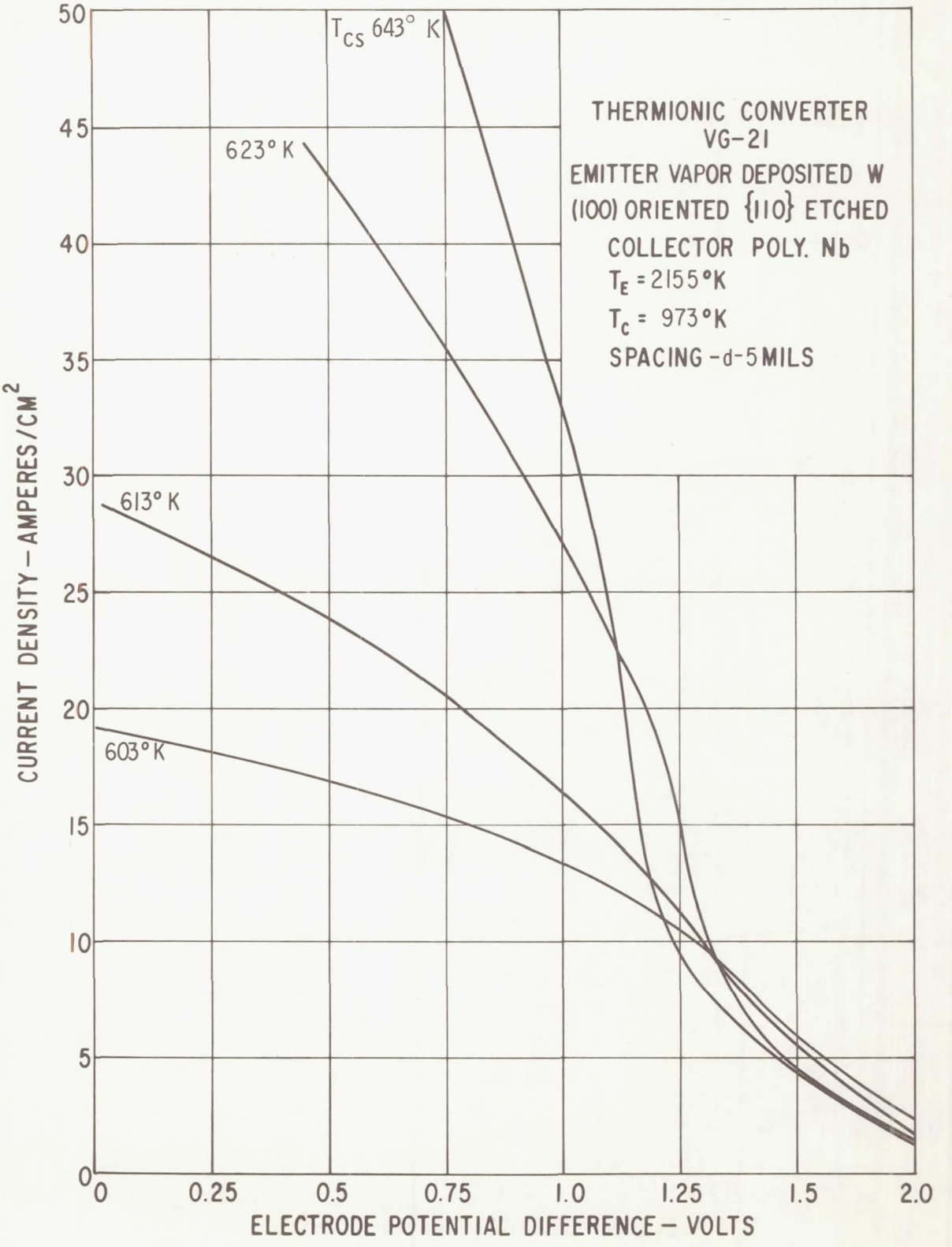

Figure 12. - Load lines for $T_E = 2155^O$ K.

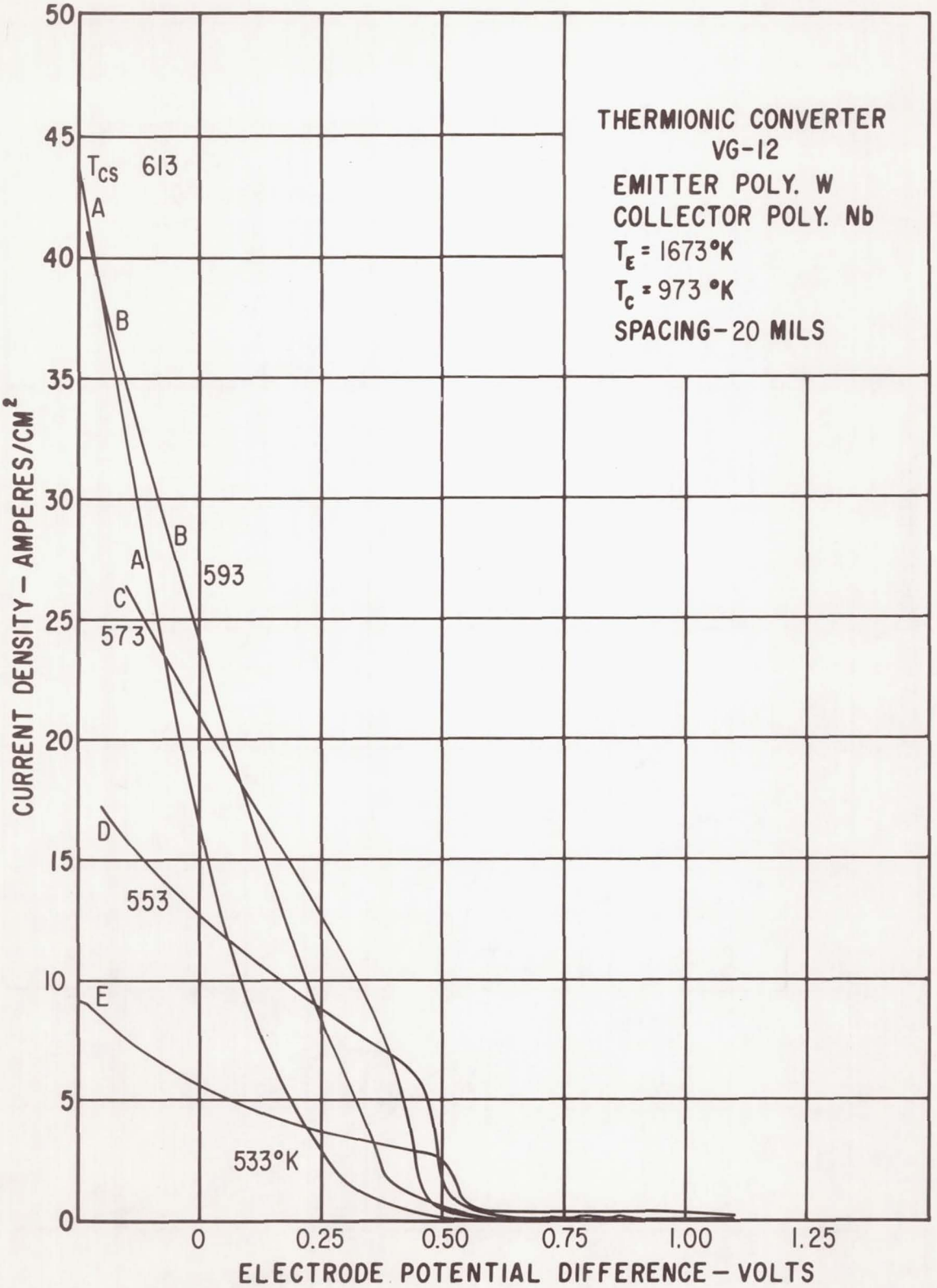

Figure 13. - Load lines for VG-12 at $T_E = 1673^O$ K.

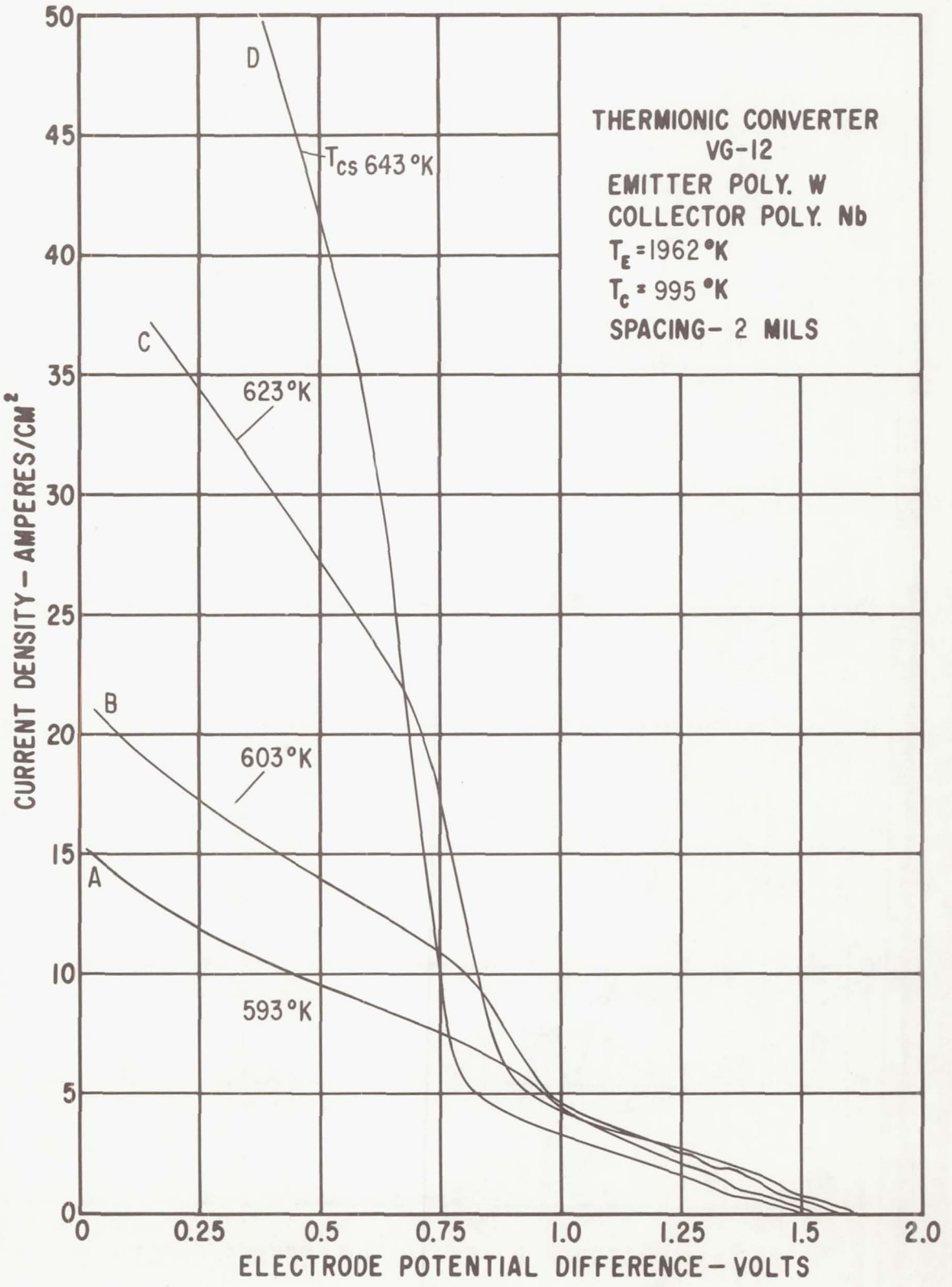

Figure 14. - Load lines for VG-12 at $T_E = 1962^{O}$ K.

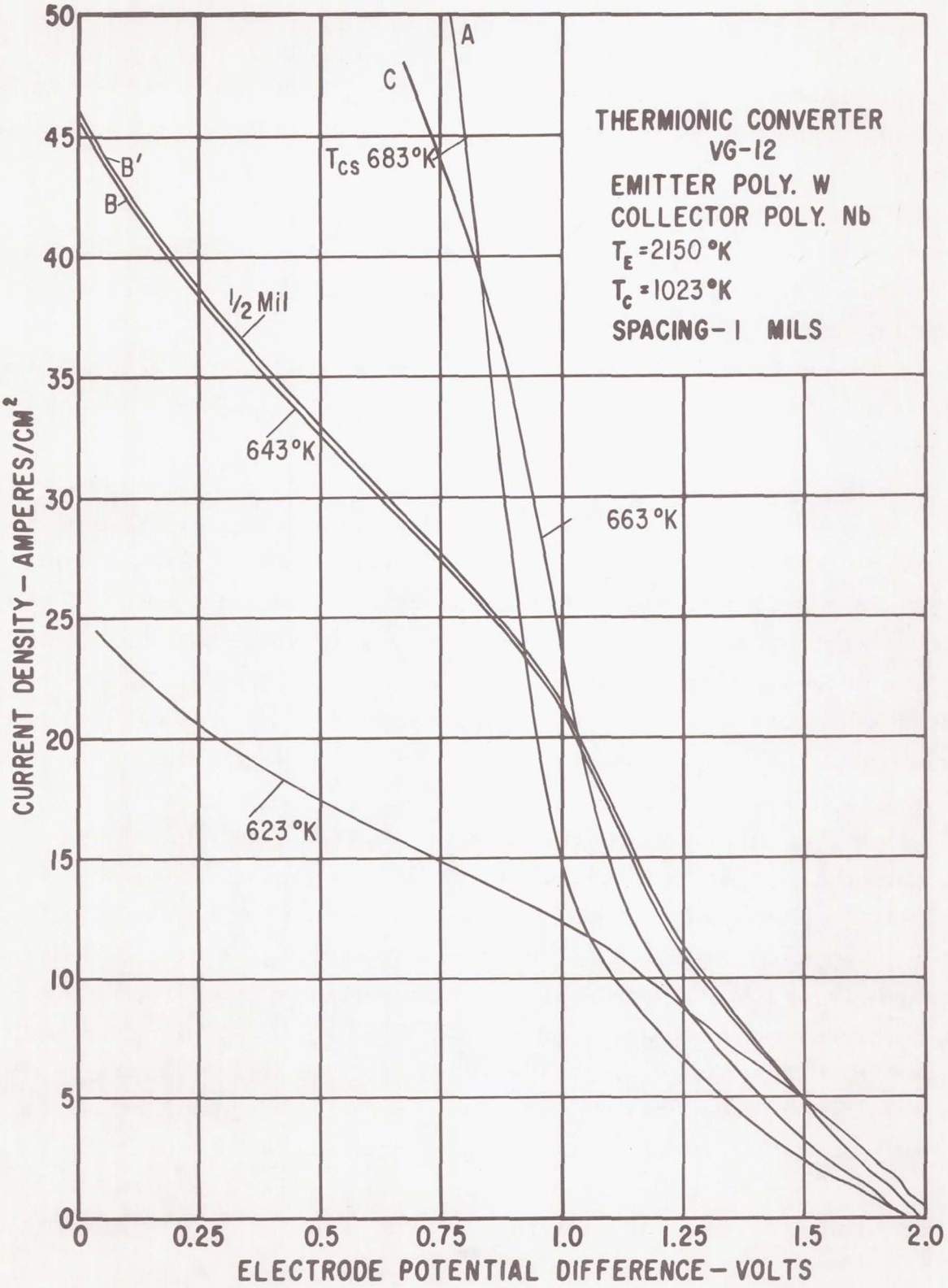

Figure 15. - Load lines for VG-12 at $T_E = 2150^{\circ}$ K.

Figure 16 gives the output power, power-in, and efficiency for this converter at T_E = 2155°K, T_C = 973°K and a spacing of 2 mils as a function of current density. This output power is from the first run at 2155°K, before observable aging had taken place. The power-in is calculated for a cylindrical geometry similar to the proposed designs for a single cell in a nuclear fuel rod assembly. Efficiency curves computed this same way for other converters have usually peaked at 20 amps/cm^2 or less. The unusual feature of this converter, which is caused by the low cesium pressure operation, is the high output voltage at high current densities and consequently higher efficiency; therefore, this converter has its peak efficiency at 25 to 30 amps/cm^2. Also, the efficiency is higher than any others measured to date at this laboratory.

In addition to lower plasma losses, there is another advantage in operating a thermionic converter at a lower cesium vapor pressure; namely, a more optimum cesium coverage may be obtained on the collector. If one plots the work function of a metal surface in cesium vapor as a function of the ratio of the collector temperature to cesium temperature, the work function starts at 1.79 eV, which is the work function of liquid cesium, and decreases as (T_C/T_{Cs}) increases to a minimum of 1.4 or 1.5 eV.

The optimum cesium reservoir temperature is determined by the optimum emitter cesium coverage. If this optimum cesium reservoir temperature (T_{Cs}) is high, the collector temperature (T_C) must be high to obtain the optimum ratio T_C/T_{Cs} for a minimum collector work function. Usually back emission from the collector prevents one from running the collector temperature at the optimum ratio T_C/T_{Cs}. If an improved emitter surface better adsorbs cesium to obtain the optimum cesium coverage at a lower cesium reservoir temperature, then the back emission limit is reached at a ratio of T_C/T_{Cs} closer to the optimum ratio, and this permits the converter to be operated at a slightly lower collector work function. For this converter at an emitter temperature of 1924°K, see Figure 11, it is estimated

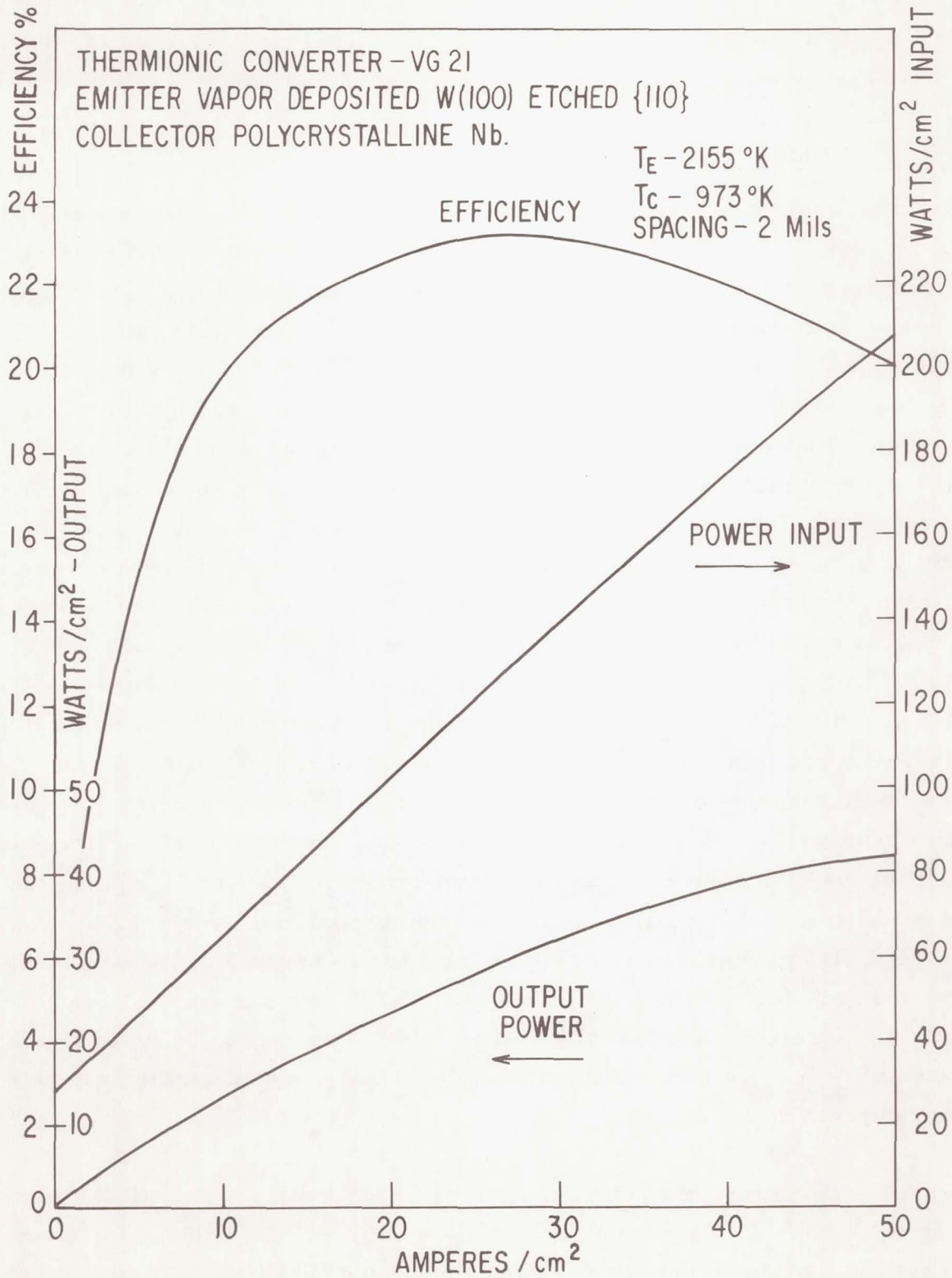

Figure 16. - Performance of VG-21 at $T_E = 2155^{\circ}$ K before aging.

that this effect at a reservoir temperature of 593°K will lower the collector work function by about 0.03 eV as compared with a reservoir temperature of 643°K in Figure 14.

AGING THE EMITTER

After observing the initial change in the converter's characteristic when operated at 2155°K, the converter was deliberately operated at this temperature to observe the change with time. Figure 17 shows the change that occurred during a run of 381 minutes at 2155°K. Each day before operating at 2155°K, a load line was taken at 2057°K and at the end of the day's run, the temperature was reduced to 2057°K again and another load line taken. These data are shown in Figure 18. Curve (1) was the initial load line, curve (2) was taken at the end of the first day's run--namely, after 95 minutes of operation at 2155°K. The most striking change occurs for the short circuit which was reduced from 36 amps/cm^2 to 28 amps/cm^2. This change probably reflects a slightly lower cesium coverage and, therefore, a higher work function for the surface. Curve (3) is the initial load line taken the next day. Notice that the short circuit current has apparently returned again to 36 amps/cm^2. This apparent overnight healing while the emitter was cool may be caused by a monolayer of oxygen which deposited on the emitter during the night. This effect would only require an oxygen partial pressure of 10^{-10} torr or less. The odd-numbered curves represent the initial load lines each day and the even-numbered curves represent the final load lines each day. Notice that superimposed on this overnight recovery effect is a steady degradation in the short circuit current, presumably this is the result of the rounding of the edges of the etched surface as shown in Figure 9. Figure 19 is a plot of the short circuit currents of Figure 18 as a function of time. This curve illustrates the steady degradation of the short circuit current density.

After aging for 21.8 hours at 2155°K, new families of load lines were run at T_E = 1750°K, T_E = 1840°K, and T_E = 2057°K. Figure 20 compares the envelopes of these load lines. One would conclude from this figure that

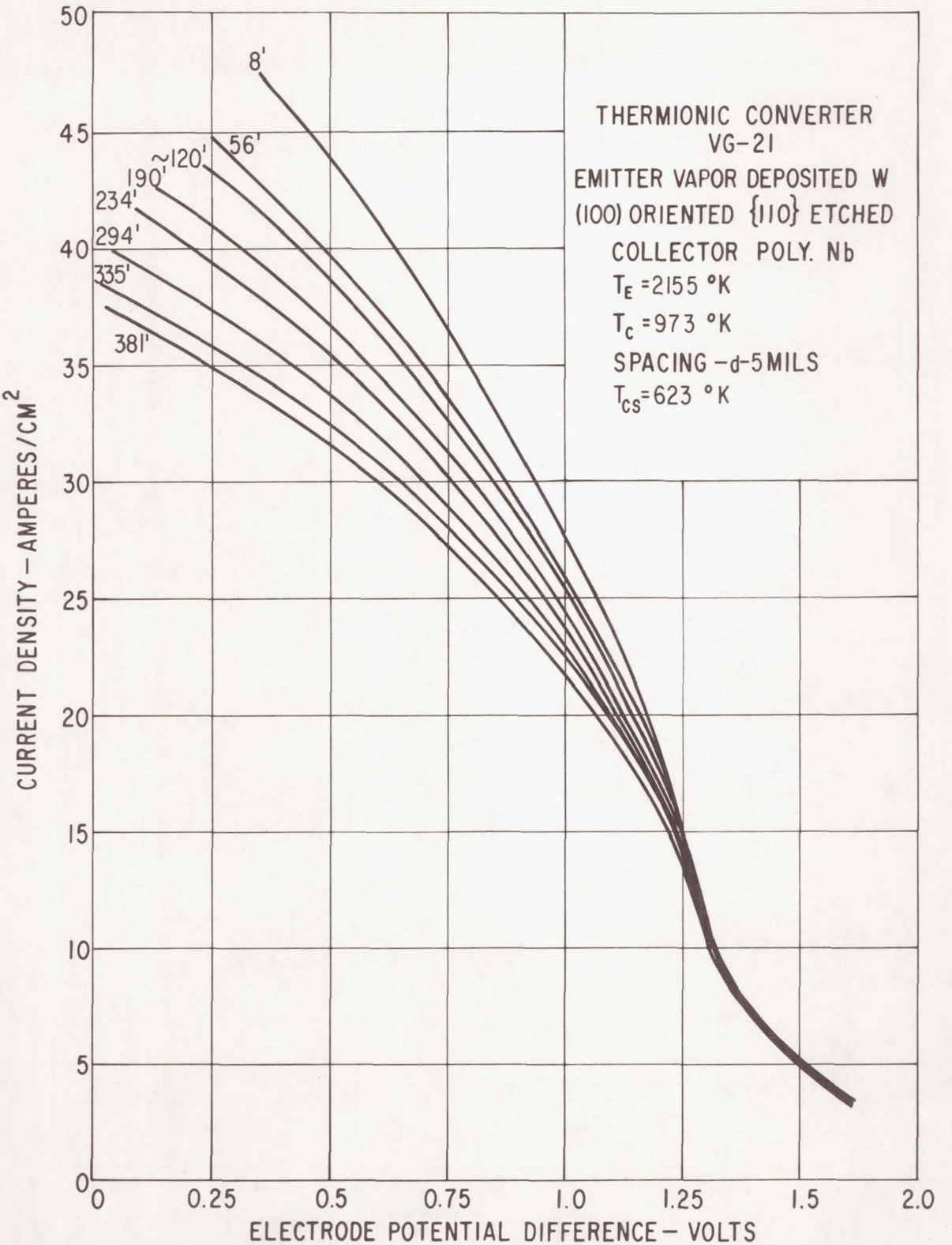

Figure 17. - Performance degradation with time at $T_E = 2155^{\circ}$ K.

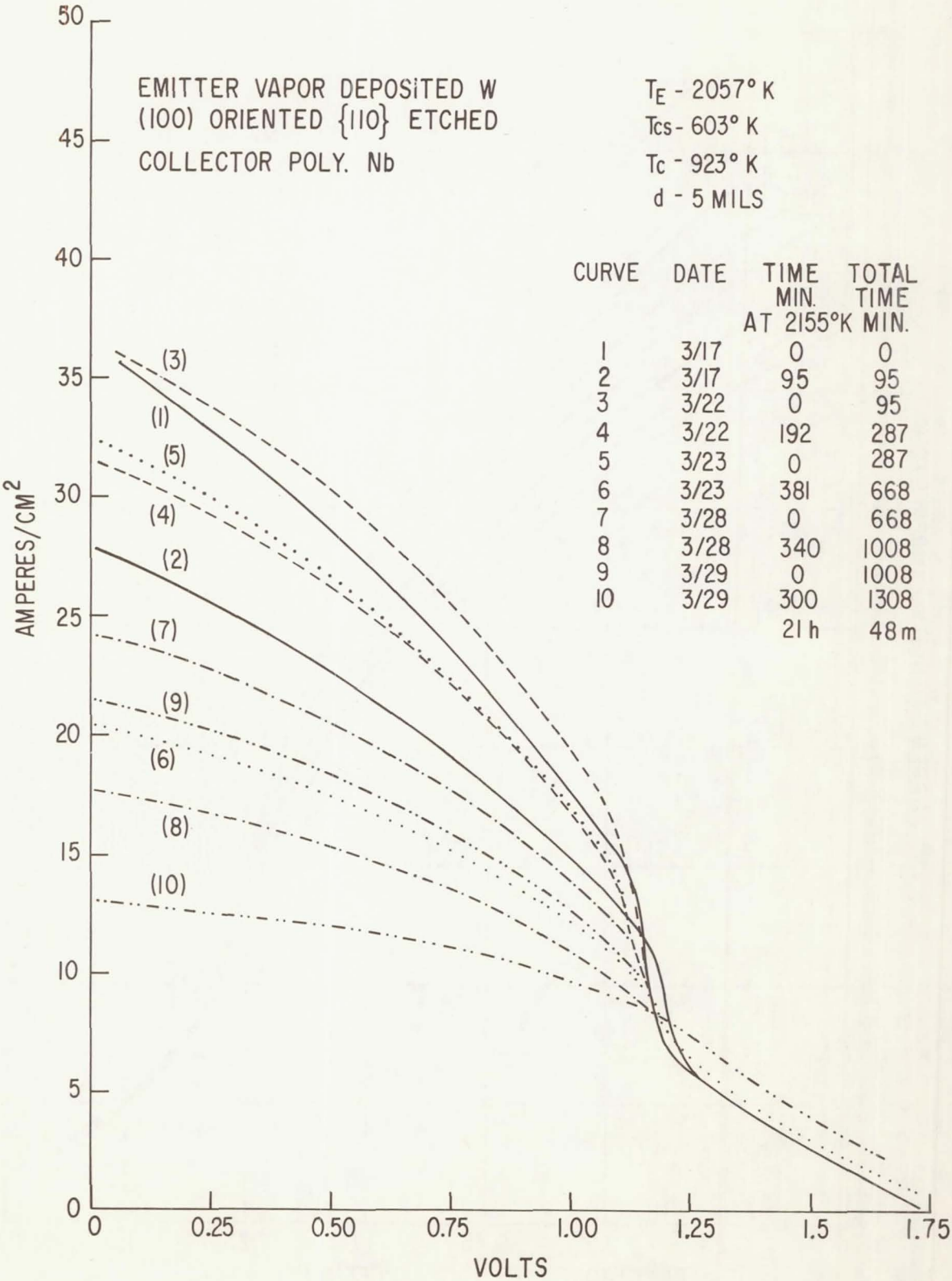

Figure 18. - Performance degradation with time and thermal cycling for $T_E = 2155^O$ K.

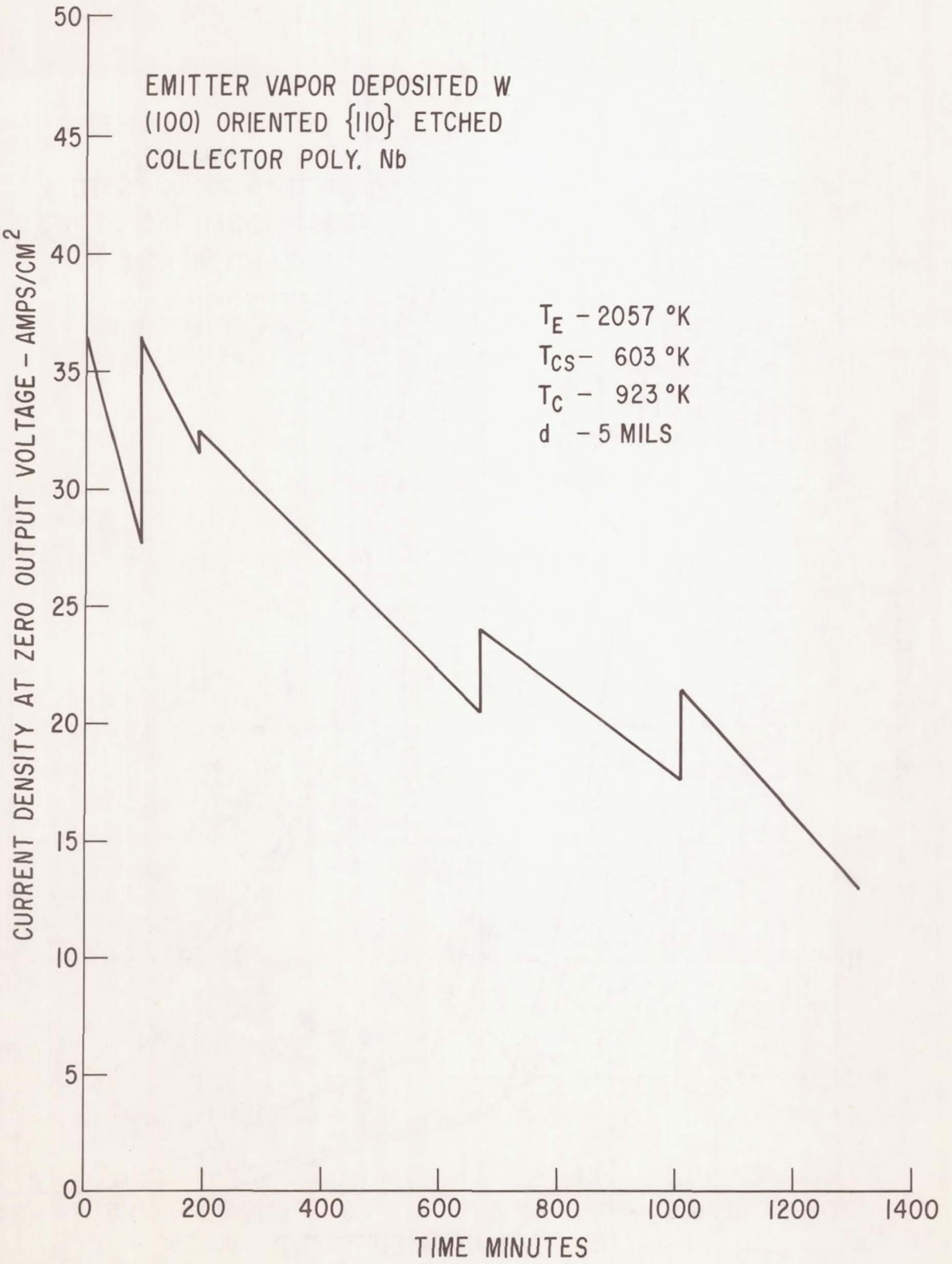

Figure 19. - Degradation of short circuit current density at $T_E = 2057^O$ K.

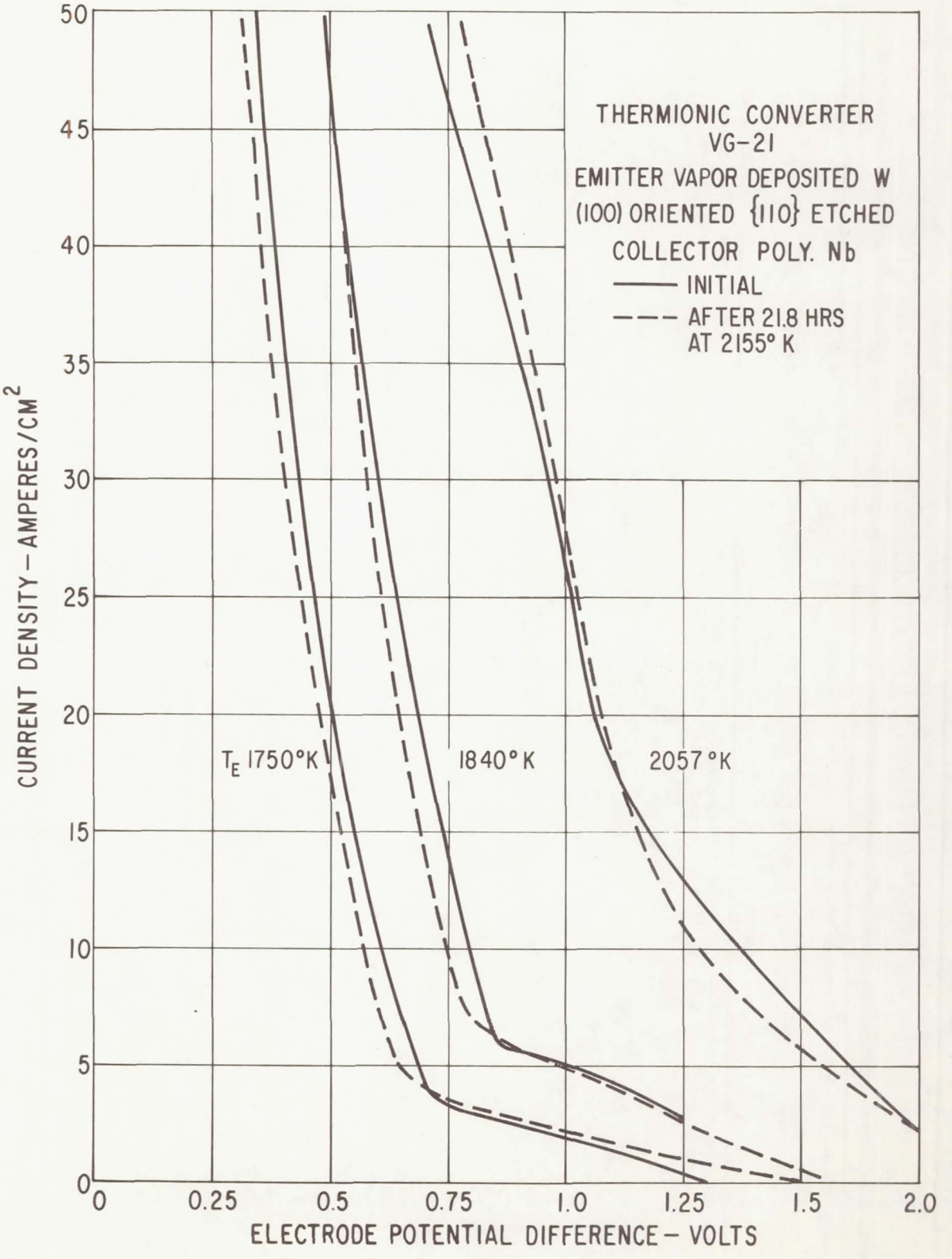

Figure 20. - Load line envelopes at various T_E before and after thermal aging.

the converter has not degraded appreciably, particularly at 2057°K. However, this figure is misleading because, in order to obtain the outputs represented by the dashed lines, one would have had to increase the cesium pressure and reduce the spacing from their initial values. Figures 21 and 22 better described the change that occurred during aging. These curves are the envelopes of load lines in which one is permitted to optimize the cesium pressure for any particular spacing. Figure 21 describes the initial output and Figure 22 describes the output characteristics after aging for 21.8 hours at 2155°K. If one were to build a fixed spaced converter with 10-mil spacing, initially at 25 amps/cm^2, from Figure 21 it would have developed 0.77 volts. From Figure 22, the output voltage would have dropped in the 21.8 hours to 0.57 volts which is a loss of 26%. There is an interesting feature in the curves of Figure 21. The curves for 1- and 2-mil spacing below 15 amps/cm^2 have higher voltages than the corresponding curves in Figure 22 and the curves have a different shape. Initially, this converter, below 15 amps/cm^2, was operating at very low cesium pressures and was operating in the condition originally described by Webster[15] in which the emitter is generating 0.002 as many ions as electrons and an essentially neutral plasma extends across the converter. This plasma does not have sheaths at the electrodes nor does it require ion generation within the interelectrode space.

The upper curves of Figures 23 and 24 show the output that could be obtained initially at T_E = 2057°K and 10- and 5-mil spacing, respectively. The curves labeled after 21.8 hours at T_E = 2155°K indicate the current densities that could be obtained at T_E = 2057°K if one had complete freedom to alter the cesium bath temperature. These curves are compared with the maximum output obtainable at this emitter temperature and spacing for the polycrystalline tungsten niobium converter. In the range of interesting current densities--i.e., 10 to 30 amps/cm^2, even after aging--the converter with the etched emitter produces more output. A crossing of the curves in Figure 23 at high current densities is probably not significant, but reflects the fact that the polycrystalline tungsten converter was operated at higher cesium coverages on the emitter.

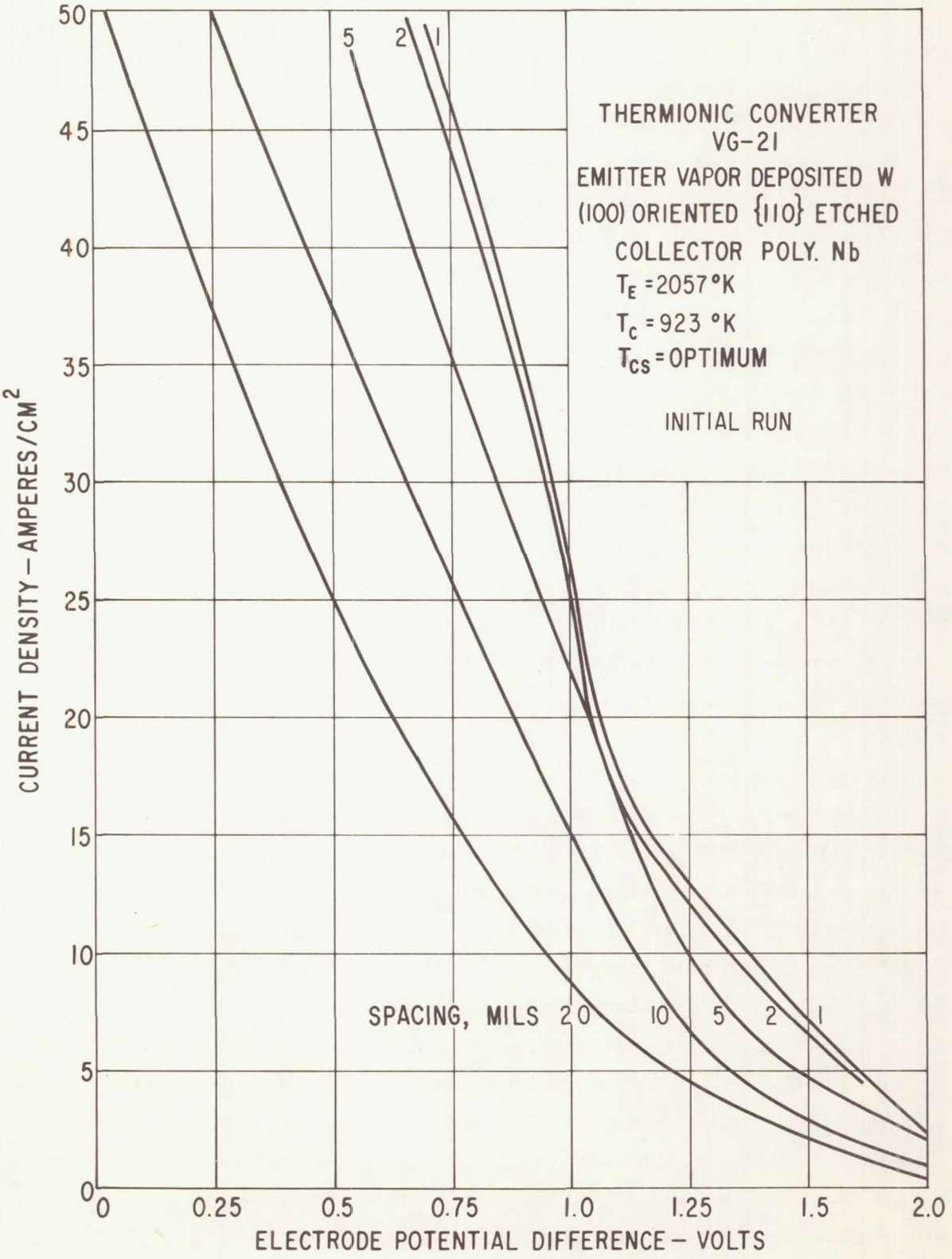

Figure 21. - Optimum load line envelopes for various spacings before thermal aging.

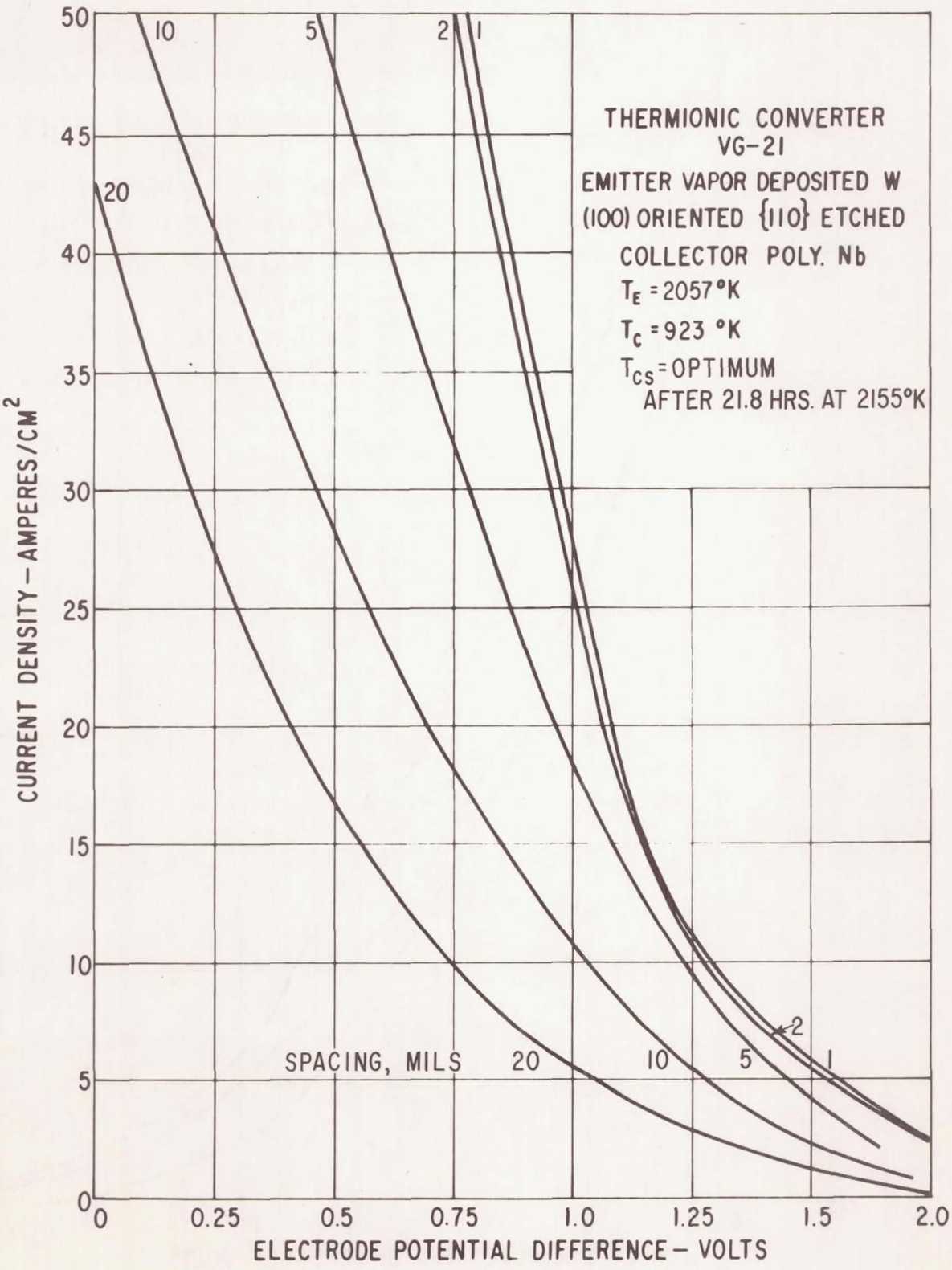

Figure 22. - Optimum load line envelopes for various spacings after thermal aging.

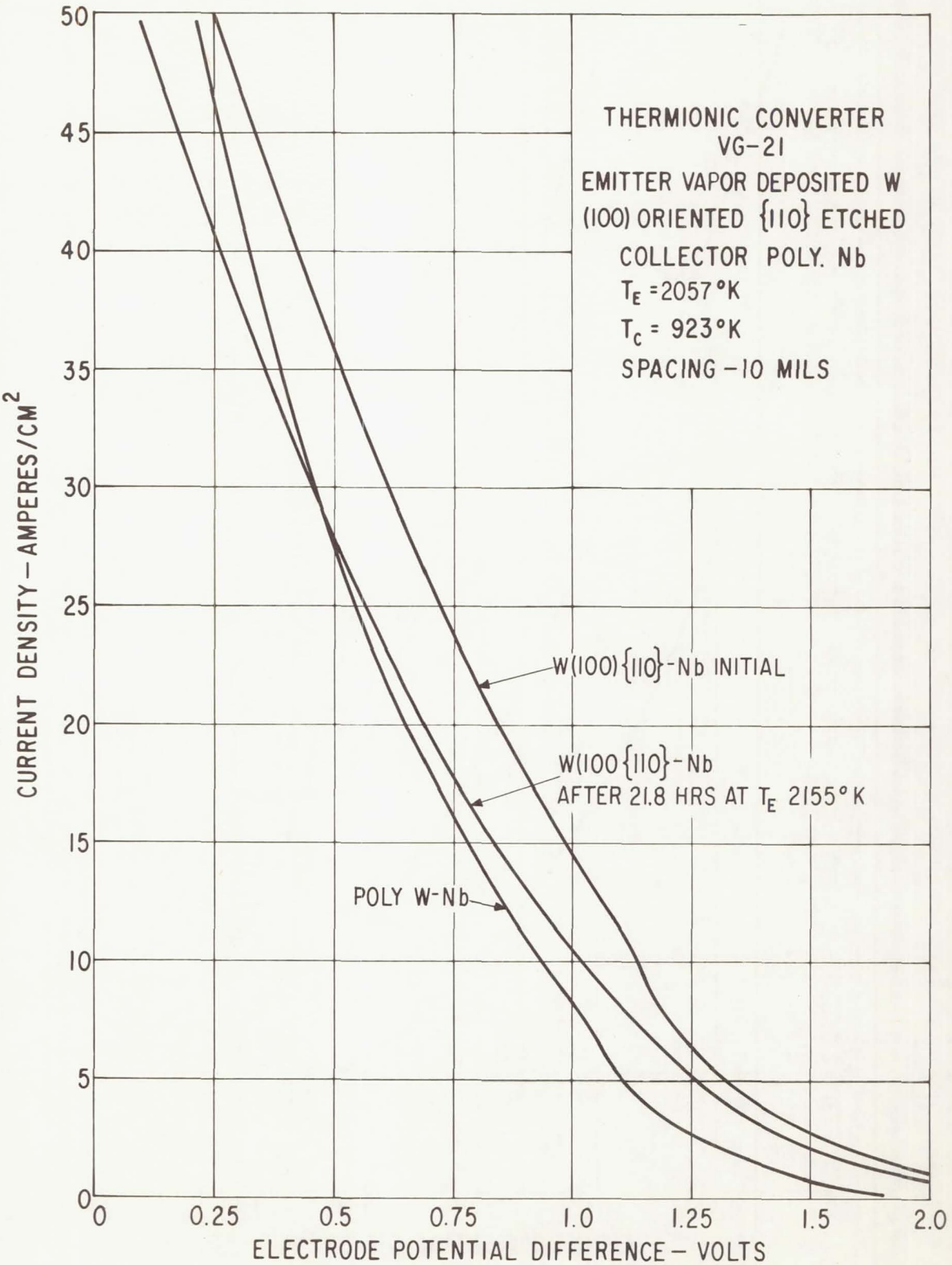

Figure 23. - Performance comparison at $T_E = 2057^O$ K and spacing d = 10 mils.

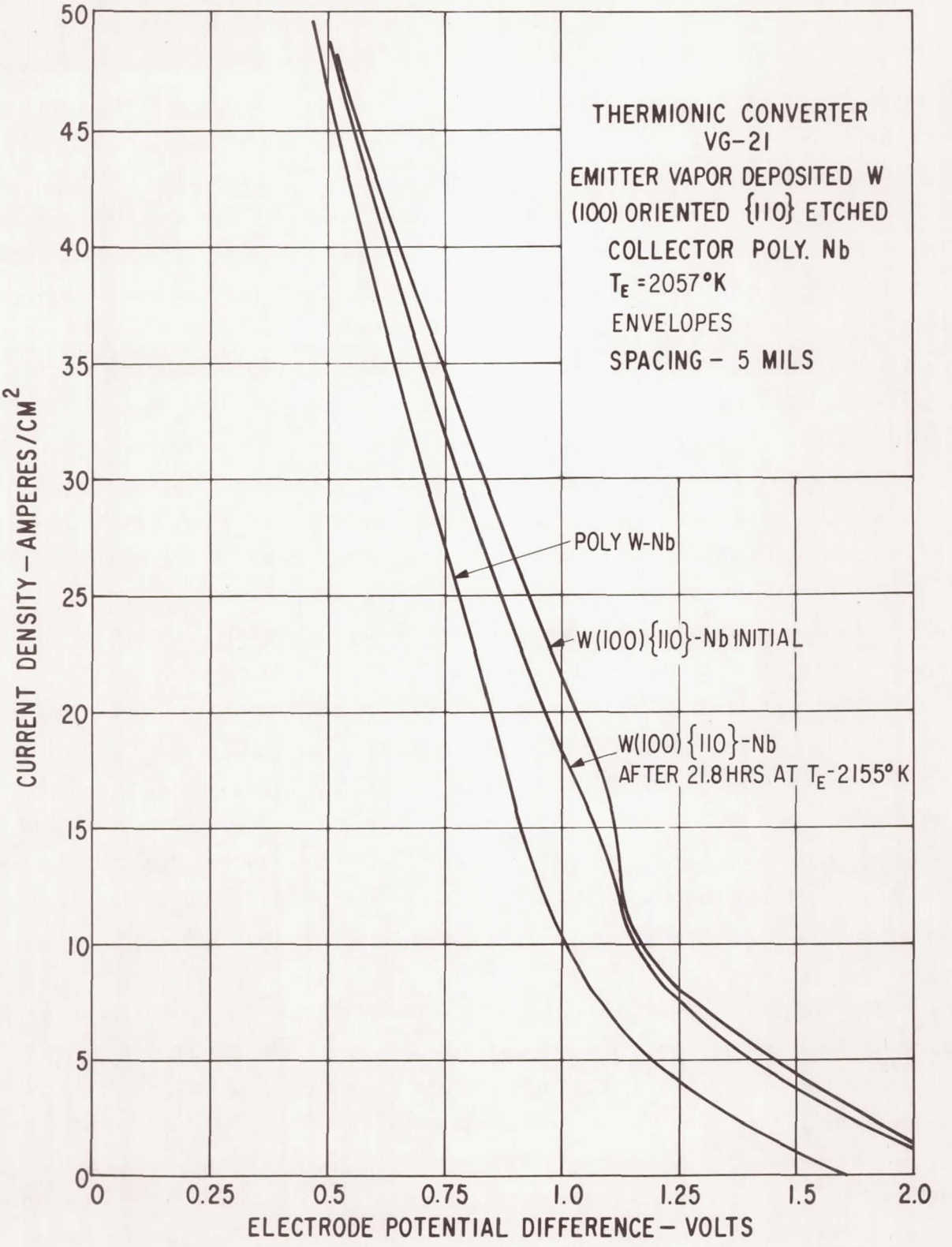

Figure 24. - Performance comparison at $T_E = 2057^O$ K and spacing d = 5 mils.

Koskinen[16] has reported a few results from tests of a thermionic converter which had a single crystal emitter with the (110) tungsten planes exposed. Koskinen's converter had a molybdenum collector. Believing that molybdenum is superior to niobium as a converter collector material, the output voltage of Koskinen's converter should be in the order of 0.05 to 0.10 volts greater for similar conditions of operation. The solid curves of Figure 25 compare Koskinen's converter with the converter described here with the etched emitter surface. The etching increases the surface area about 40% over the geometrical cross-section of the emitter. There has been some doubt among the converter specialists as to whether one could realize the advantage of this increased area. For example, under operating conditions that would form a double sheath adjacent to the emitter, the highest potential barrier for the electrons is in the center of this sheath. If the sheath extends beyond the geometrical pattern of the etch pits, the cross sectional area of the sheath rather than the area of the emitting surface may determine the current density in the converter. The current density of the upper solid line was multiplied by 0.7 to obtain the dashed line of Figure 25. If the upper curve represents the current density assuming the geometrical area of the emitter, the dashed curve represents the current density at the surface of the etched emitter structure. Comparing the dashed curve with Koskinen's curve and remembering that Koskinen's converter had a more favorable collector material, the two outputs seem quite comparable. This suggests that it is advantageous to increase the surface area of the emitter and that the effective current density is increased by the area increase.

The degradation in the output of the converter and the change in the work function of the emitter were not entirely due to a change in the area of the emitter. The initial etching changed the emitter from a (100) surface to predominantly one with the (110) surface exposed and, at the same time, increased the area. As we see from Figure 9, the area was not greatly reduced by the thermal etching; that is, the emitter surface did not become planar. As the sharp edges and valleys were removed, the new rounded

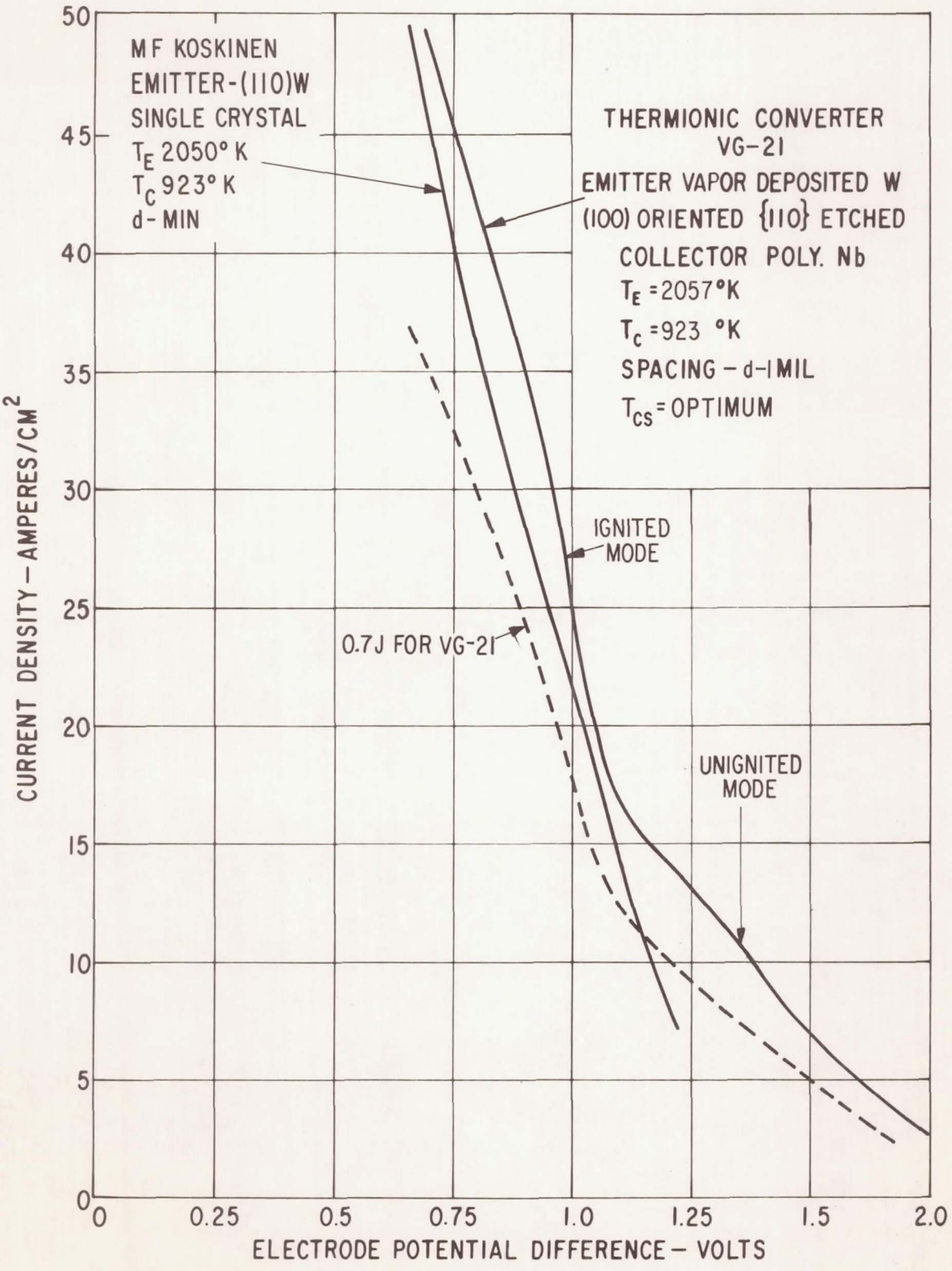

Figure 25. - Performance comparison of etched and unetched emitter surfaces.

surfaces exposed areas with crystal planes that had lower work function surfaces than the (110) planes. In terms of the work function, the final surface was very patchy. This means some areas would more strongly adsorb cesium that would other areas. Past experience has shown that patchy work function surfaces do not produce good thermionic converter emitter surfaces because it is impossible to optimize the cesium pressure for optimum cesium coverage of all patches.

CONCLUSIONS

As predicted by Webster,[11] a tungsten emitter with primarily the (110) crystal faces exposed adsorbs cesium more strongly than a polycrystalline tungsten emitter. In this study, a converter with a vapor deposited tungsten emitter etched to expose the (110) crystal facets, demonstrated this phenomena by operating at lower cesium pressure in order to obtain the proper cesium coverage on the emitter. As a result, there was less power lost in the cesium plasma. Also, a better cesium coverage on the collector at the lower cesium pressure slightly increased the output voltage. This improvement may be used advantageously to produce more output power with a given input power or to operate the converter at a wider interelectrode spacing.

In etching the base (100) oriented tungsten emitter to expose the (110) facets, there is an effective increase in the surface area of approximately 40%. This increase in the effective emitting areas, resulted in a corresponding increase in the current density. Thus, it will be possible to operate at higher power densities at essentially constant efficiency.

This converter did not maintain the initial high operating performance partially because thermal etching changed the surface area, but more importantly, because a greater spread in the work function of the surfaces was created by reducing the number of (110) etched facets and increasing the number of facets with undesirable crystalline planes exposed.

REFERENCES

(1) Wilson, V. C. and Lawrence, J., Adv. Energy Conv., 4, 195 (1964).

(2) Wilson, V. C., Therm. Conv. Spec. Conf., p. 285 (1964).

(3) Lawrence, J., Therm. Conv. Spec. Conf., p. 291 (1964).

(4) Wilson, V. C., Webster, H. F. and Lawrence, J., International Thermionic Power Conf., London, England, Sec. IIIA (1965).

(5) Lawrence, J. and Perdew, J. P., Therm. Conv. Spec. Conf., p. 289 (1965).

(6) Ibid., Figure 5.

(7) Lawrence, J. and Wilson, V. C., Therm. Conv. Spec. Conf., p. 6 (1966).

(8) Wilson, V. C. and Lawrence, J., "Characteristics of a Variable Spaced Planar Thermionic Converter with a Tungsten Emitter and a Niobium Collector," General Electric Company, NASA CR-1033 (May 1968).

(9) Wilson, V. C. and Lawrence J., Therm. Conv. Spec. Conf. (1967); also, ref. 8.

(10) Houston, J. M. and Webster, H. F., Adv. in Electronics, 17, p. 150 (1962), Academic Press, New York.

(11) Ibid., p. 146.

(12) Ibid., p. 150.

(13) Lawrence, J. and Wilson, V. C., Therm. Conv. Spec. Conf., Houston, Texas, p. 6 (1966).

(14) Festa, J. V. and Danko, J. C., Proceedings of Conf. on Chem. Vapor Deposition of Refractory Metals, Alloys and Compounds, Gatlinburg, Tennessee (September 1967).

(15) Wilson, V. C. and Webster, H. F., 19th Annual Proceedings Power Sources Conf. (1965).

(16) Koskinen, M. F., Therm. Conv. Spec. Conf., San Diego, California, p. 366 (1965).

APPENDIX A

FAMILIES OF LOAD LINES

Fig. No.	T_E °K	T_C °K	T_{Cs} °K	Spacing Mils
26	1660	873	533 to 573	1
27	1665	873	" "	2
28	1650	878	" "	5
29	"	873	" "	10
30	"	875	" "	20
31	"	823 to 923	553	10
32	1750	923	553 to 593	1
33	1745	"	" "	2
34	"	"	" "	5
35	"	"	" "	10
36	1750	"	" "	20
37	1745	823 to 923	573	10
38	1840	923	553 to 593	1
39	"	"	" "	2
40	"	"	" "	5
41	"	"	" "	10
42	"	"	" "	20
43	1924	923	553 to 593	1
44	"	"	" "	2
45	"	"	" "	5
46				
47	"	"	" "	20
48	1962	923	563 to 613	1
49	"	"	" "	2
50	"	"	" "	5
51	"	"	" "	10
52	"	"	" "	20
53	2057	923	573 to 613	1
54	"	"	" "	2
55	"	"	" "	5
56	"	"	" "	10
57	"	"	" "	20

Fig. No.	T_E °K	T_C °K	T_{Cs} °K	Spacing Mils
58	1600	848	553	5
59	1600	"	"	10
60	1600	"		20
61	1673	848	553 to 573	1
62	"	"	" "	2
63	"	"	" "	5
64	"	"	" "	10
65	"	"	" "	20
66	1866	923	558 to 603	1
67	"	"	" "	2
68	"	"	" "	5
69	"	"	" "	10
70	"	"	" "	20
71	2057	923	573 to 613	1
72	"	"	" "	2
73	"	"	" "	5
74	"	"	" "	10
75	"	"	" "	20
76	2155	973	603 to 643	1
77	"	"	" "	2
78	"	"	" "	5
79	"	"	" "	10
80	"	"	" "	20
Converter operated 21.8 hours at 2155° K				
81	2057	923	603 to 643	1
82	"	"	" "	2
83	"	"	" "	5
84	"	"	" "	10
85	"	"	" "	20

Fig. No.	T_E °K	T_C °K	T_{Cs} °K	Spacing Mils
86	1840	900	583 to 603	1
87	"	"	" "	2
88	"	"	" "	5
89	"	"	" "	10
90	"	"	" "	20
91	1750	900	573 to 603	1
92	"	"	" "	2
93	"	"	" "	5
94	"	"	" "	10
95	"	"	" "	20

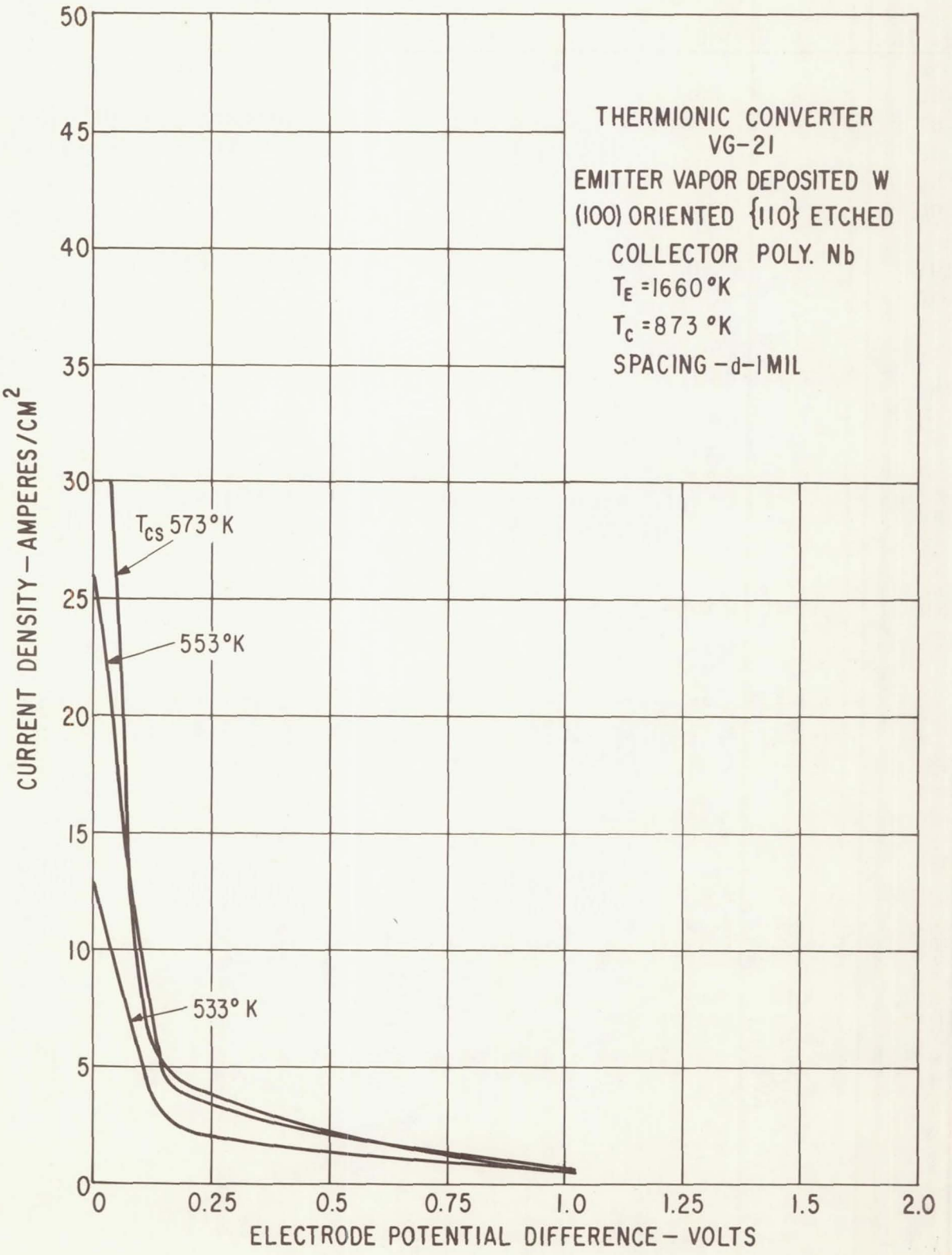

Figure 26. - Load lines for $T_E = 1660^O$ K, $T_C = 873^O$ K, and spacing d = 1 mil.

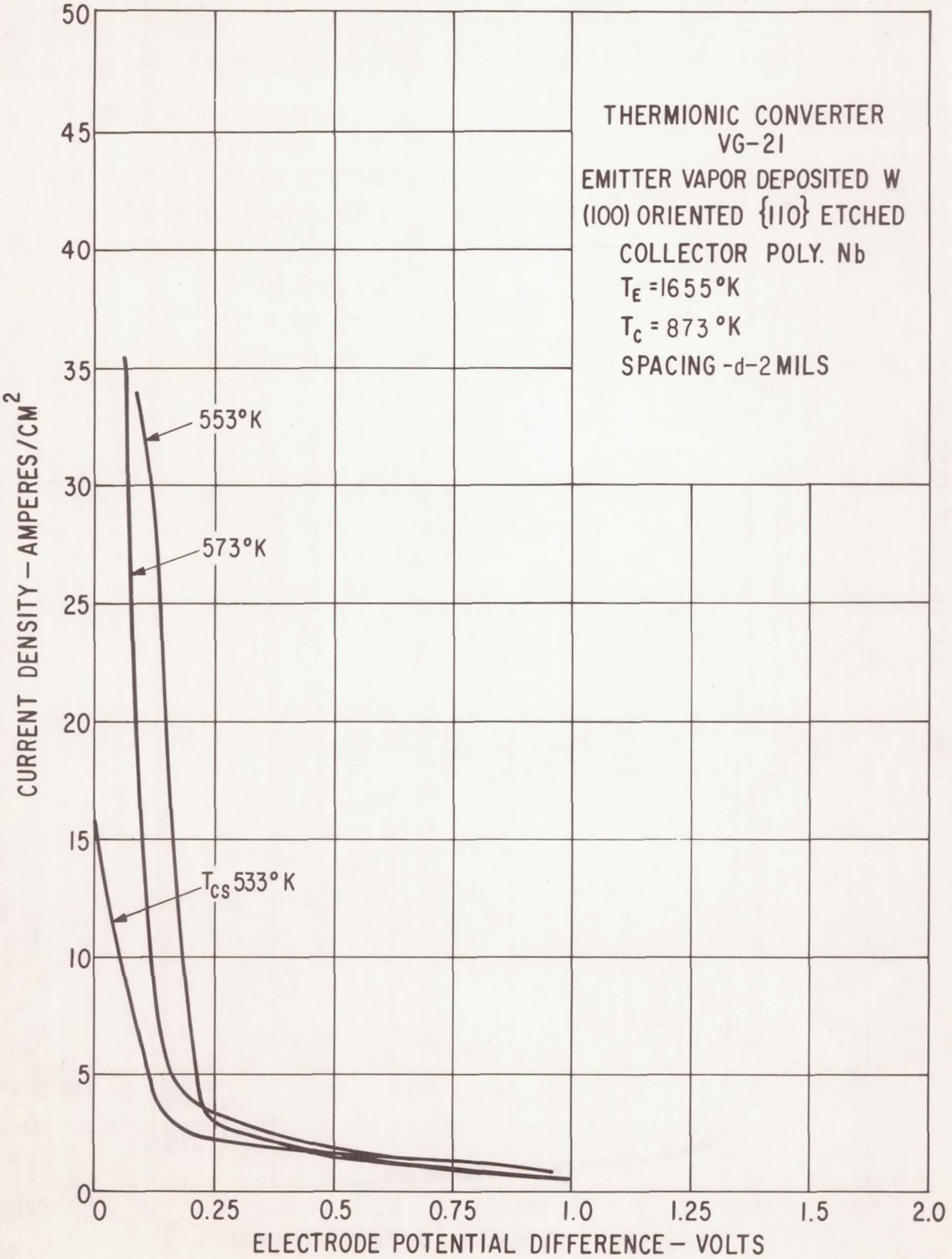

Figure 27. - Load lines for T_E = 1655° K, T_C = 873° K, and spacing d = 2 mils.

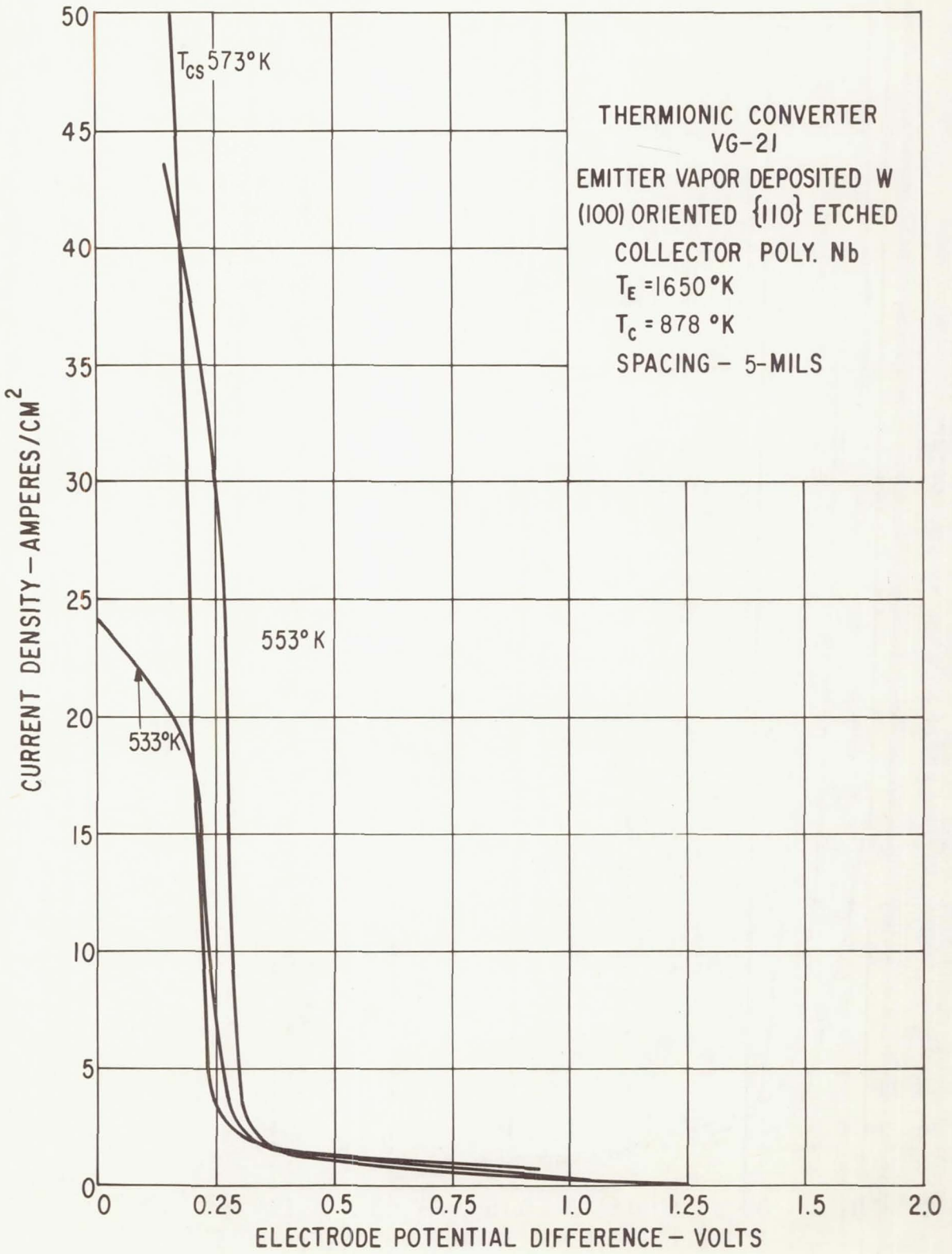

Figure 28. - Load lines for $T_E = 1650^O$ K, $T_C = 878^O$ K, and spacing d = 5 mils.

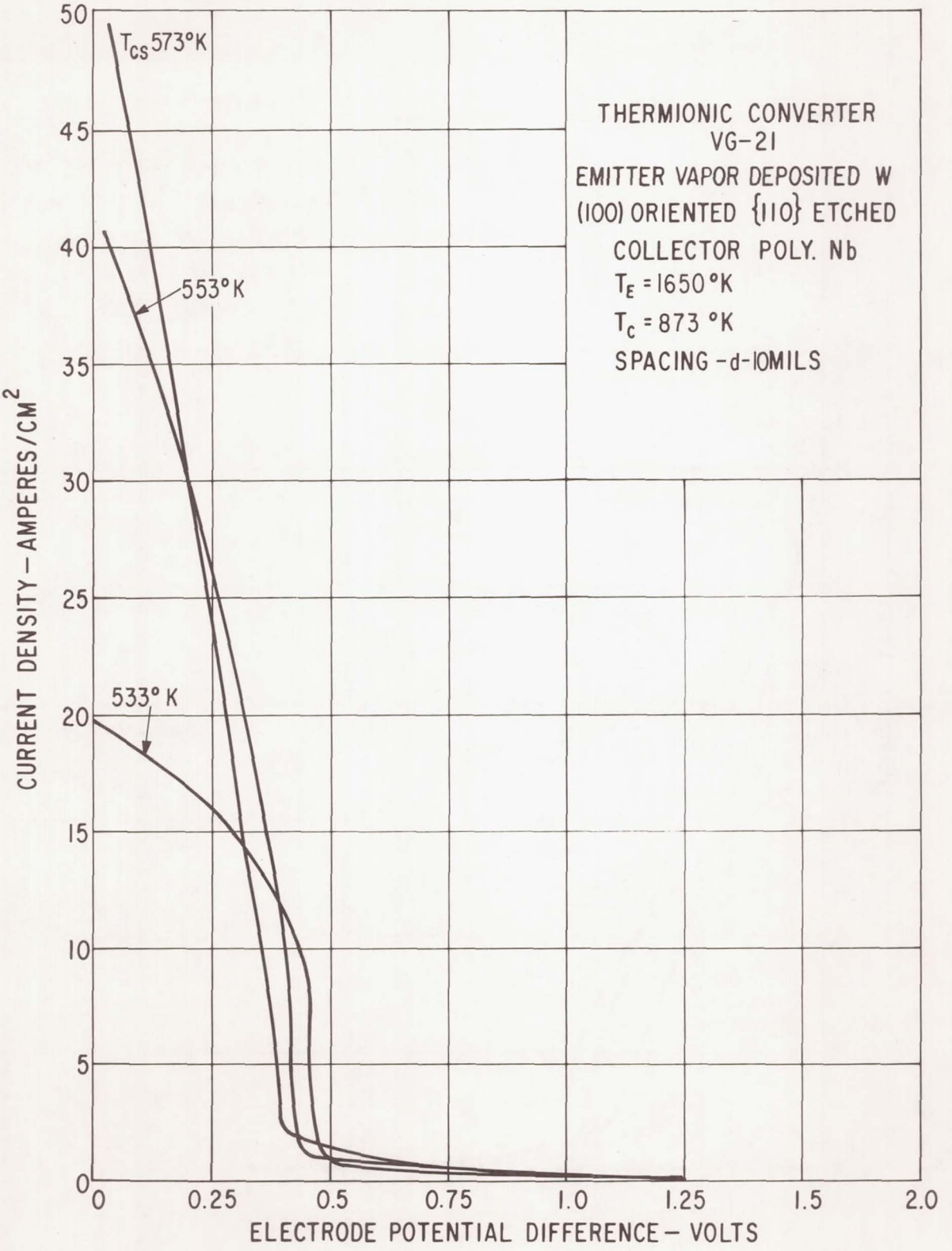

Figure 29. - Load lines for $T_E = 1650^O$ K, $T_C = 873^O$ K, and spacing d = 10 mils.

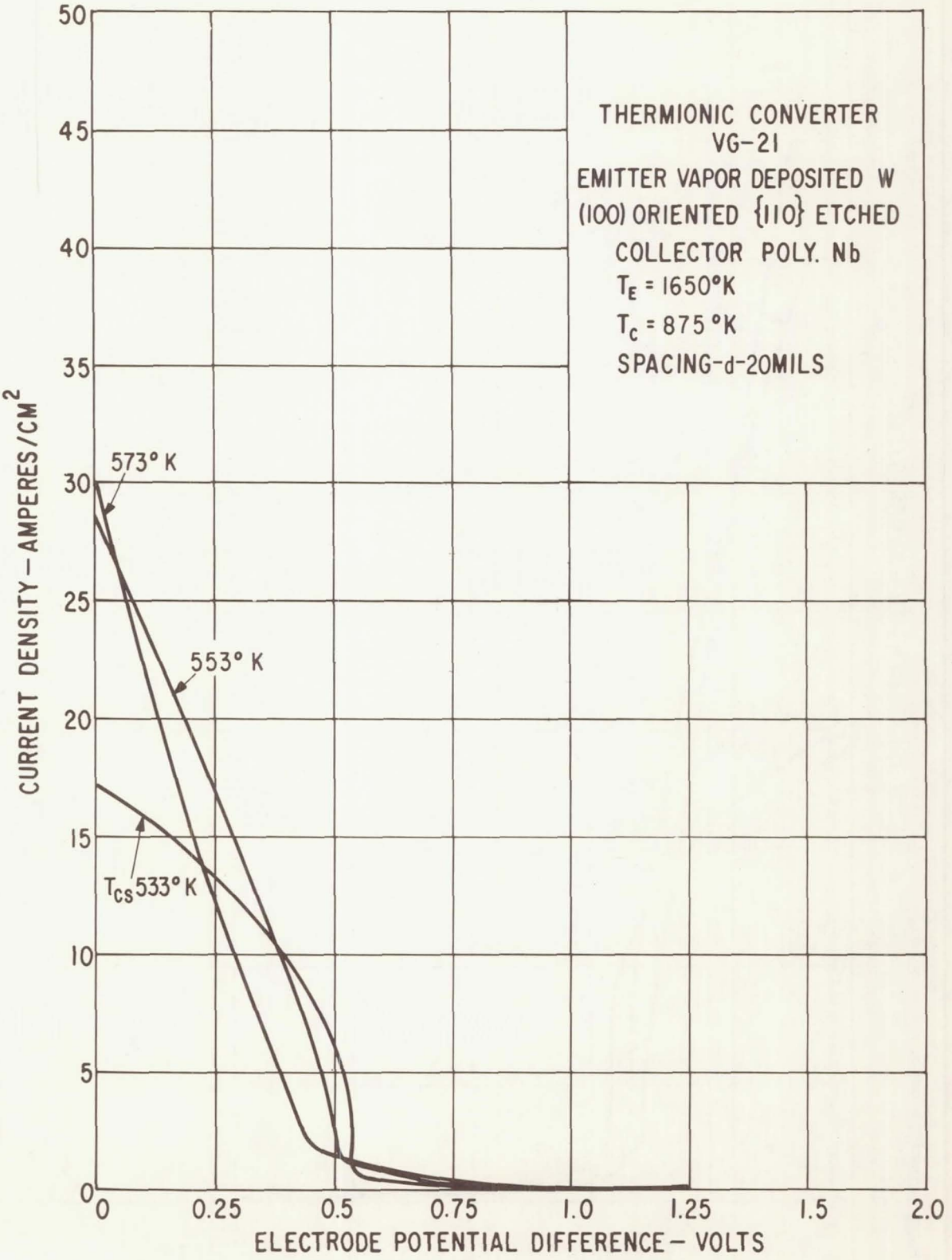

Figure 30. - Load lines for $T_E = 1650^O$ K, $T_C = 875^O$ K, and spacing d = 20 mils.

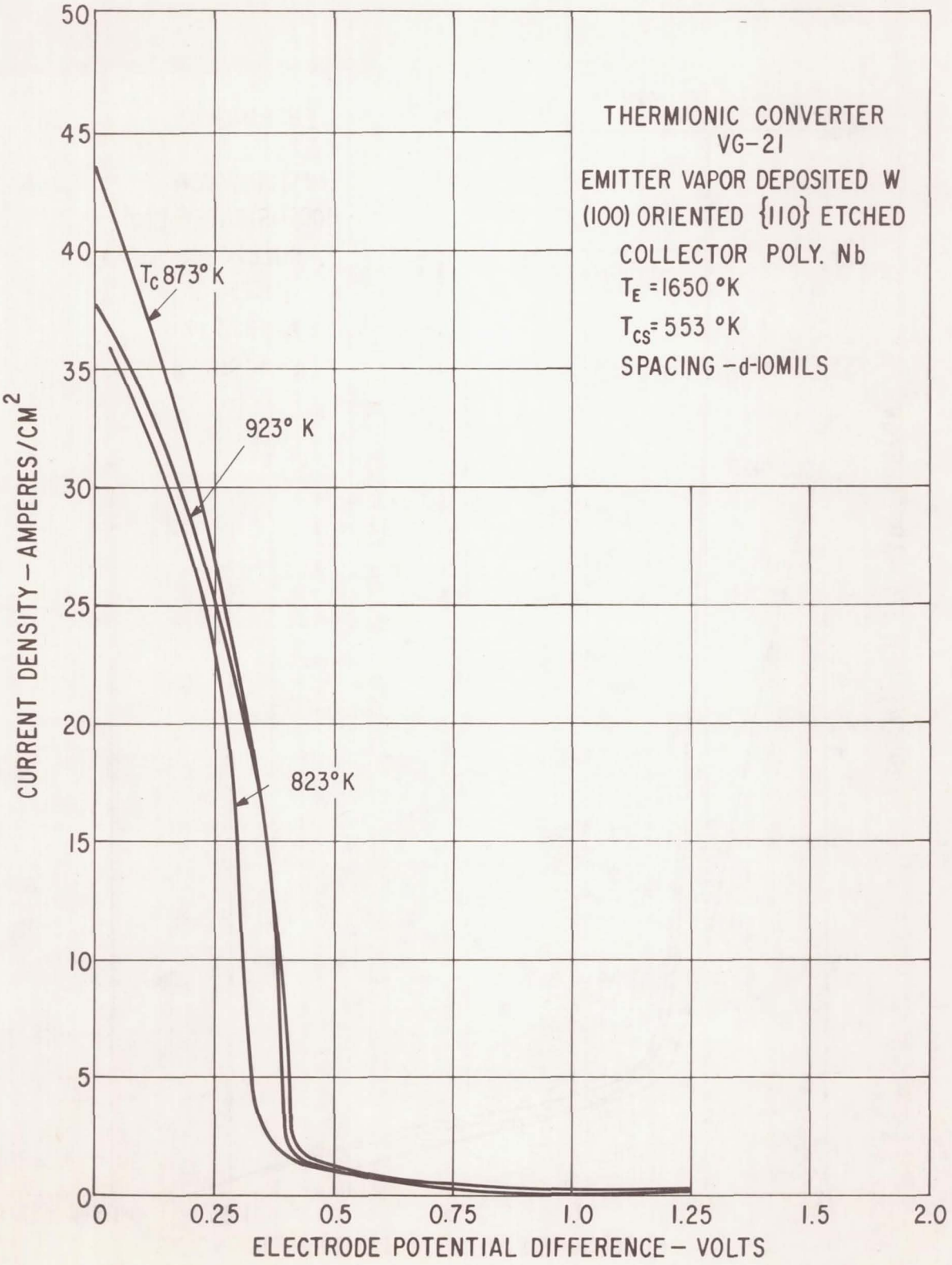

Figure 31. - Load lines for $T_E = 1650^O$ K, $T_{cs} = 553^O$ K, and spacing d = 10 mils.

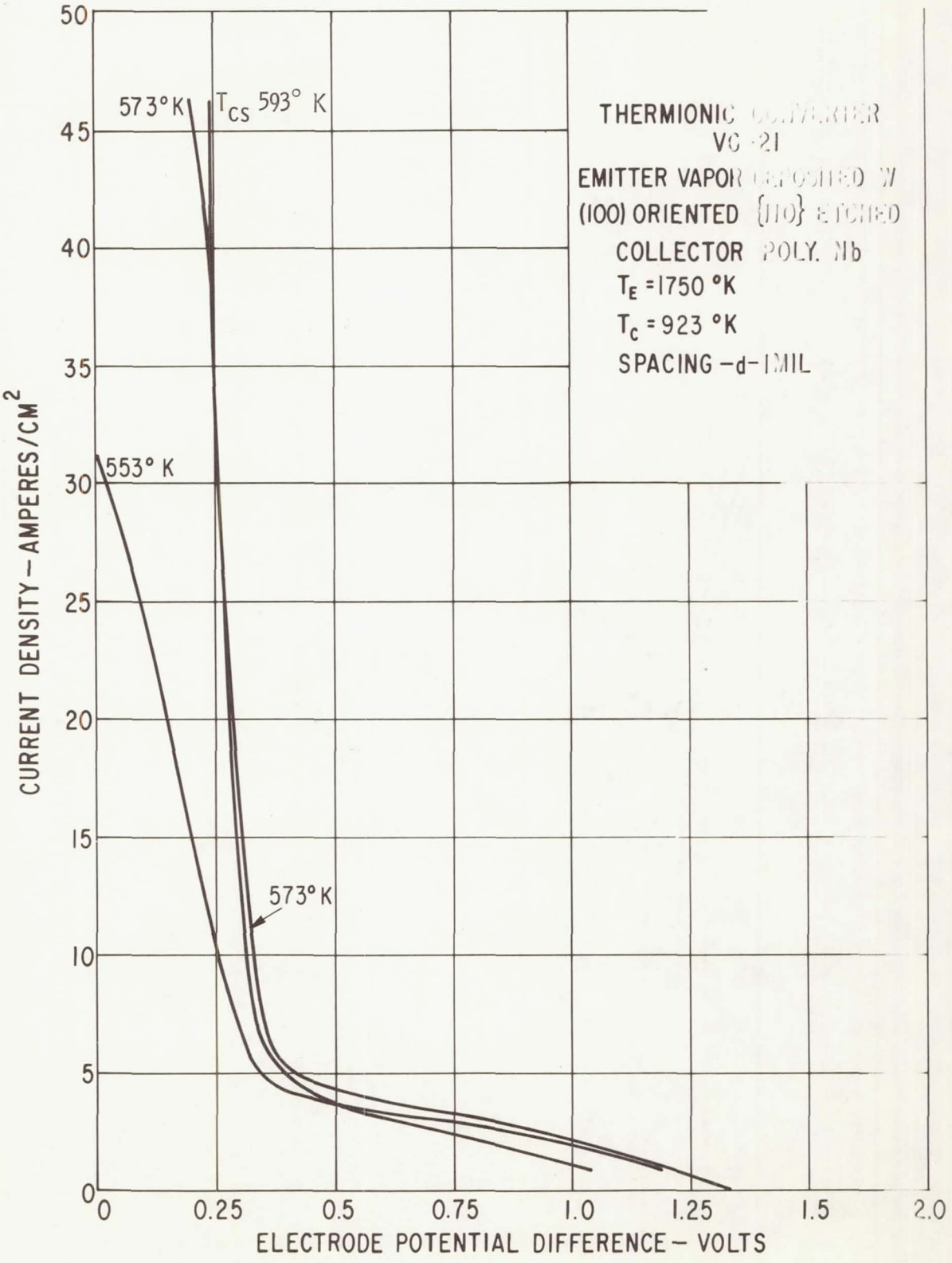

Figure 32. - Load lines for $T_E = 1750^O$ K, $T_C = 923^O$ K, and spacing d = 1 mil.

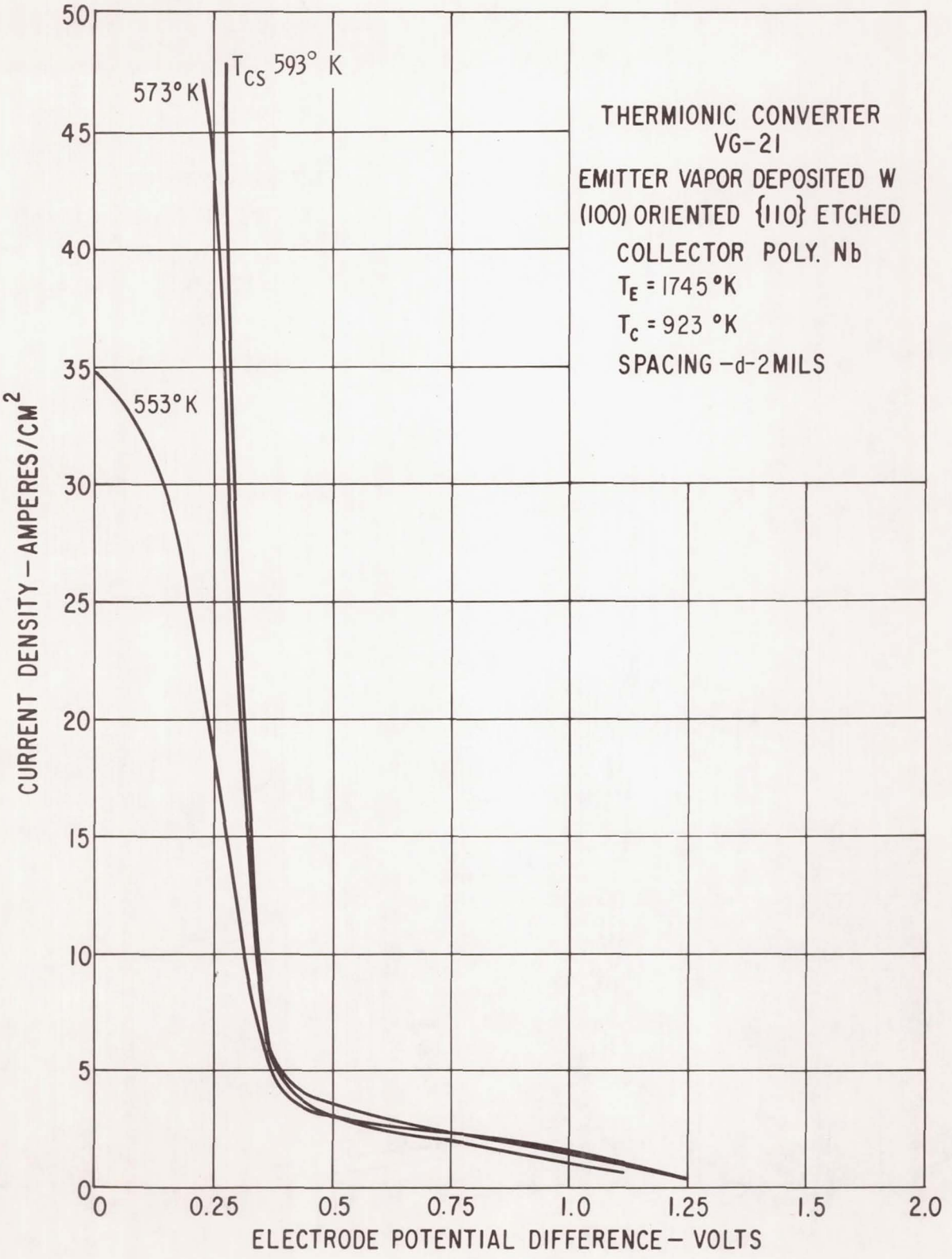

Figure 33. - Load lines for $T_E = 1745^O$ K, $T_C = 923^O$ K, and spacing d = 2 mils.

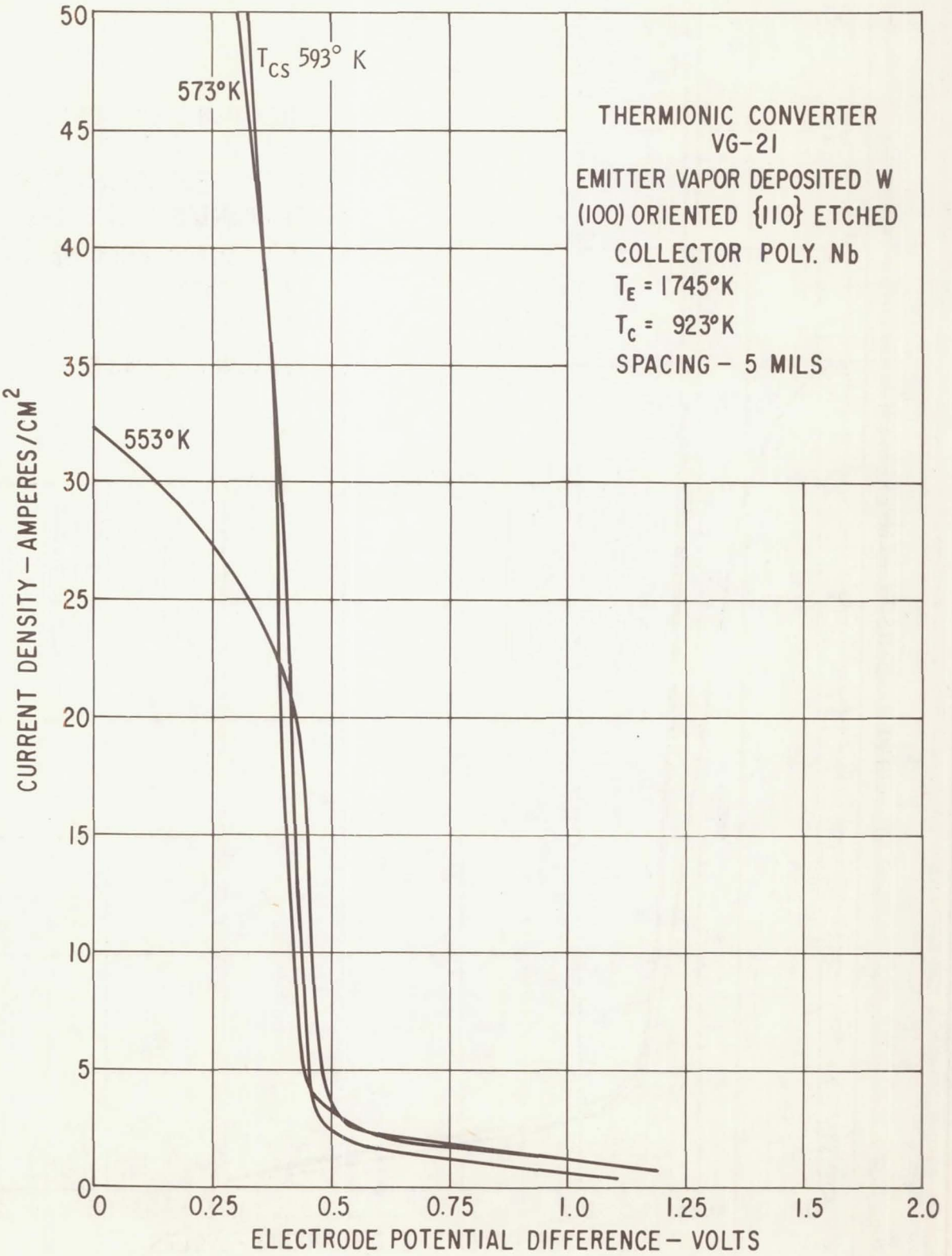

Figure 34. - Load lines for $T_E = 1745^{\circ}$ K, $T_C = 923^{\circ}$ K, and spacing d = 5 mils.

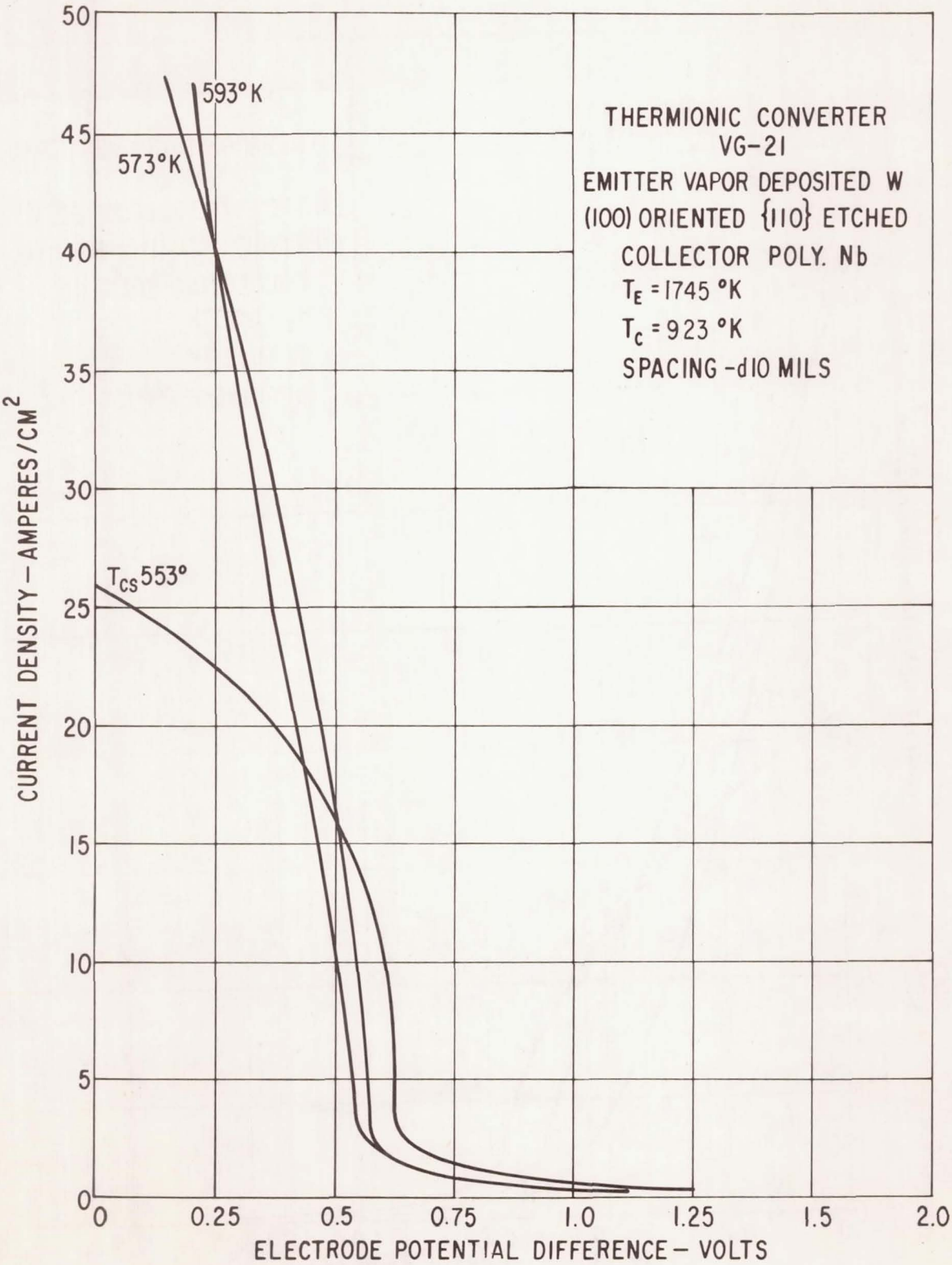

Figure 35. - Load lines for $T_E = 1745^O$ K, $T_C = 923^O$ K, and spacing d = 10 mils.

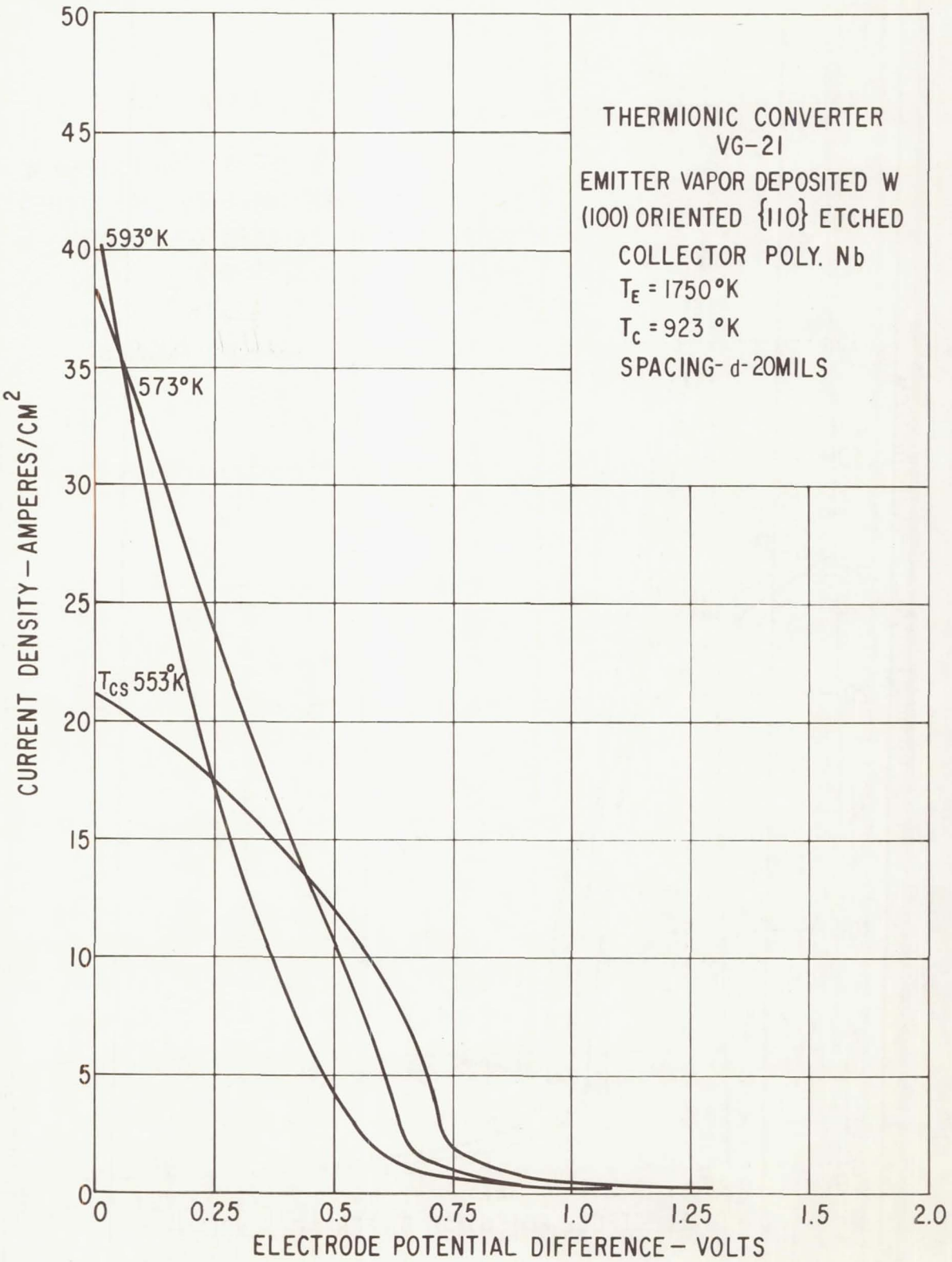

Figure 36. - Load lines for $T_E = 1750^O$ K, $T_C = 923^O$ K, and spacing d = 20 mils.

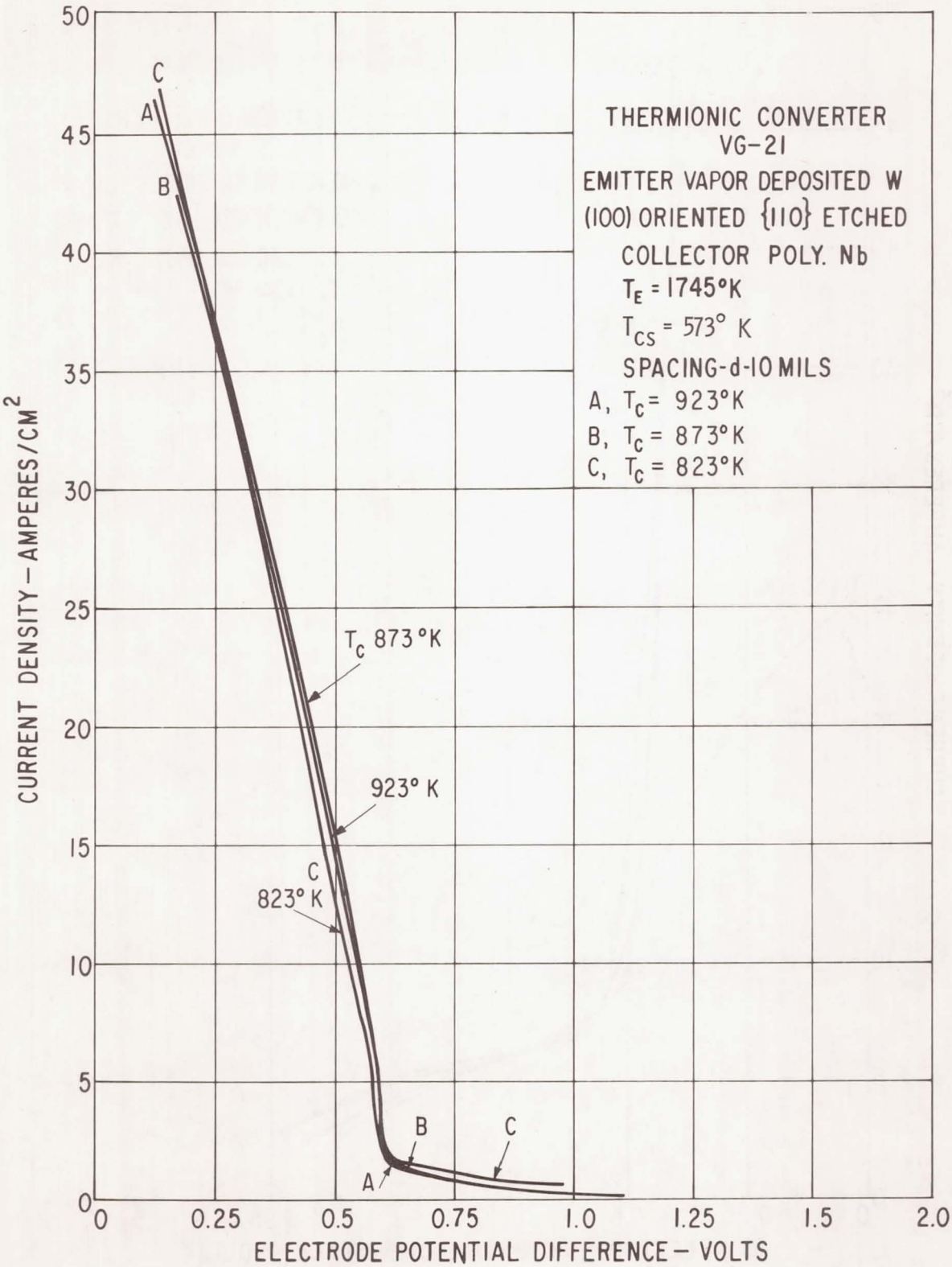

Figure 37. - Load lines for $T_E = 1745^O$ K, $T_{CS} = 573^O$ K, and spacing d = 10 mils.

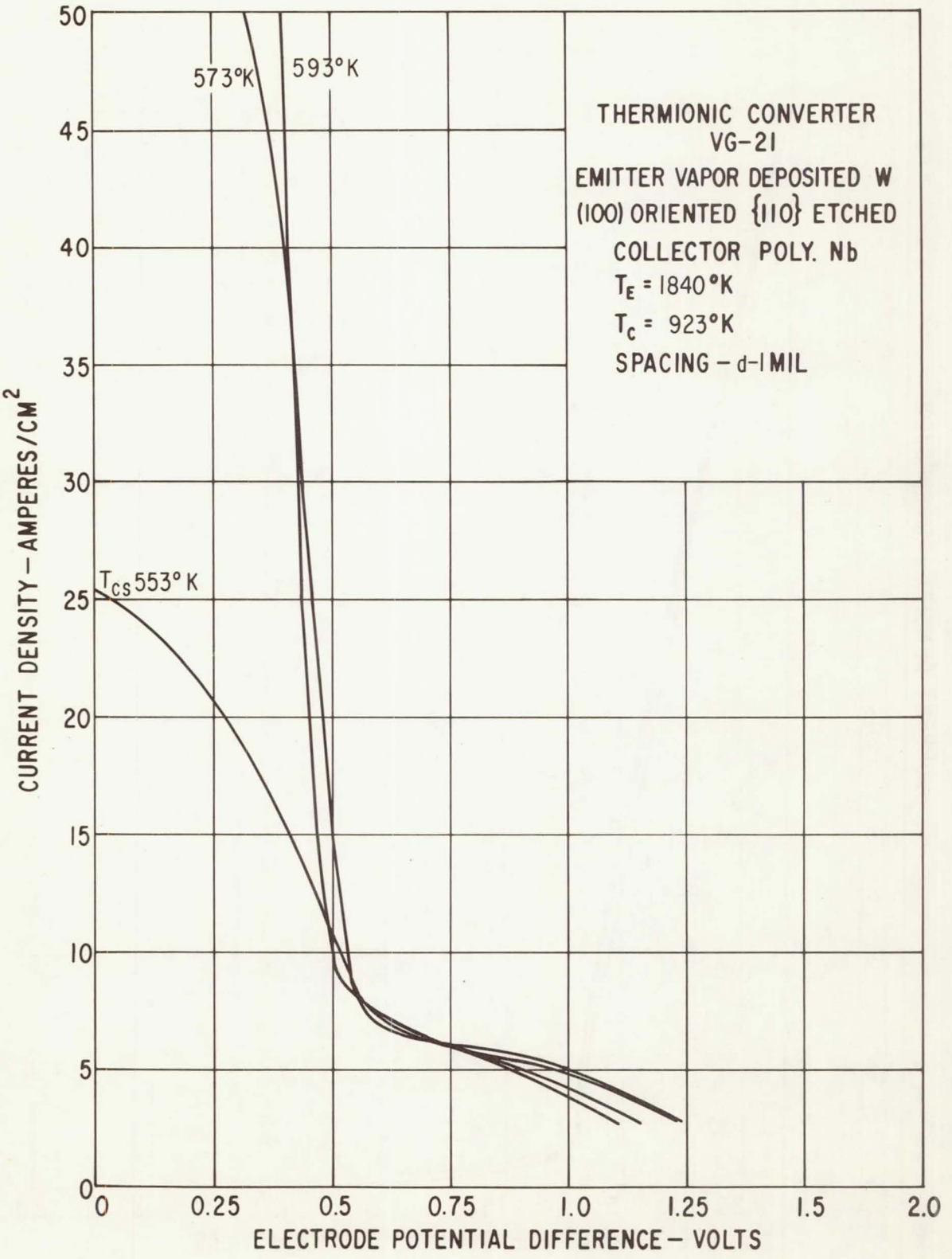

Figure 38. - Load lines for $T_E = 1840^o$ K, $T_C = 923^o$ K, and spacing d = 1 mil.

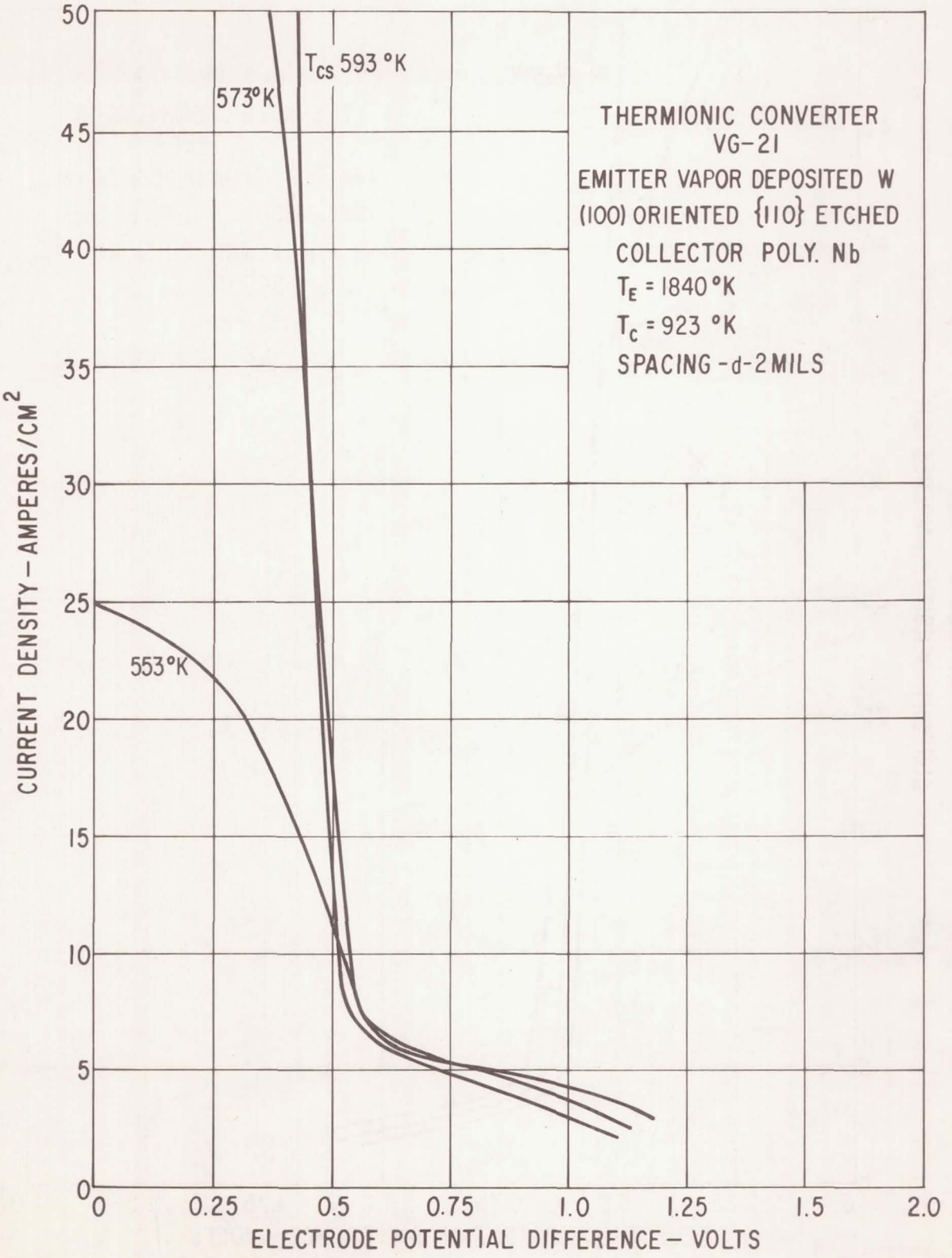

Figure 39. - Load lines for $T_E = 1840^O$ K, $T_C = 923^O$ K, and spacing d = 2 mils.

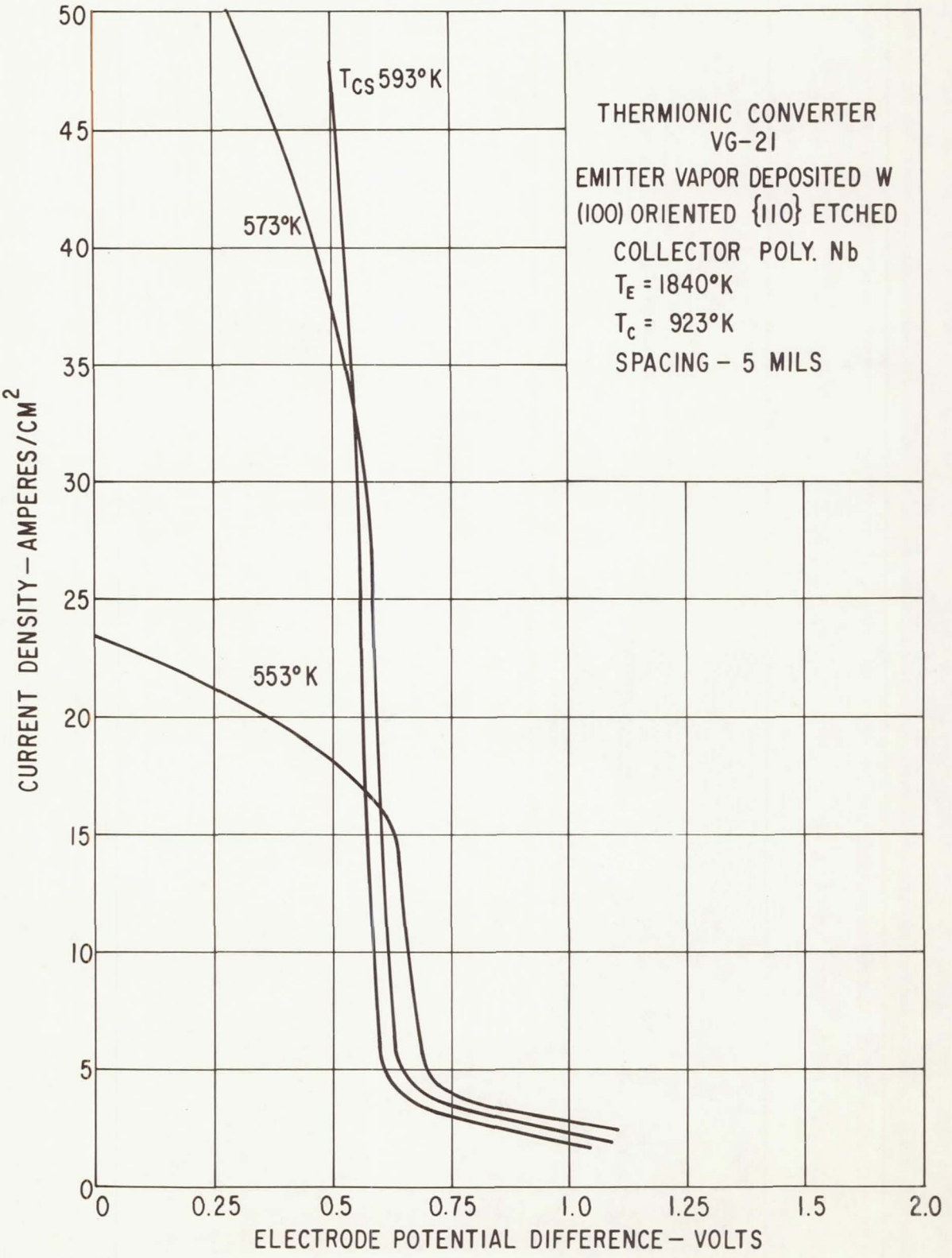

Figure 40. - Load lines for $T_E = 1840^{\circ}$ K, $T_C = 923^{\circ}$ K, and spacing d = 5 mils.

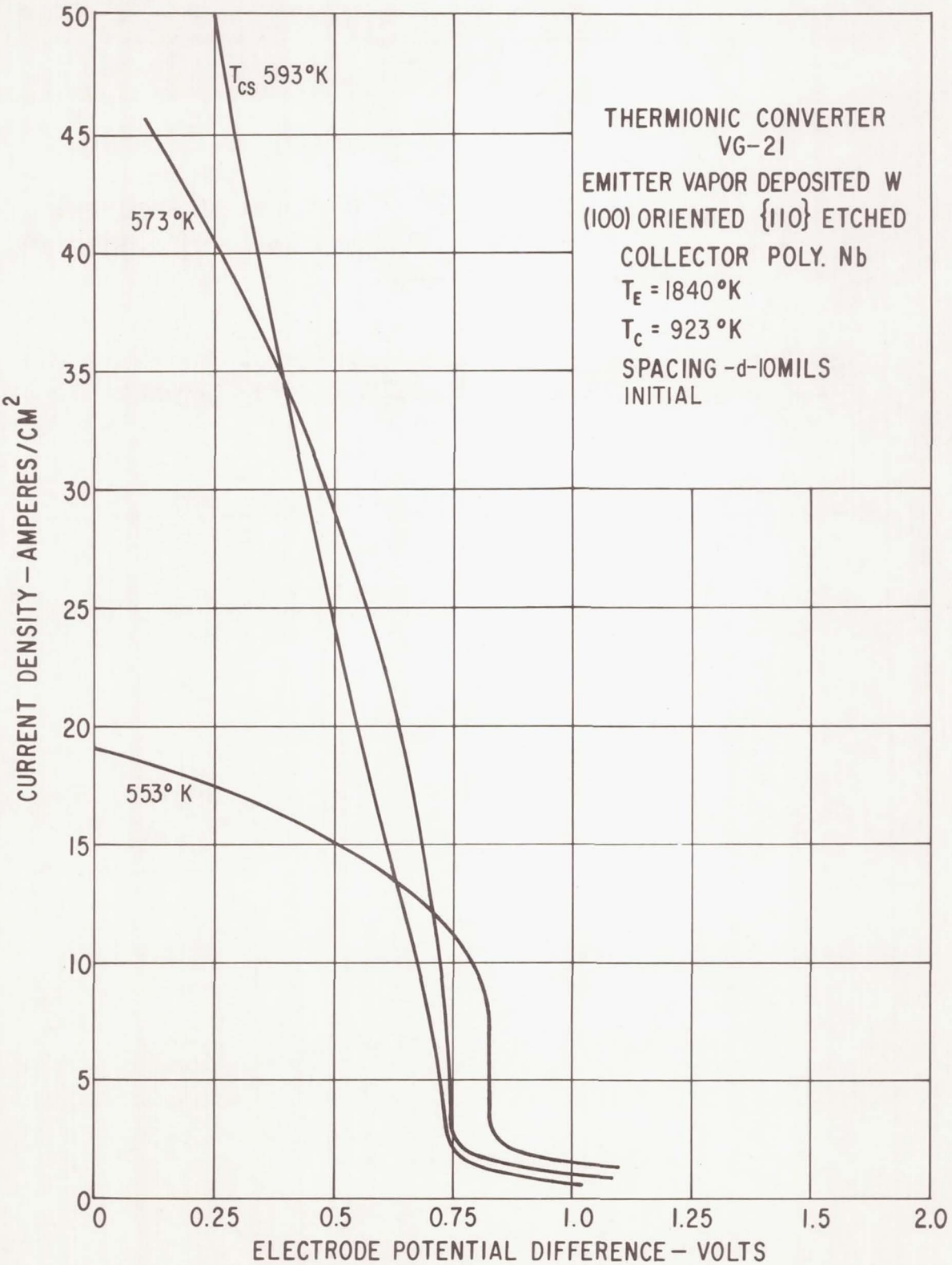

Figure 41. - Load lines for $T_E = 1840^O$ K, $T_C = 923^O$ K, and spacing d = 10 mils; before aging.

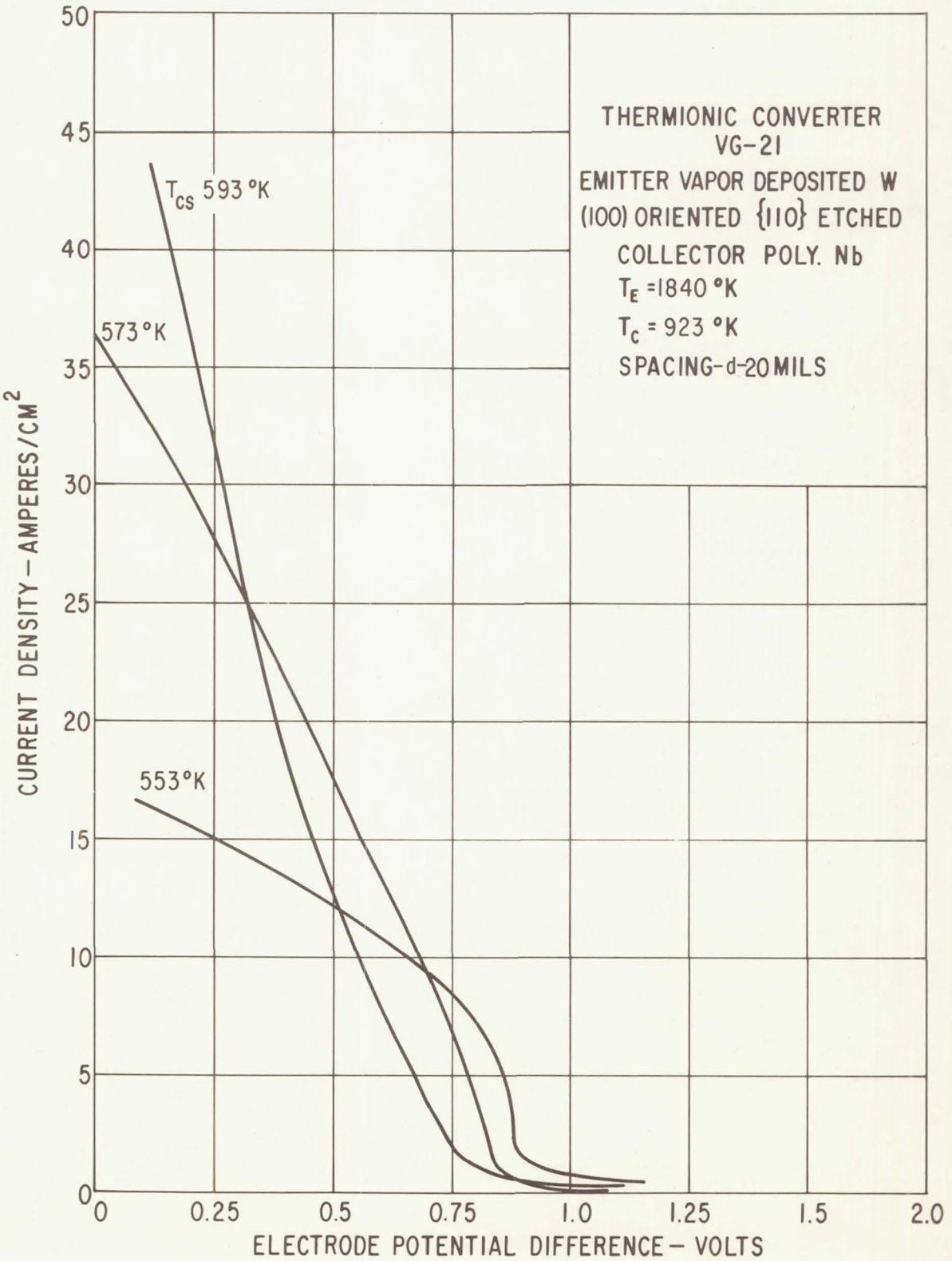

Figure 42. - Load lines for $T_E = 1840^O$ K, $T_C = 923^O$ K, and spacing d = 20 mils.

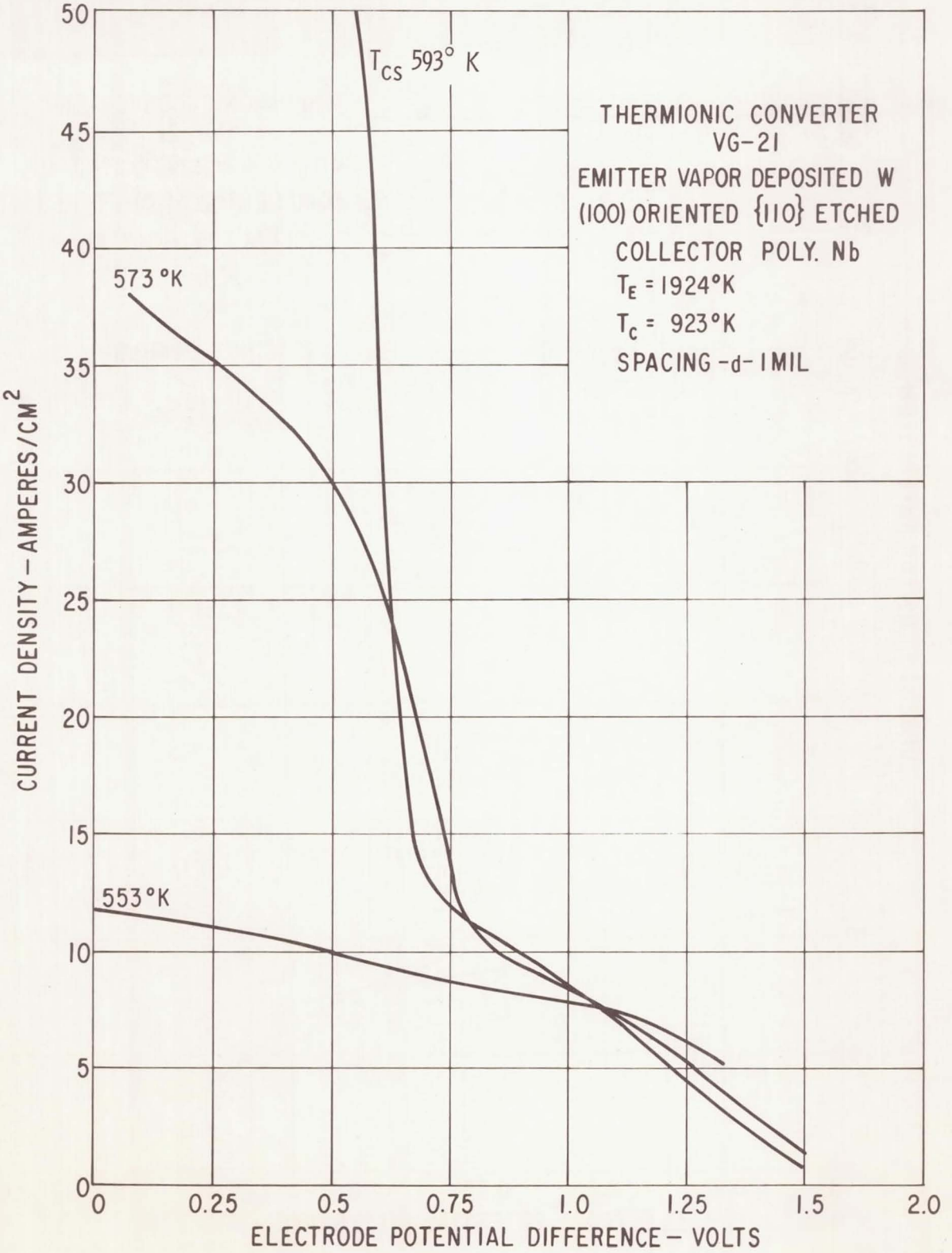

Figure 43. - Load lines for $T_E = 1924^O$ K, $T_C = 923^O$ K, and spacing d = 1 mil.

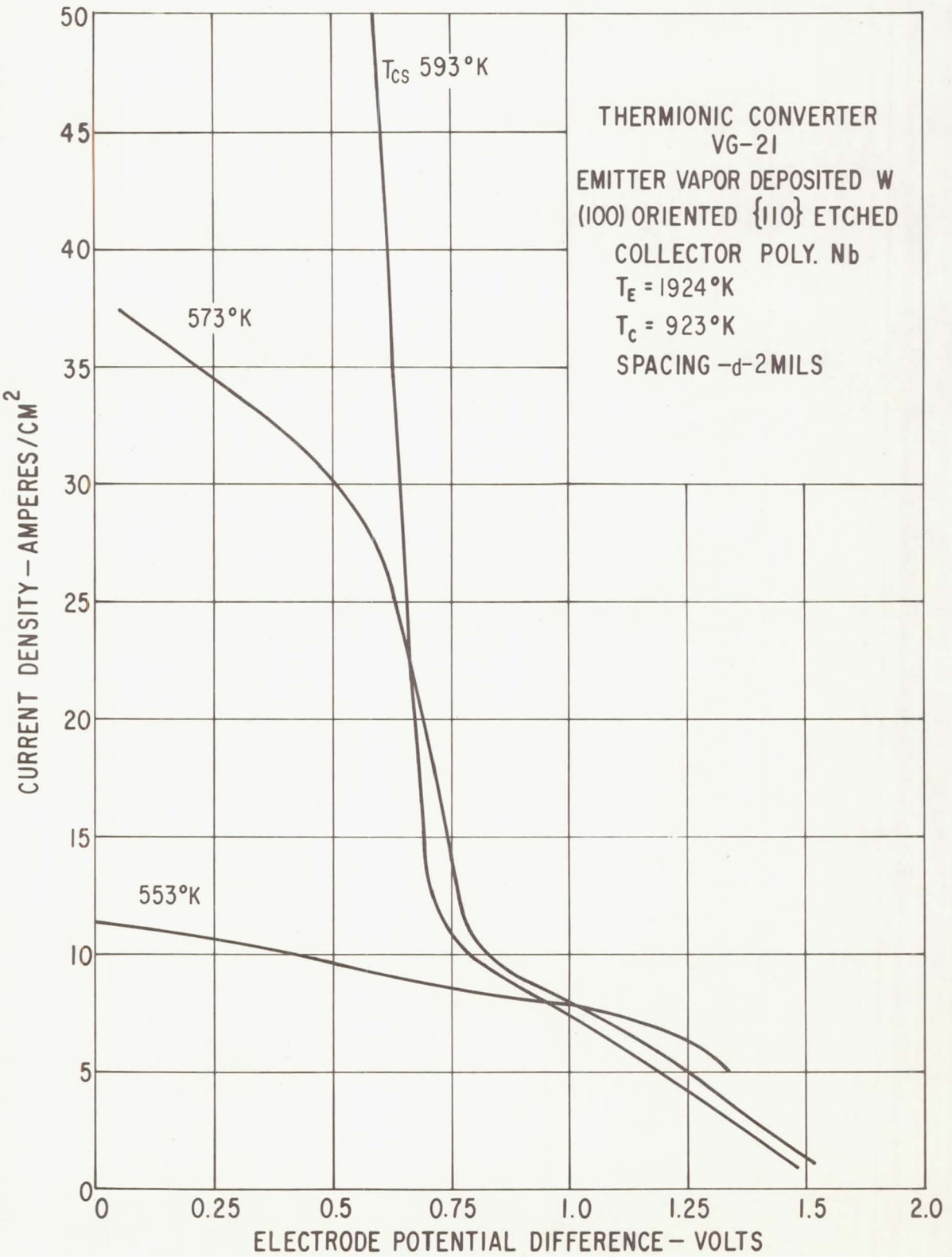

Figure 44. - Load lines for $T_E = 1924^O$ K, $T_C = 923^O$ K, and spacing d = 2 mils.

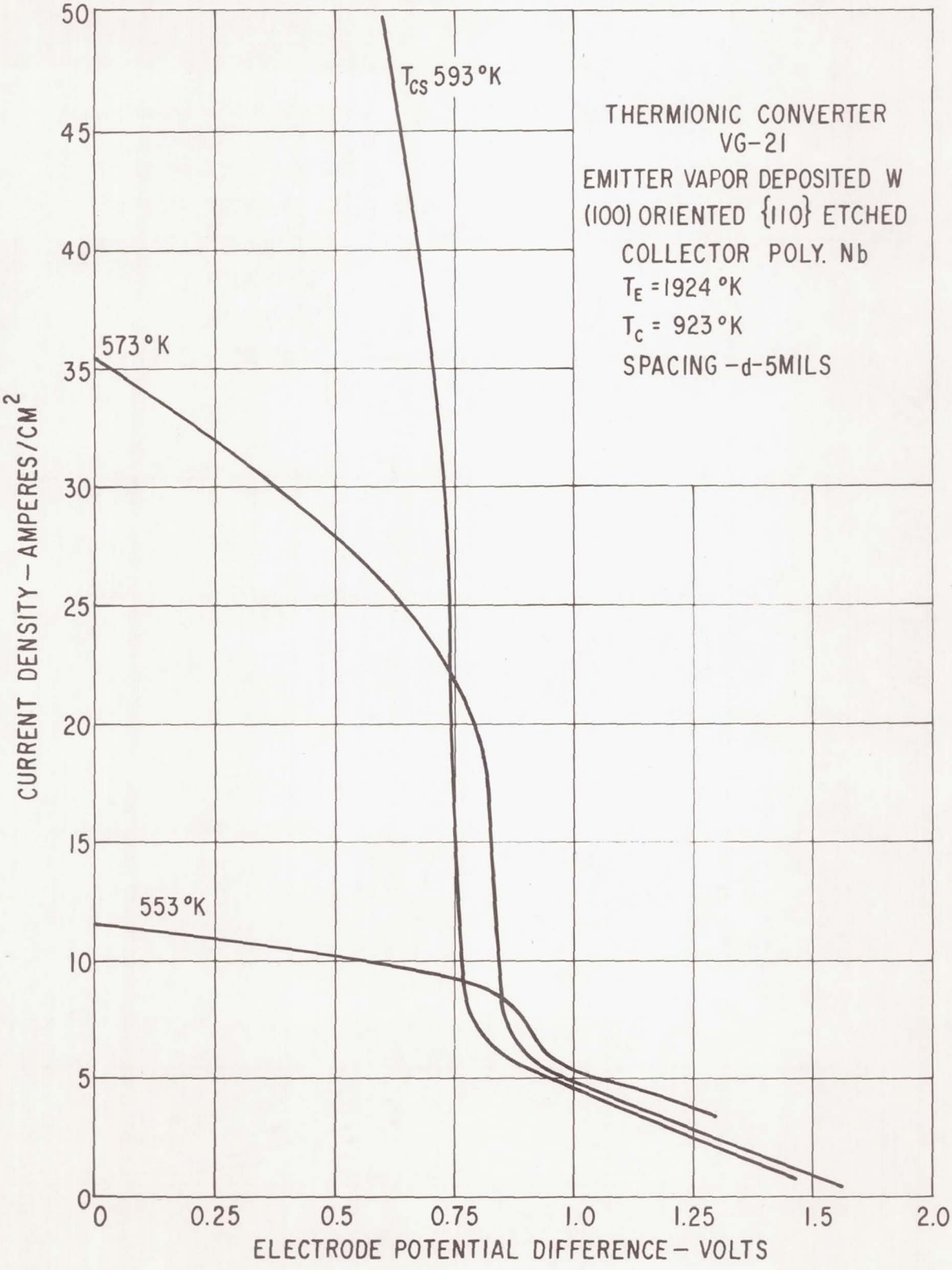

Figure 45. - Load lines for $T_E = 1924^O$ K, $T_C = 923^O$ K, and spacing d = 5 mils.

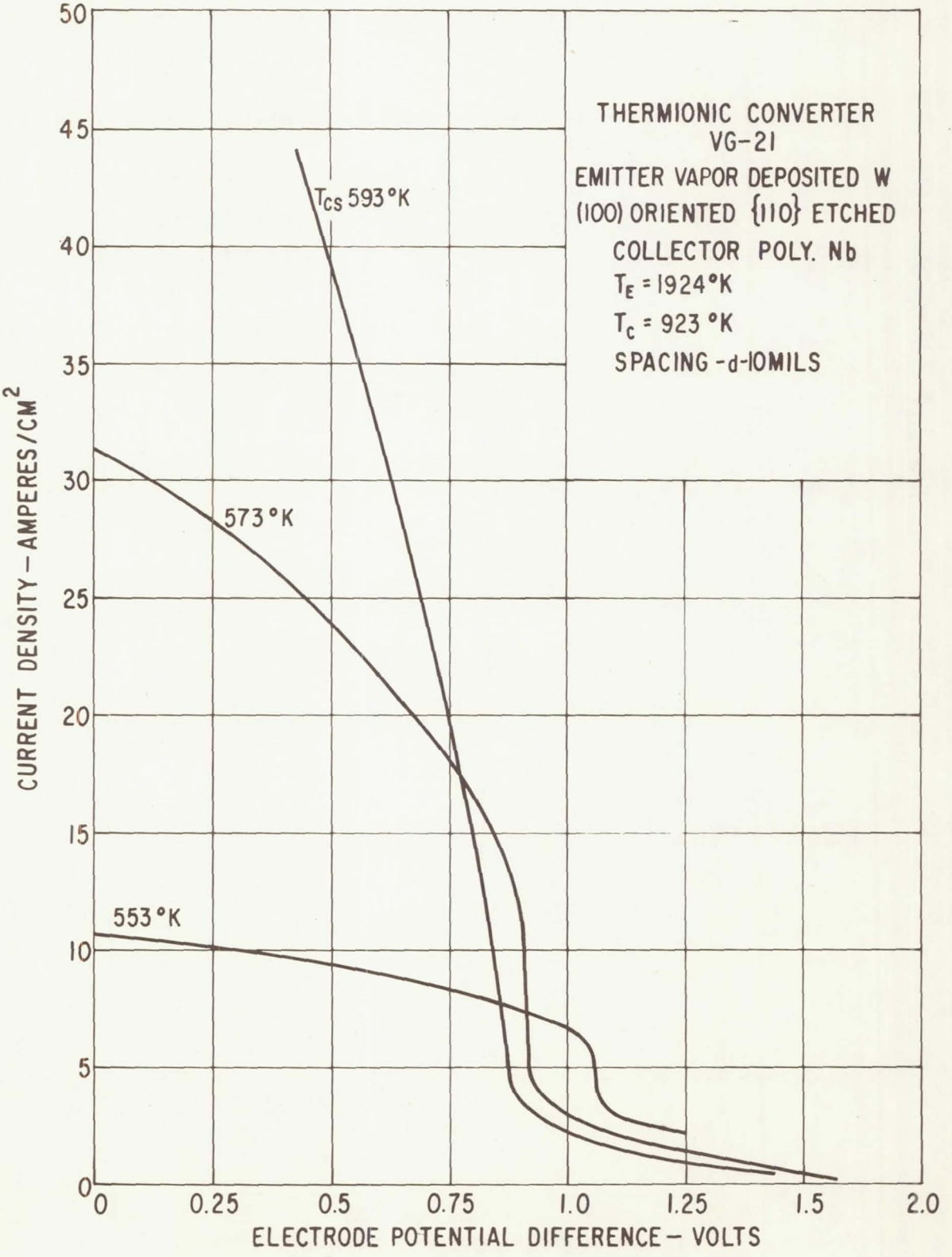

Figure 46. - Load lines for $T_E = 1924^O$ K, $T_C = 923^O$ K, and spacing d = 10 mils.

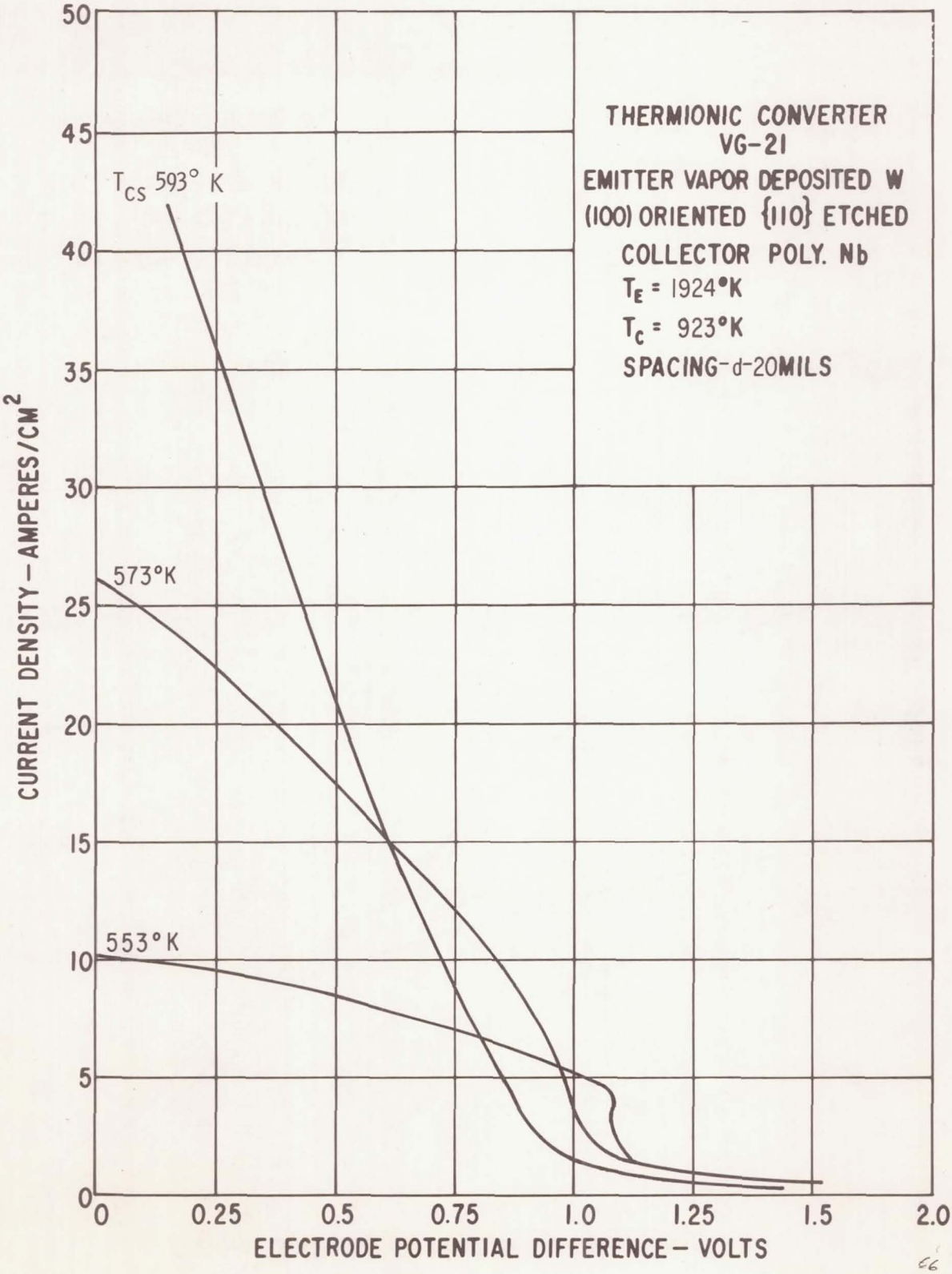

Figure 47. - Load lines for $T_E = 1924^O$ K, $T_C = 923^O$ K, and spacing d = 20 mils.

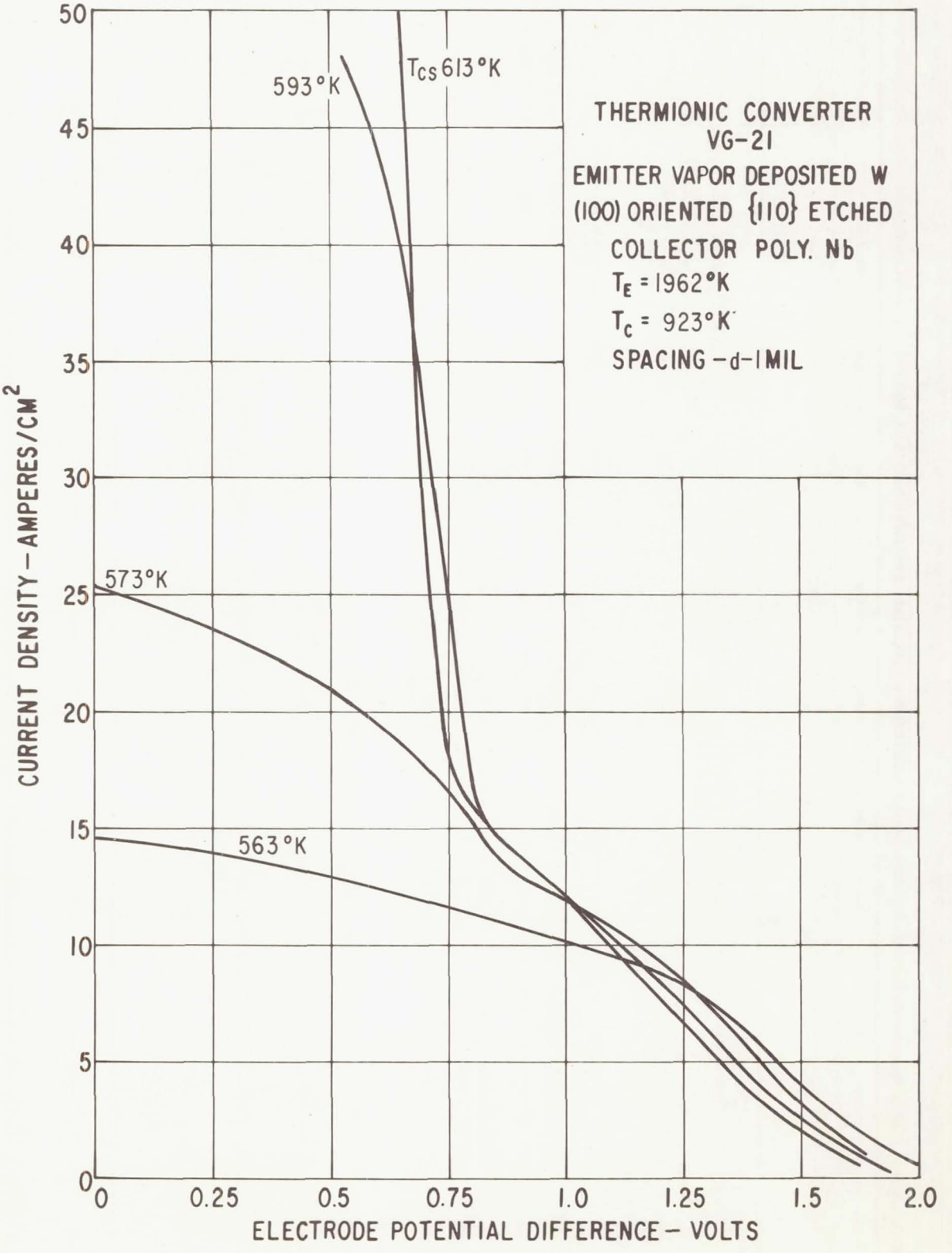

Figure 48. - Load lines for $T_E = 1962^O$ K, $T_C = 923^O$ K, and spacing d = 1 mil.

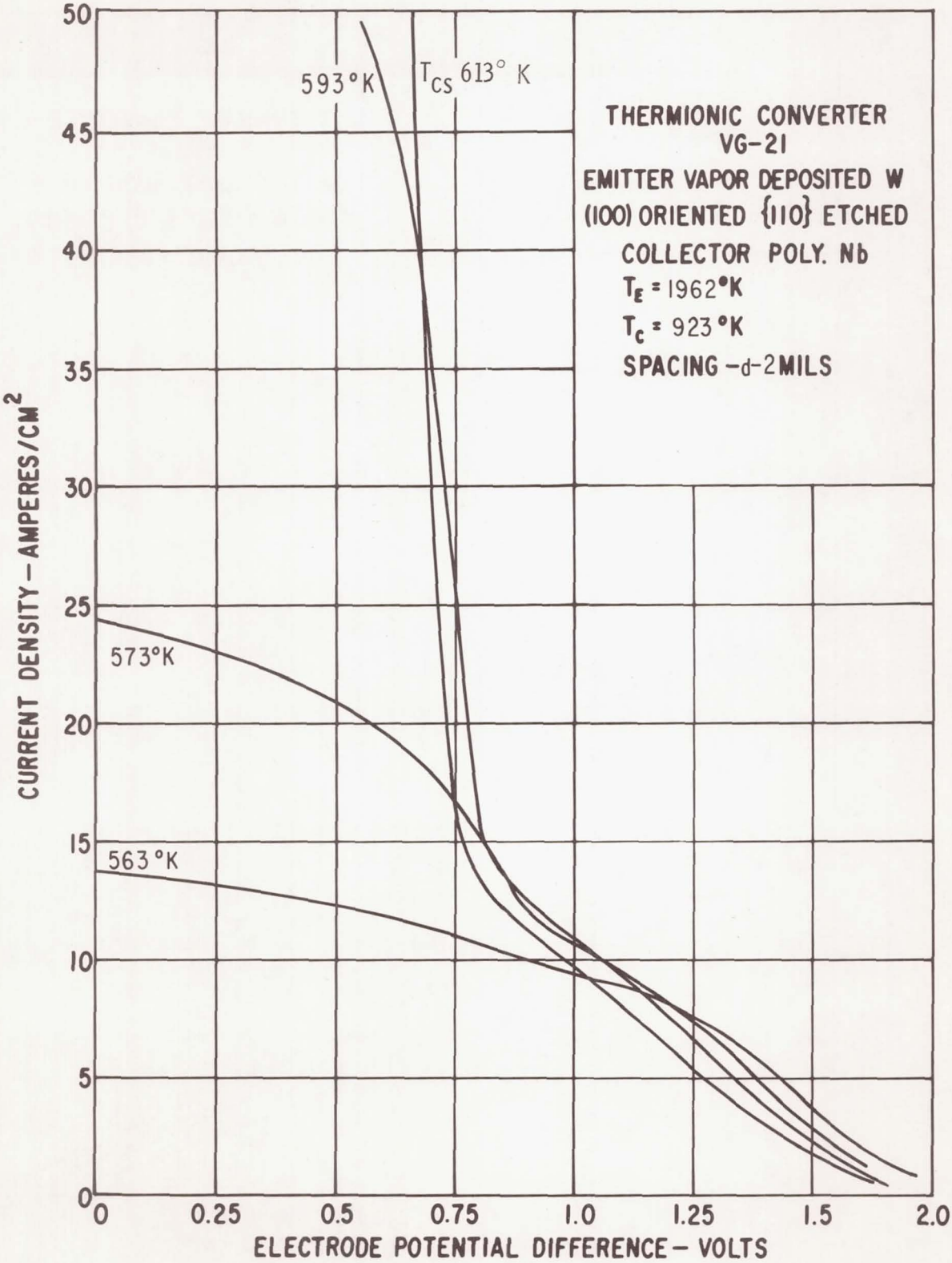

Figure 49. - Load lines for $T_E = 1962^O$ K, $T_C = 923^O$ K, and spacing d = 2 mils.

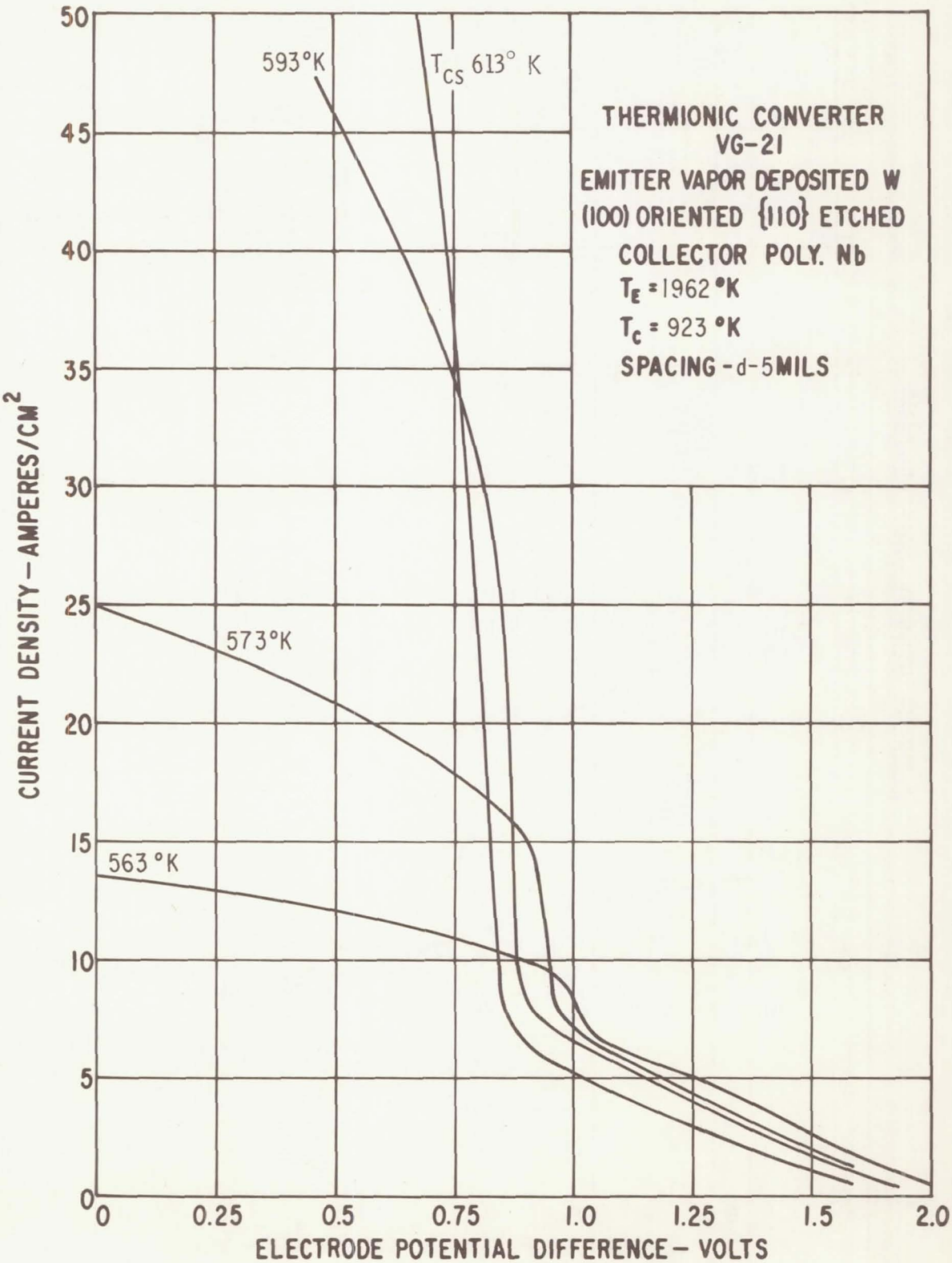

Figure 50. - Load lines for $T_E = 1962^O$ K, $T_C = 923^O$ K, and spacing d = 5 mils.

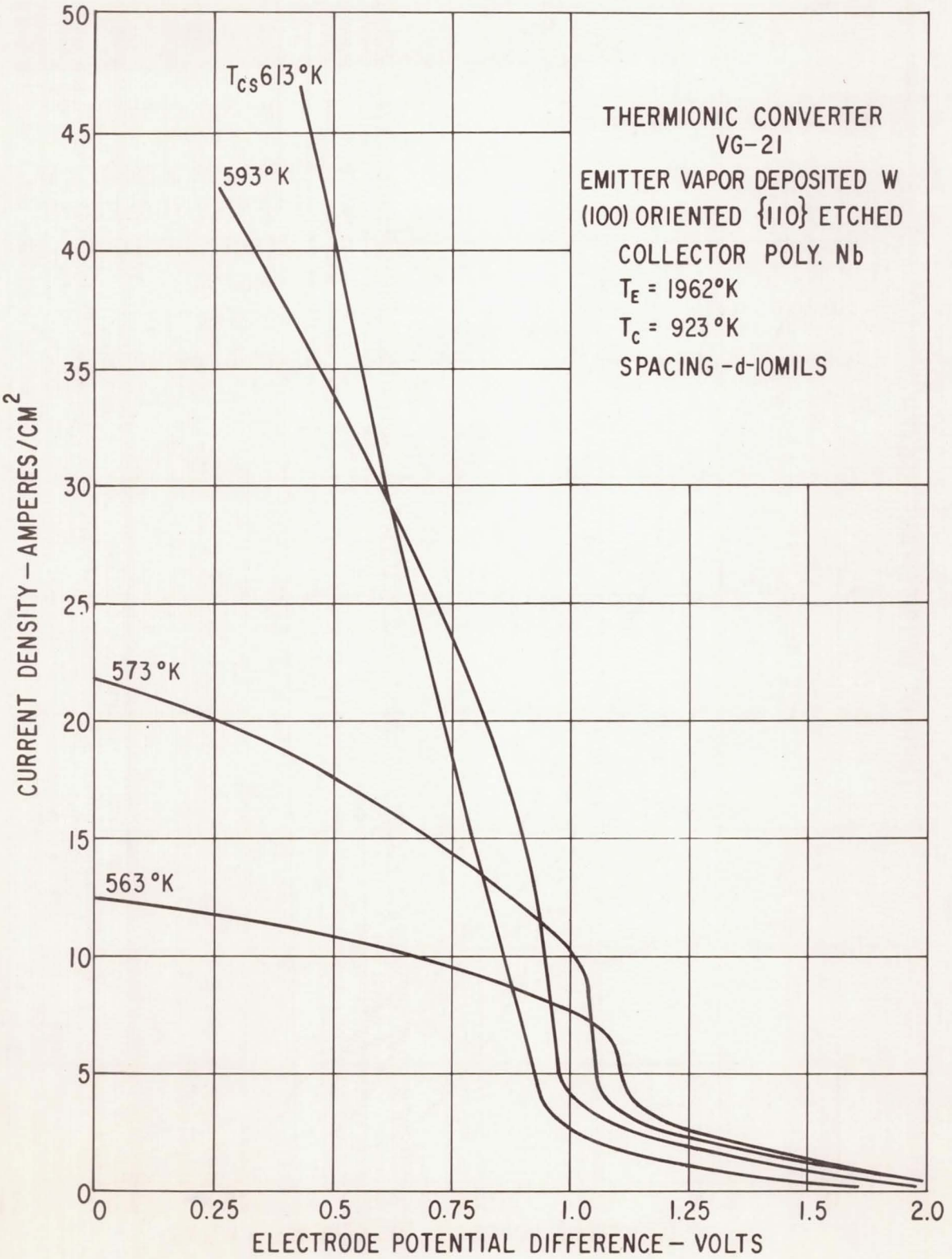

Figure 51. - Load lines for $T_E = 1962^O$ K, $T_C = 923^O$ K, and spacing d = 10 mils.

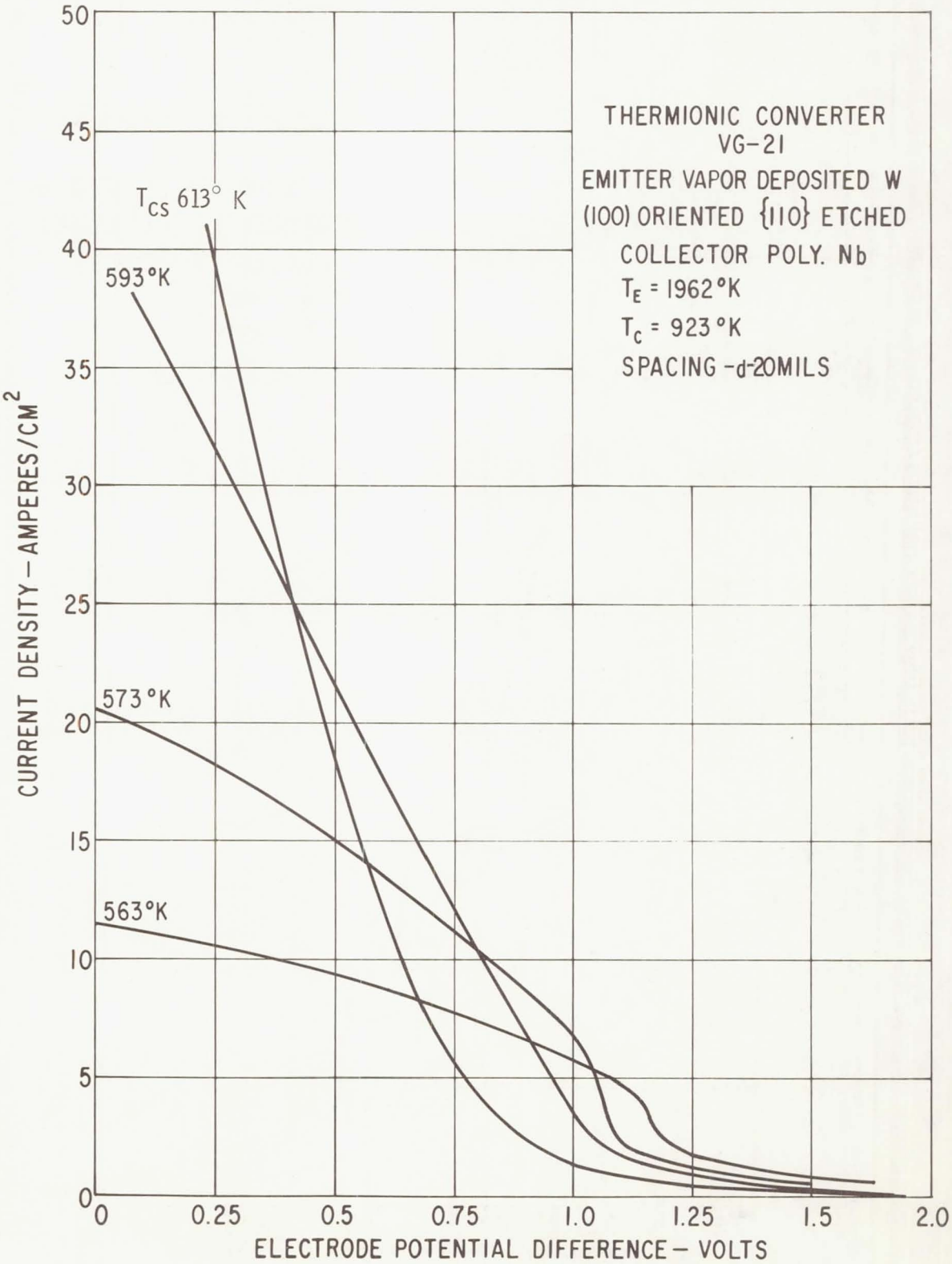

Figure 52. - Load lines for $T_E = 1962^{\circ}$ K, $T_C = 923^{\circ}$ K, and spacing d = 20 mils.

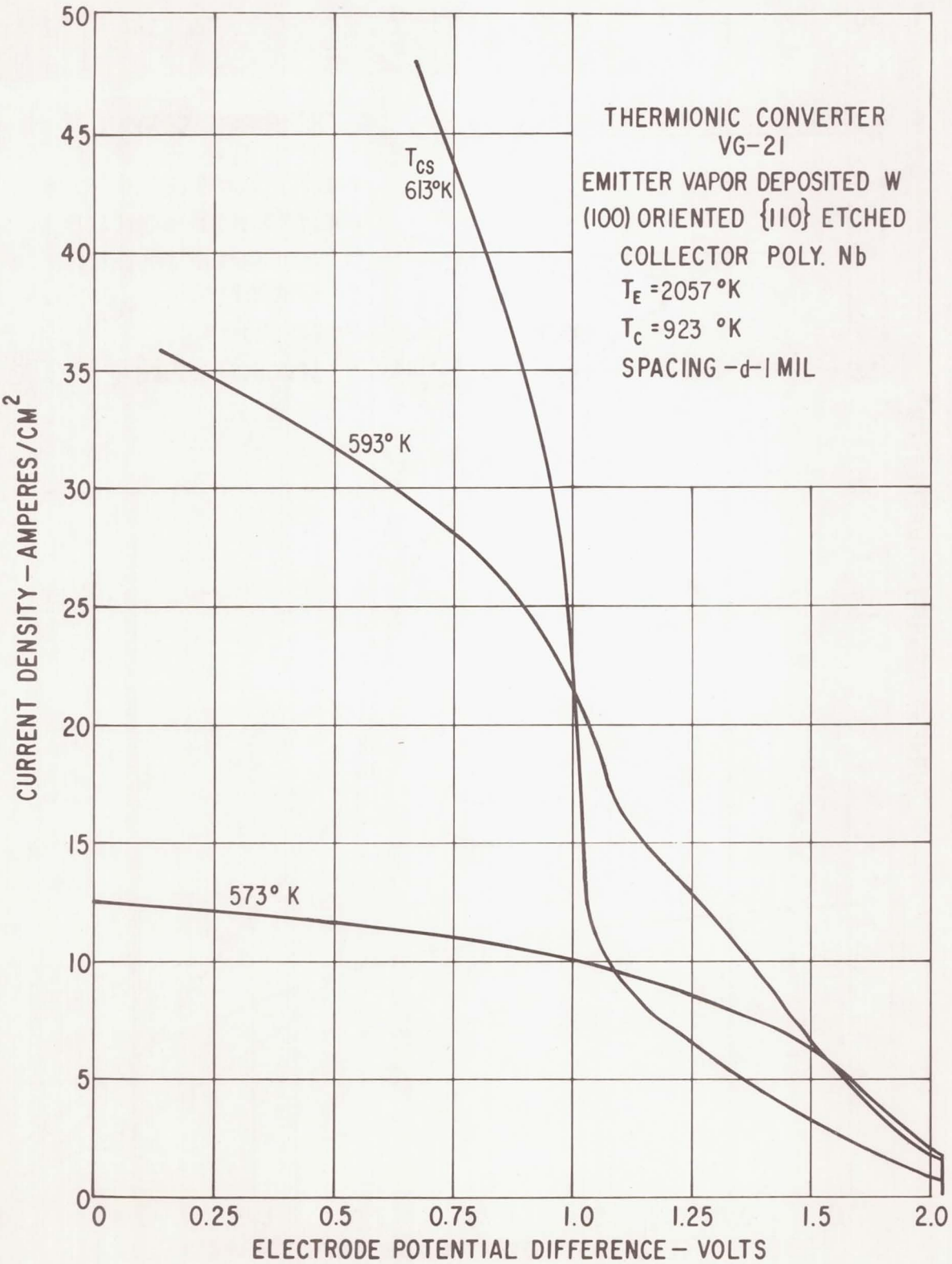

Figure 53. - Load lines for $T_E = 2057^O$ K, $T_C = 923^O$ K, and spacing d = 1 mil.

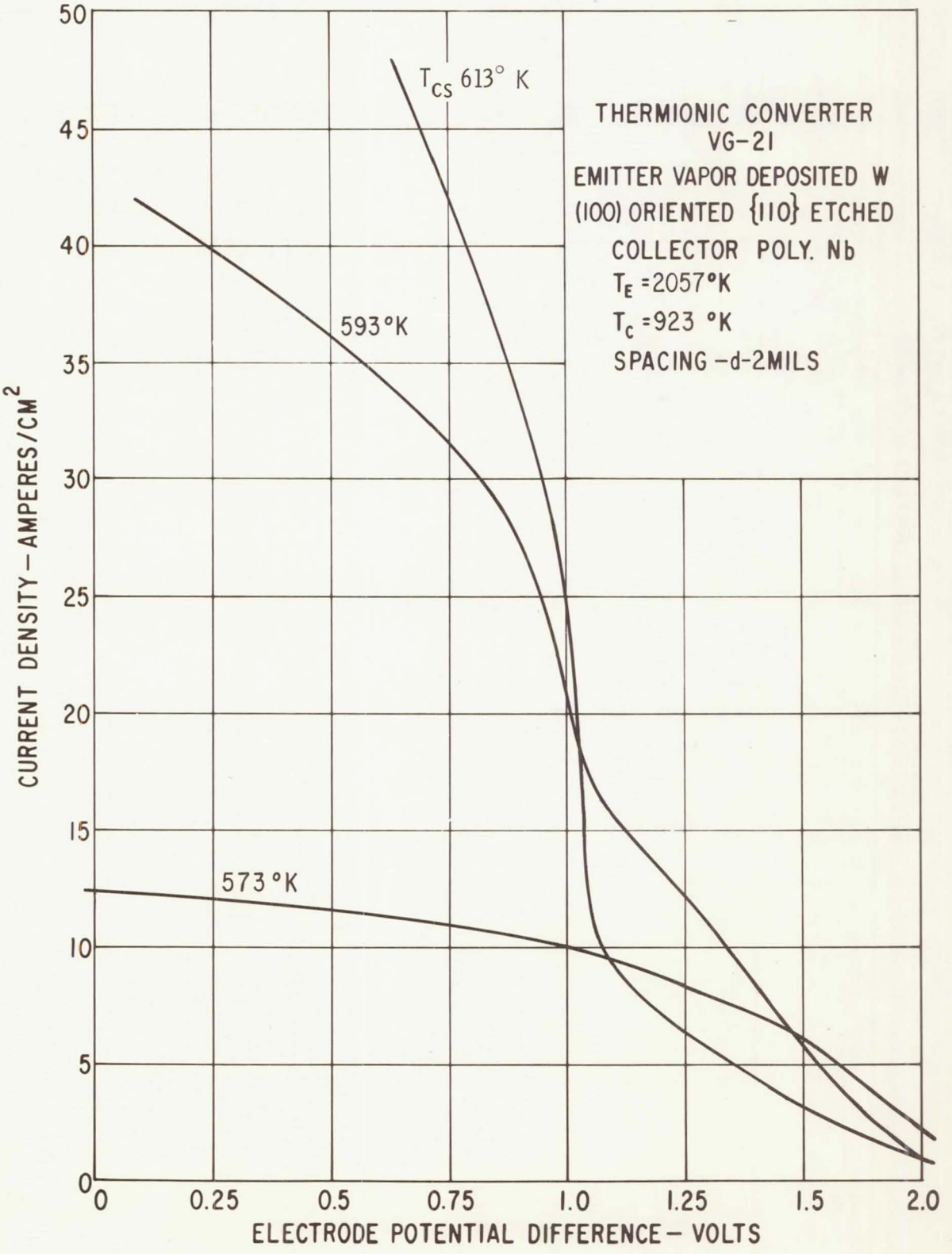

Figure 54. - Load lines for $T_E = 2057^O$ K, $T_C = 923^O$ K, and spacing d = 2 mils.

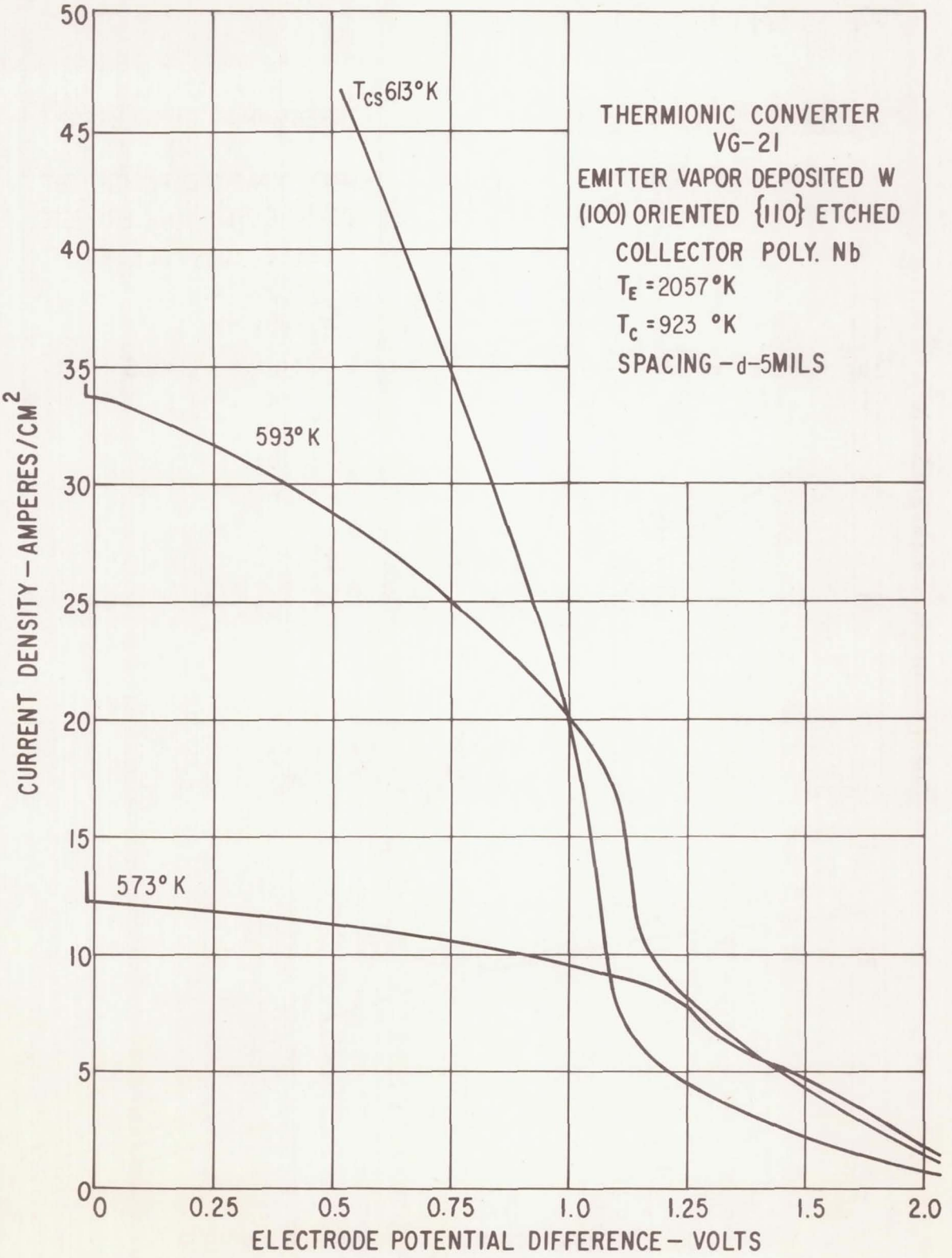

Figure 55. - Load lines for $T_E = 2057^O$ K, $T_C = 923^O$ K, and spacing d = 5 mils.

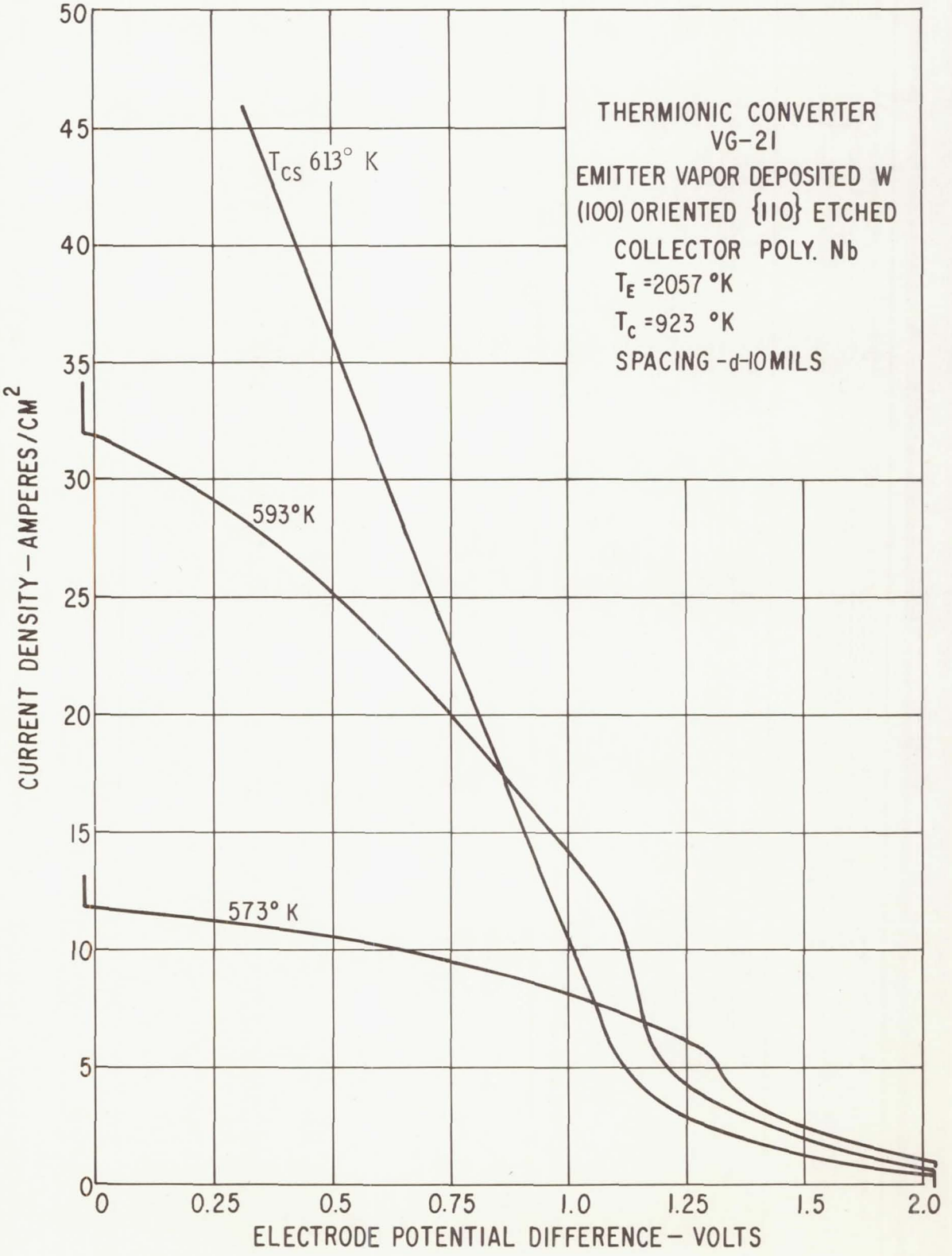

Figure 56. - Load lines for $T_E = 2057^O$ K, $T_C = 923^O$ K, and spacing d = 10 mils.

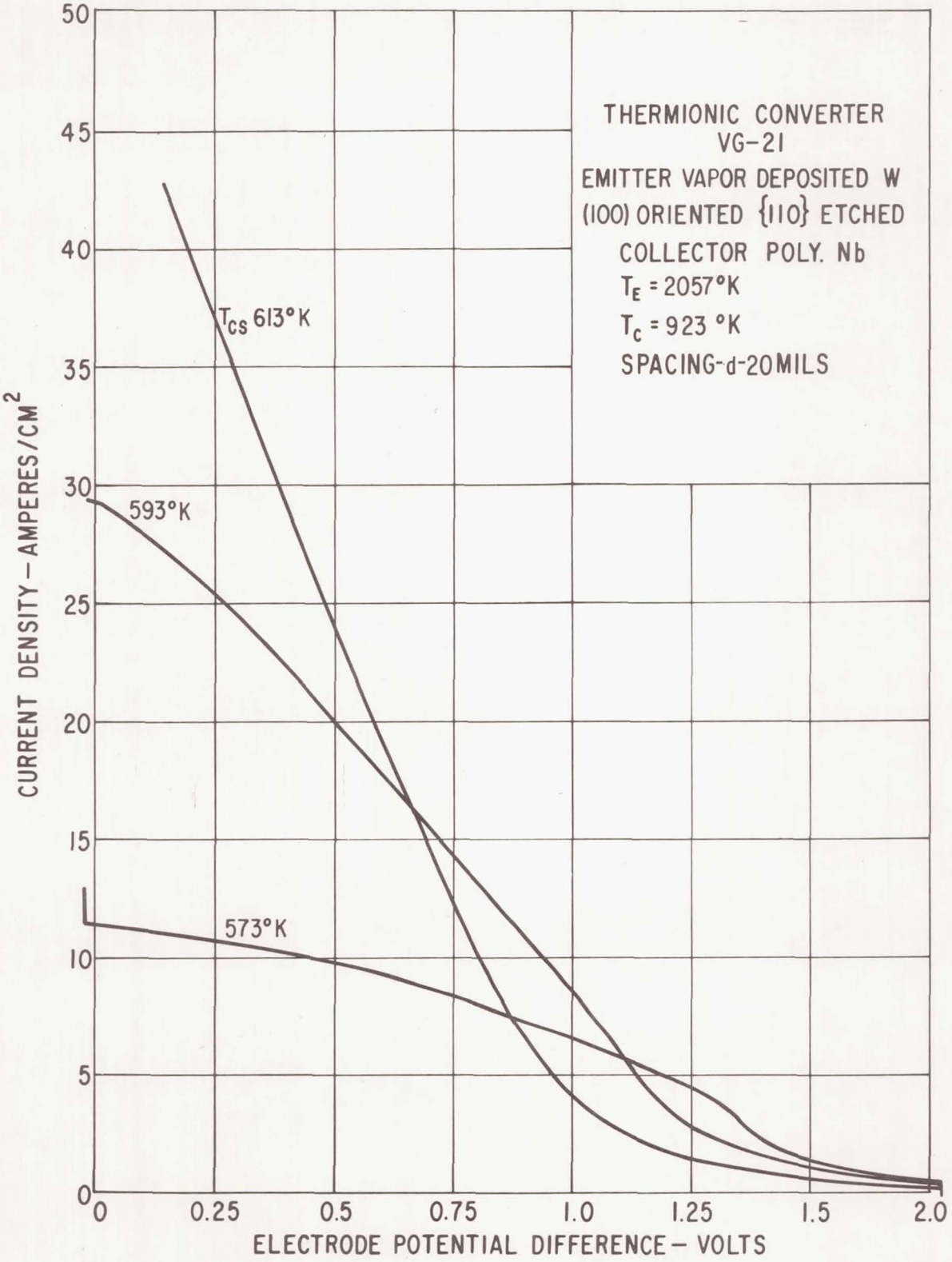

Figure 57. - Load lines for $T_E = 2057^O$ K, $T_C = 923^O$ K, and spacing d = 20 mils.

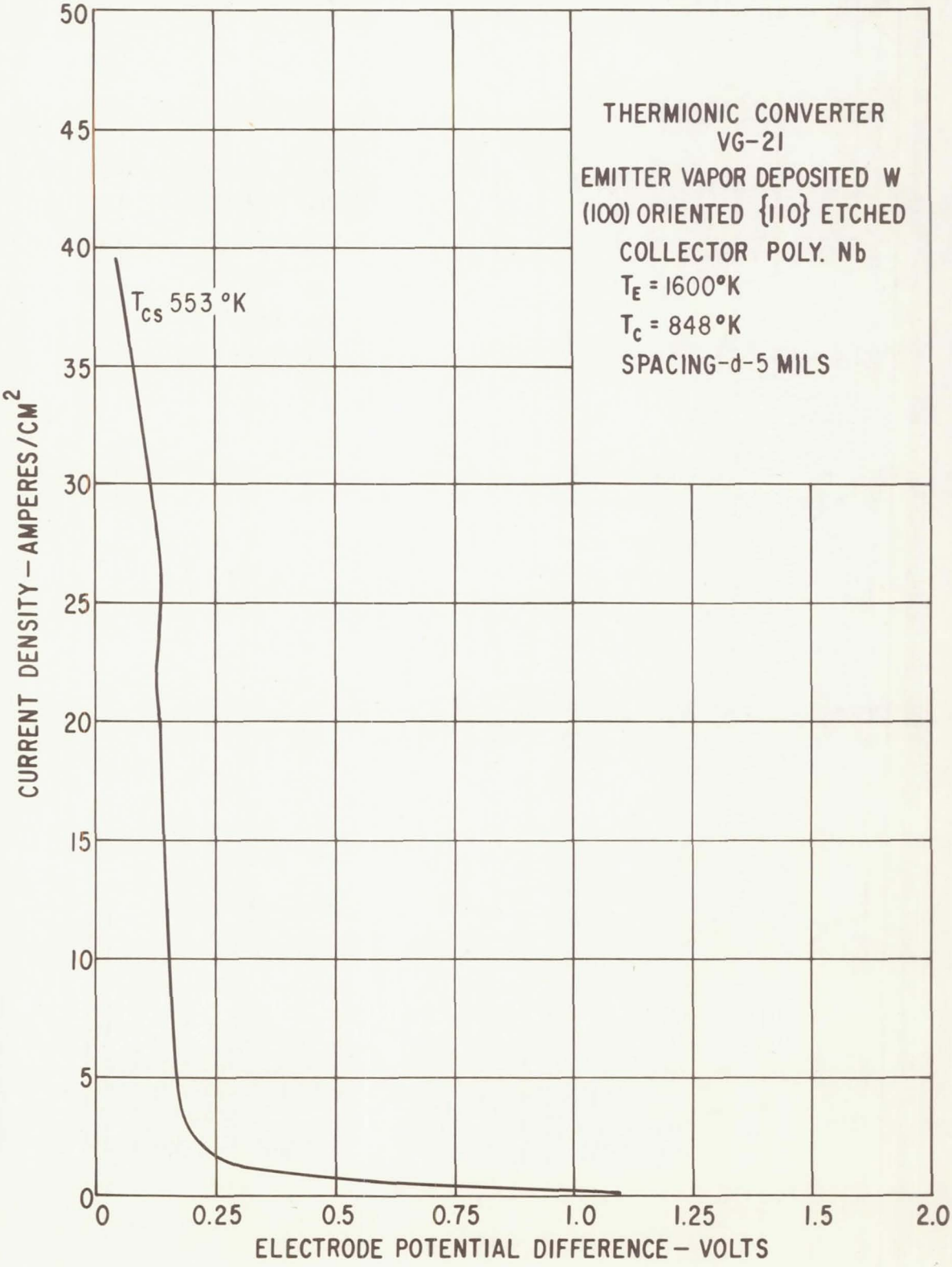

Figure 58. - Load lines for $T_E = 1600^O$ K, $T_C = 848^O$ K, and spacing d = 5 mils.

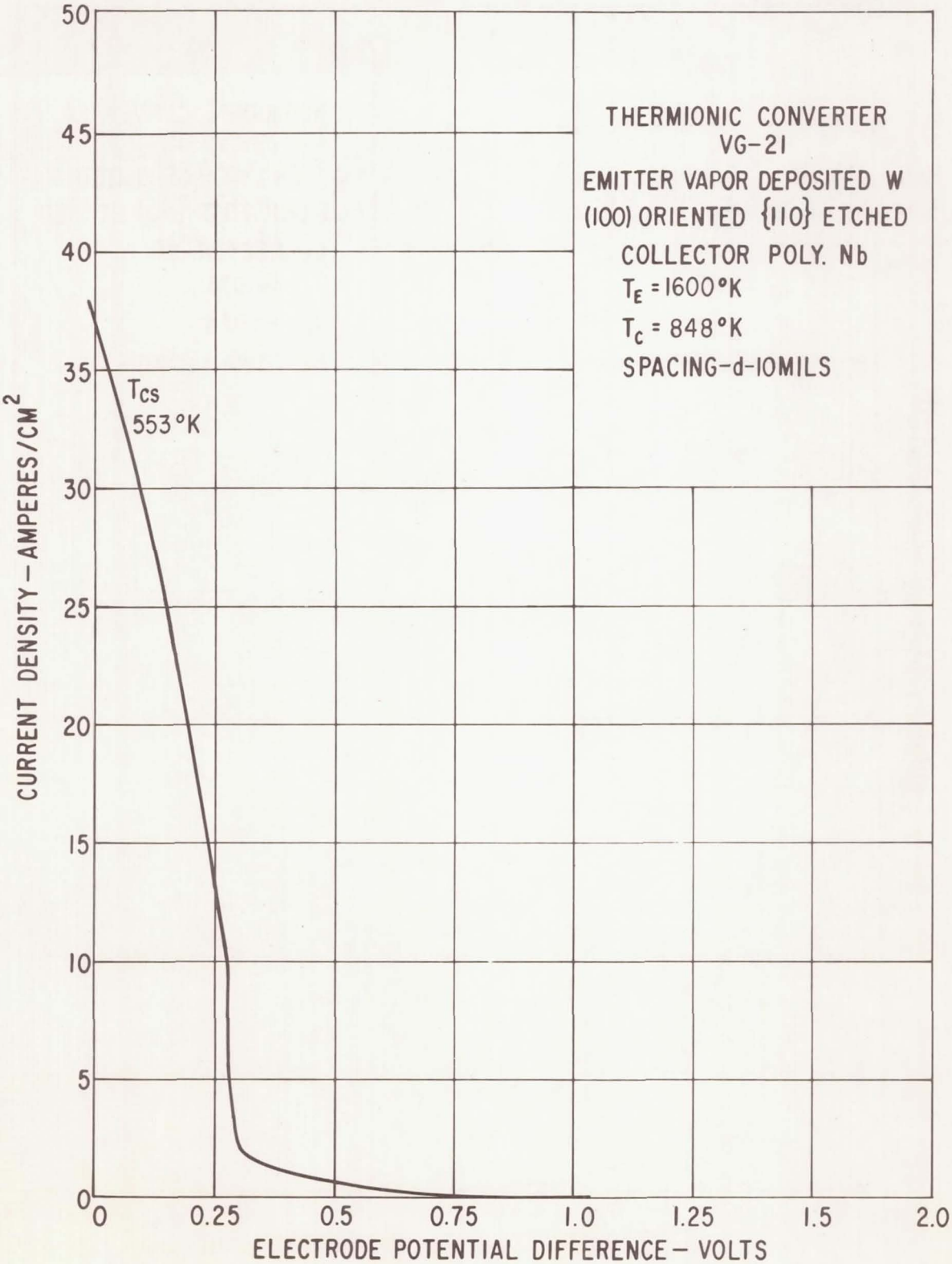

Figure 59. - Load lines for $T_E = 1600^O$ K, $T_C = 848^O$ K, and spacing d = 10 mils.

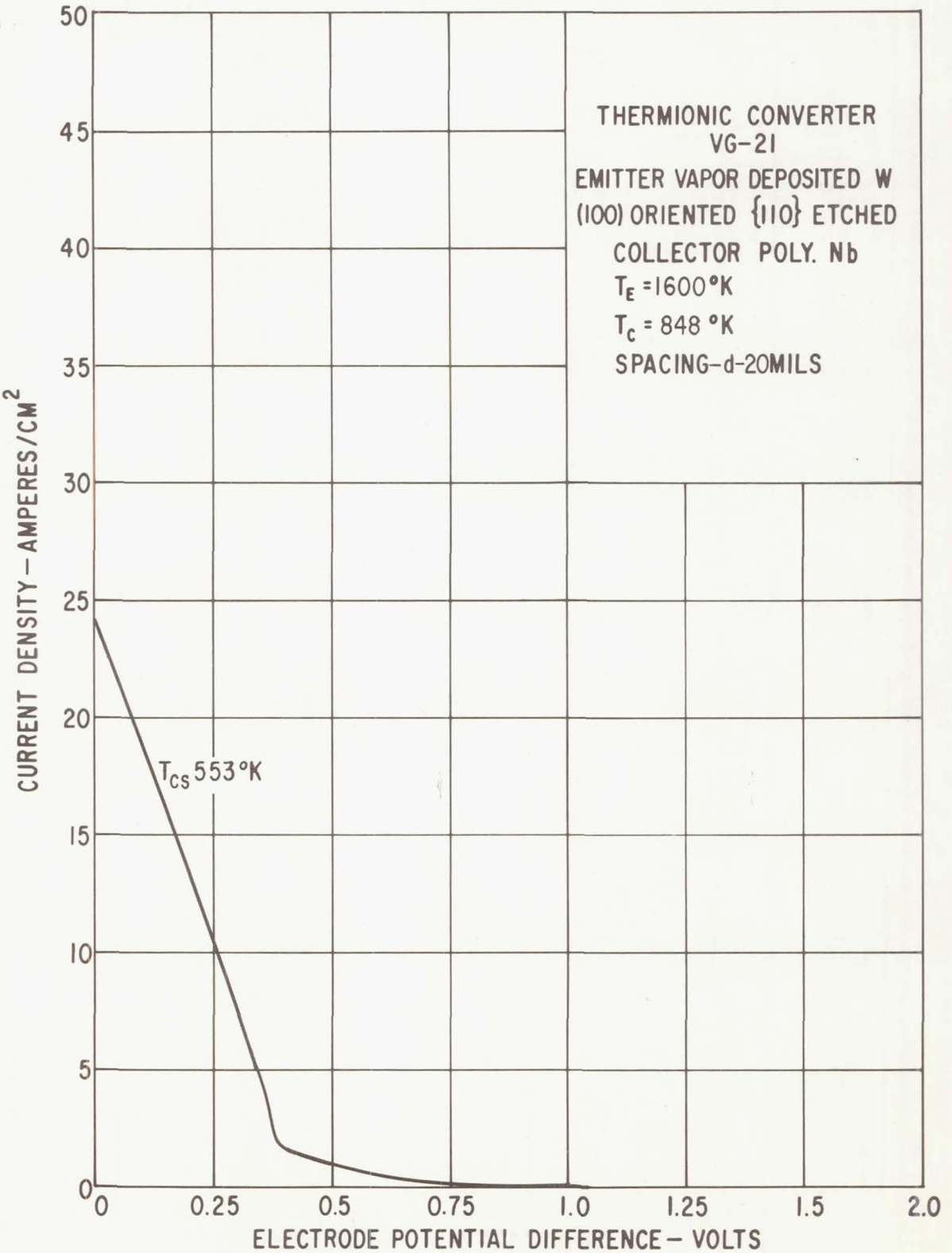

Figure 60. - Load lines for $T_E = 1600^O$ K, $T_C = 848^O$ K, and spacing d = 20 mils.

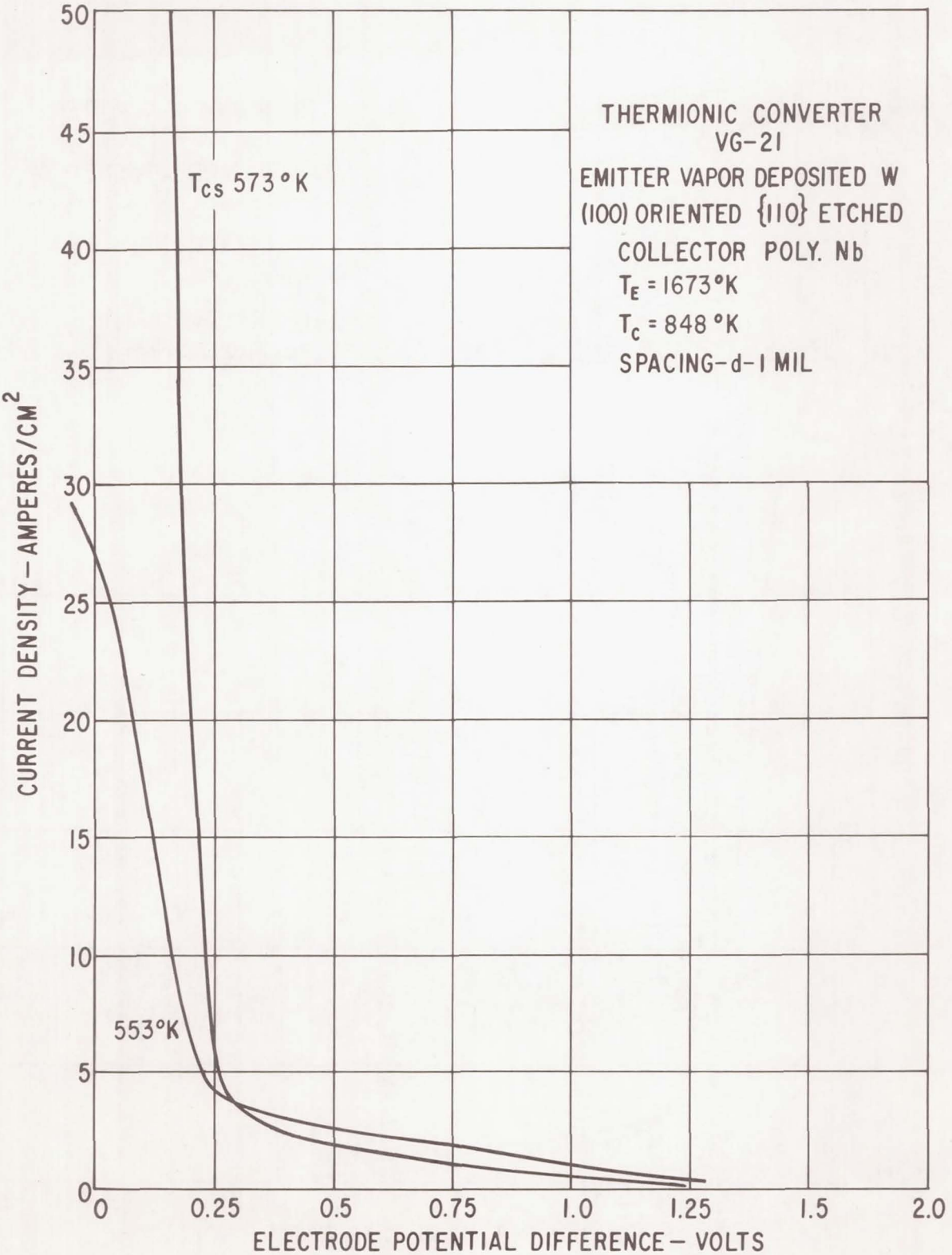

Figure 61. - Load lines for $T_E = 1673^O$ K, $T_C = 848^O$ K, and spacing d = 1 mil.

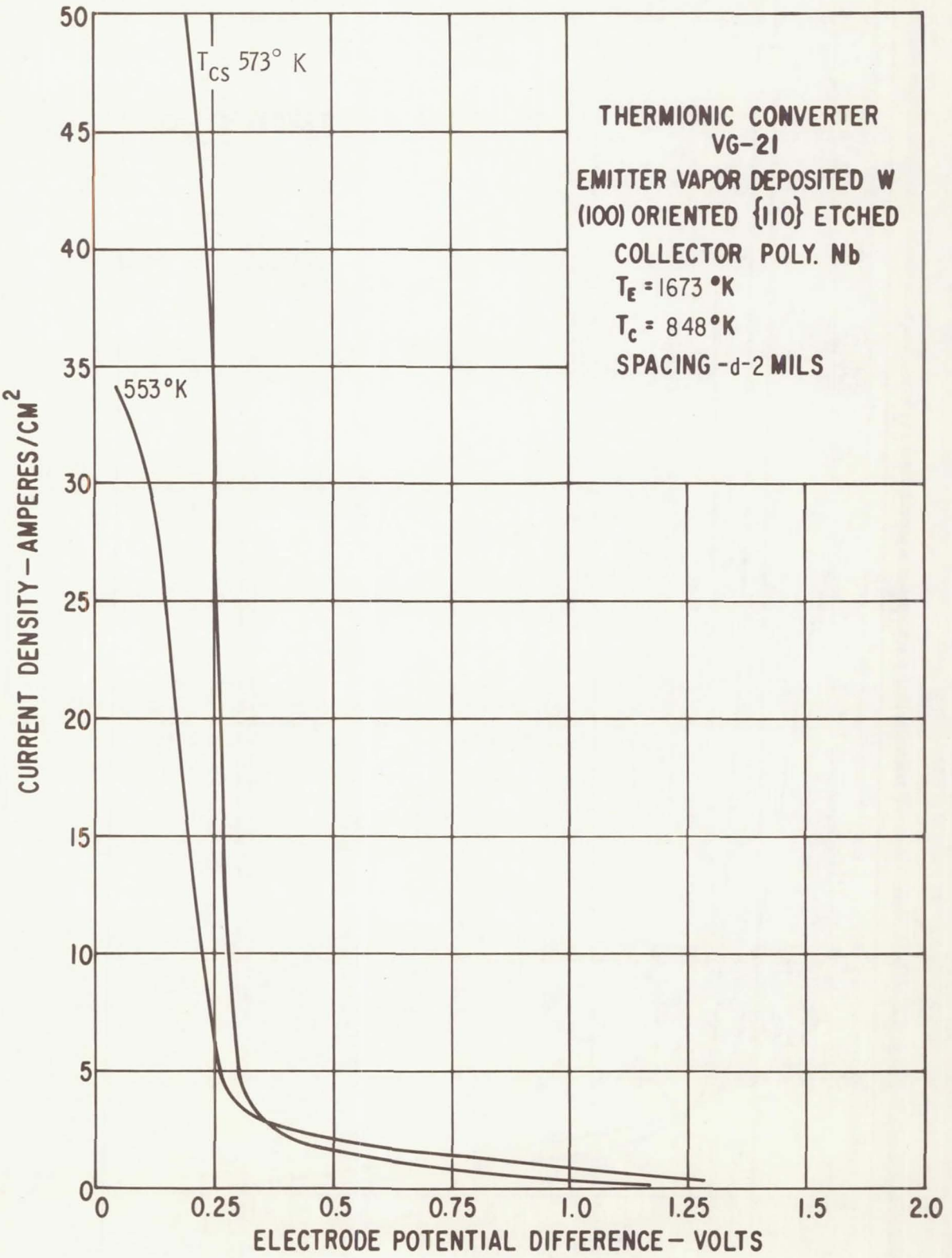

Figure 62. - Load lines for $T_E = 1673^O$ K, $T_C = 848^O$ K, and spacing d = 2 mils.

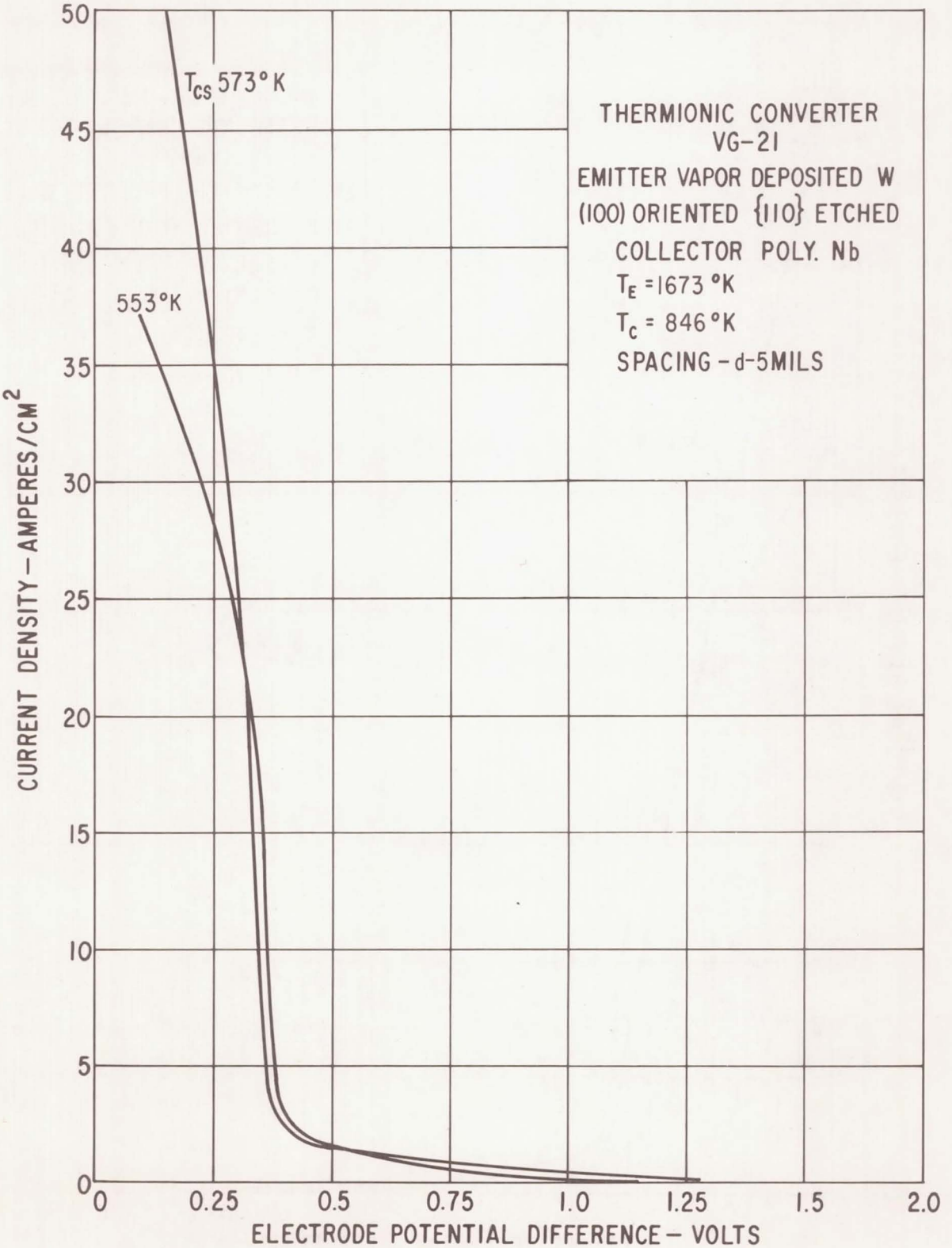

Figure 63. - Load lines for $T_E = 1673^O$ K, $T_C = 846^O$ K, and spacing d = 5 mils.

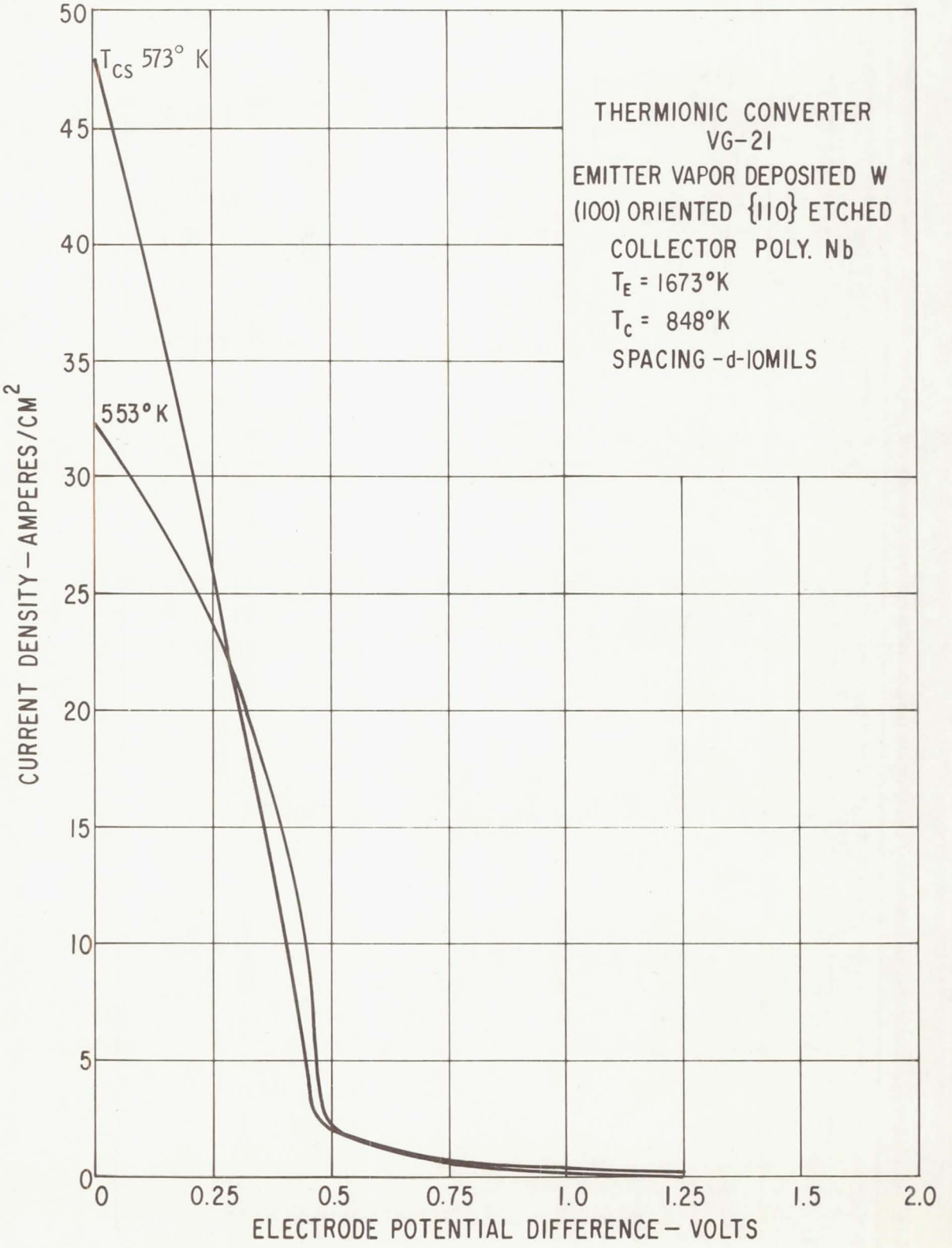

Figure 64. - Load lines for $T_E = 1673^O$ K, $T_C = 848^O$ K, and spacing d = 10 mils.

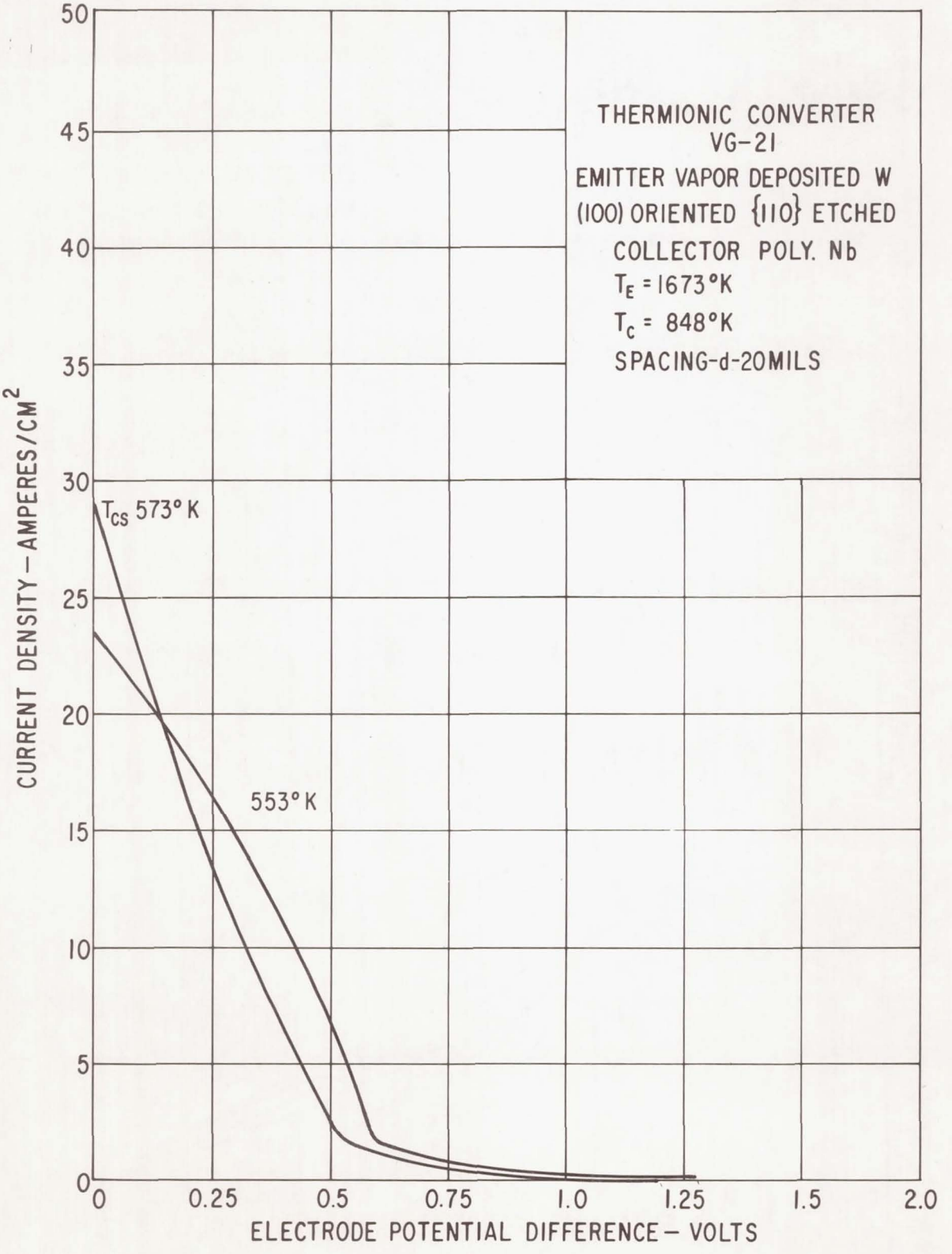

Figure 65. - Load lines for $T_E = 1673^O$ K, $T_C = 848^O$ K, and spacing d = 20 mils.

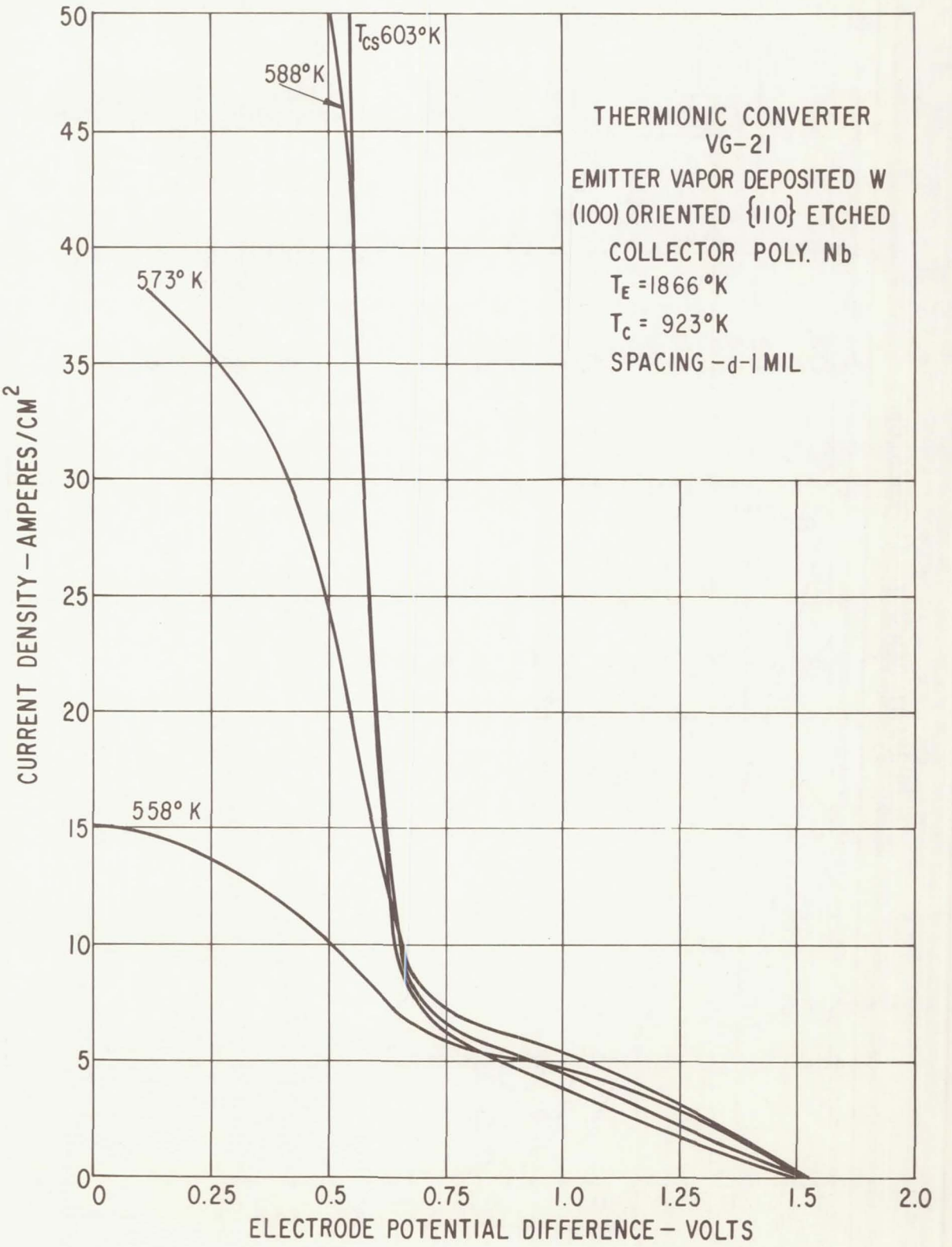

Figure 66. - Load lines for $T_E = 1866^O$ K, $T_C = 923^O$ K, and spacing d = 1 mil.

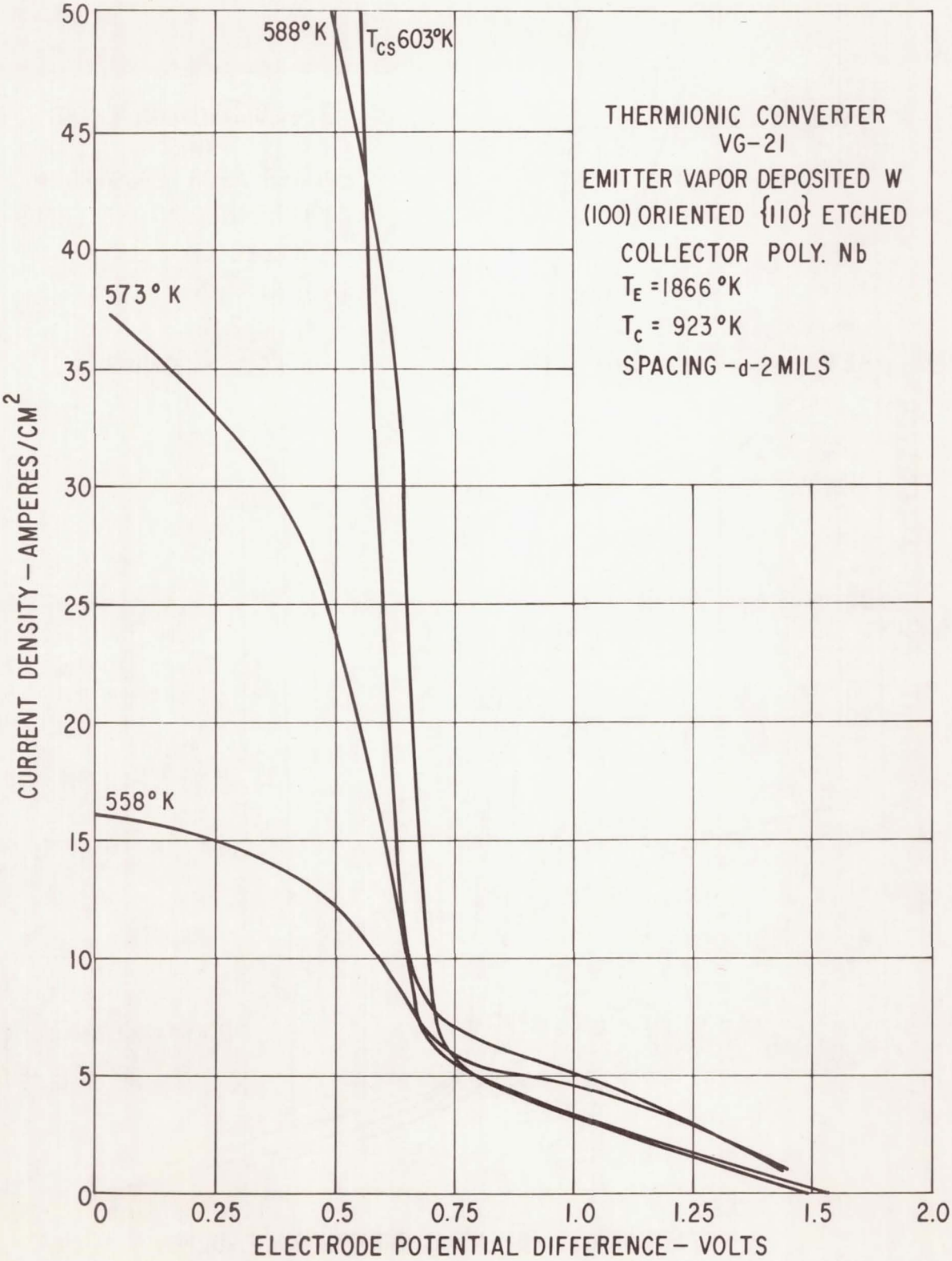

Figure 67. - Load lines for $T_E = 1866^O$ K, $T_C = 923^O$ K, and spacing d = 2 mils.

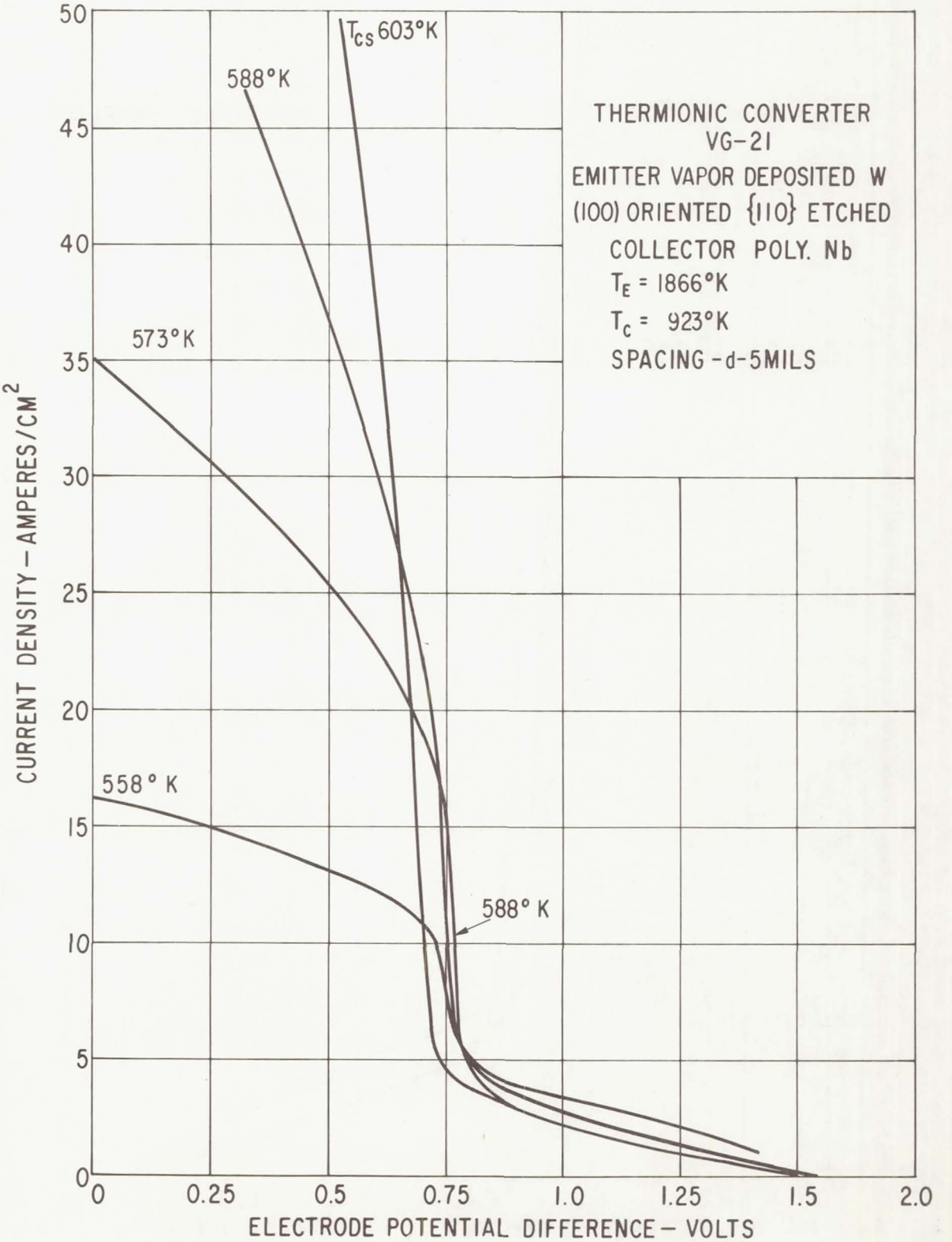

Figure 68. - Load lines for $T_E = 1866^O$ K, $T_C = 923^O$ K, and spacing d = 5 mils.

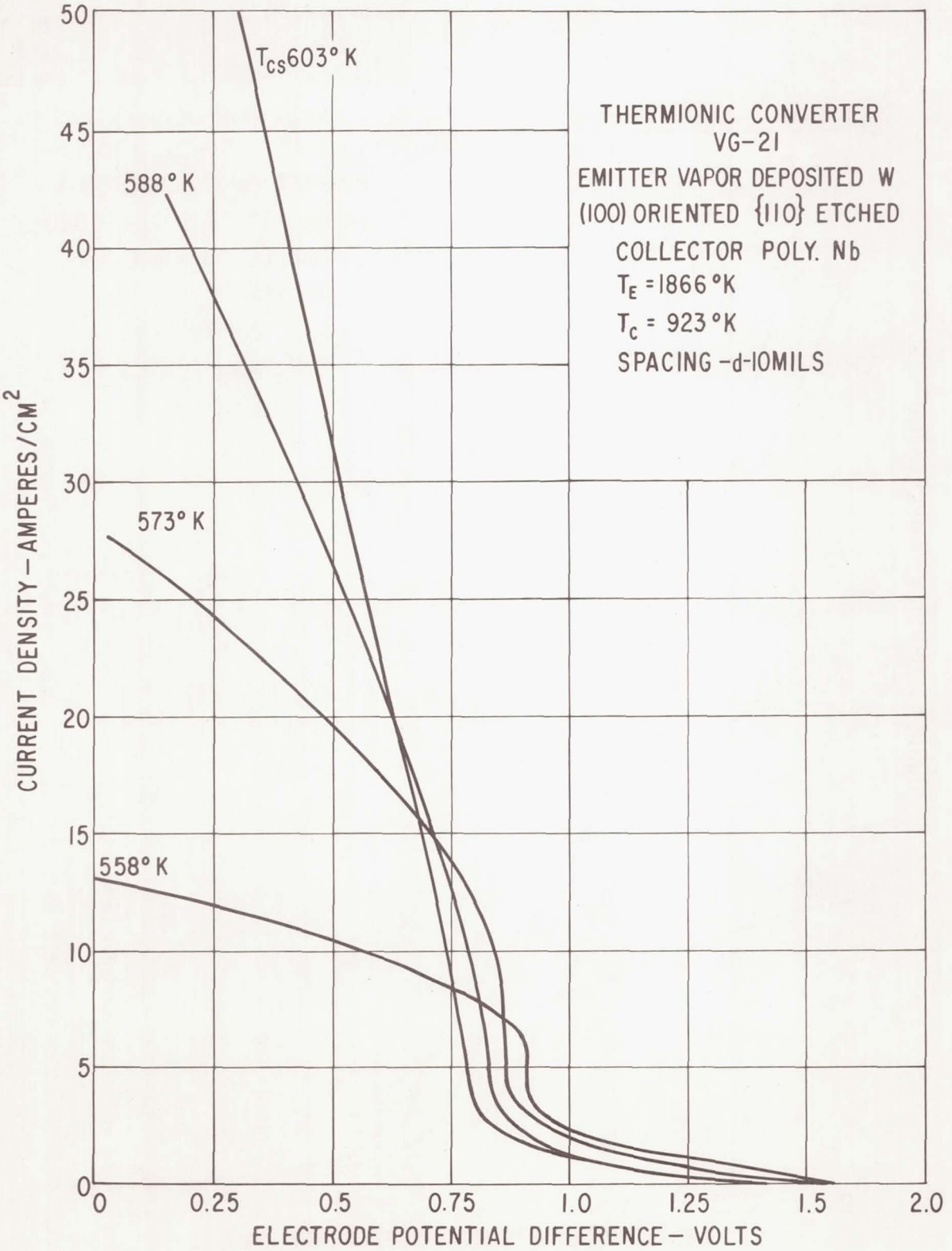

Figure 69. - Load lines for $T_E = 1866^O$ K, $T_C = 923^O$ K, and spacing d = 10 mils.

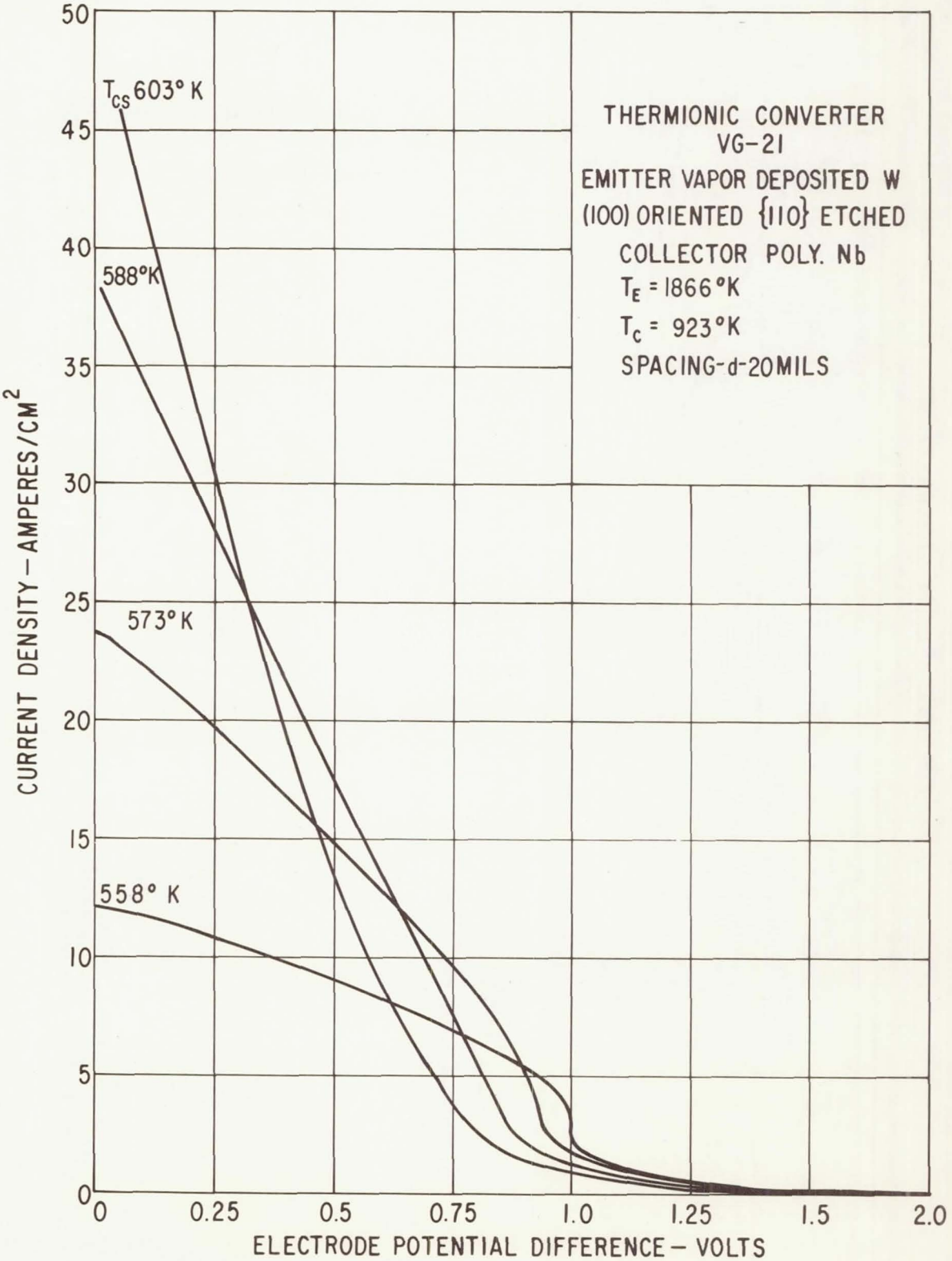

Figure 70. - Load lines for $T_E = 1866^O$ K, $T_C = 923^O$ K, and spacing d = 20 mils.

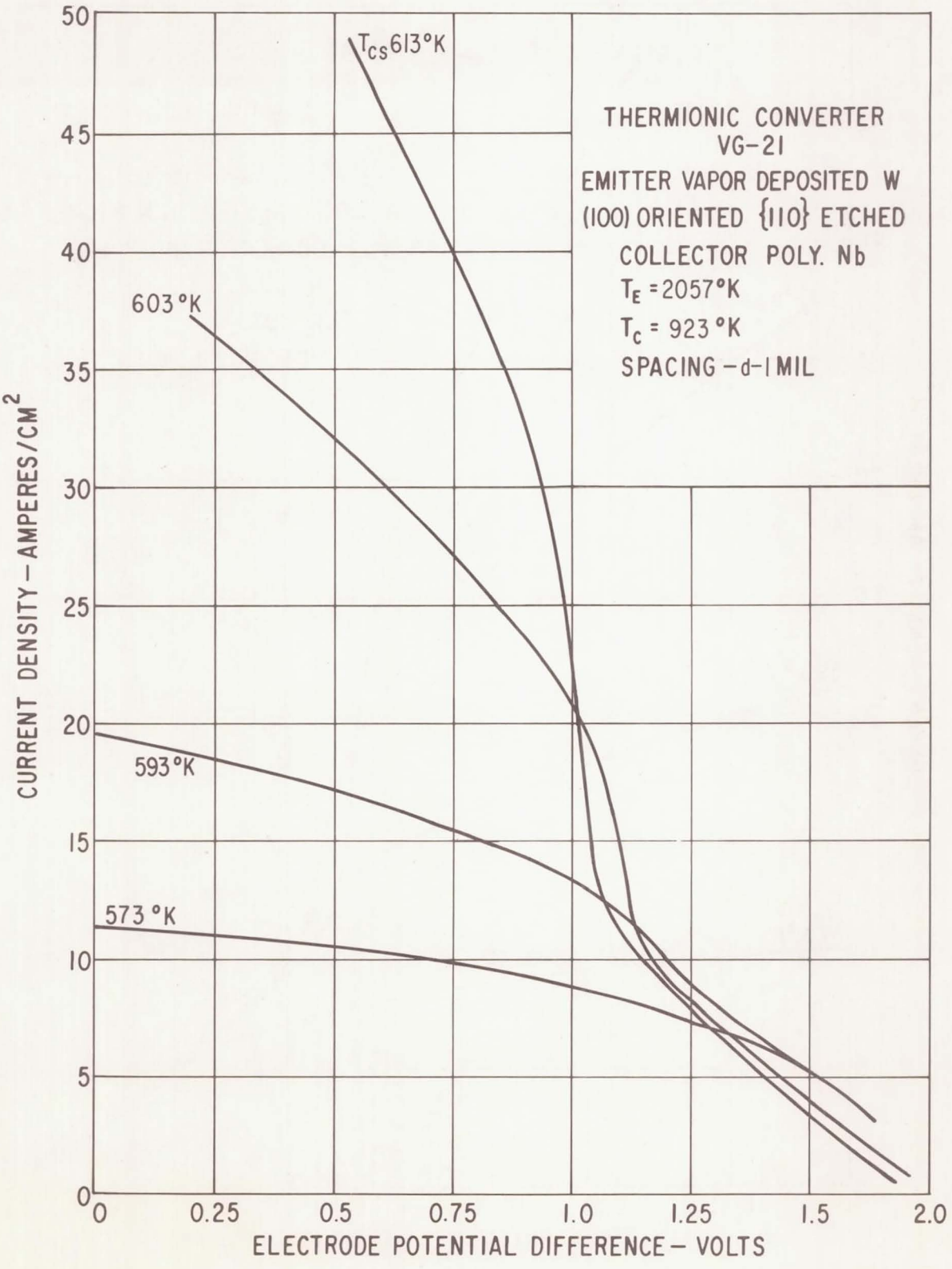

Figure 71. - Load lines for $T_E = 2057^O$ K, $T_C = 923^O$ K, and spacing d = 1 mil.

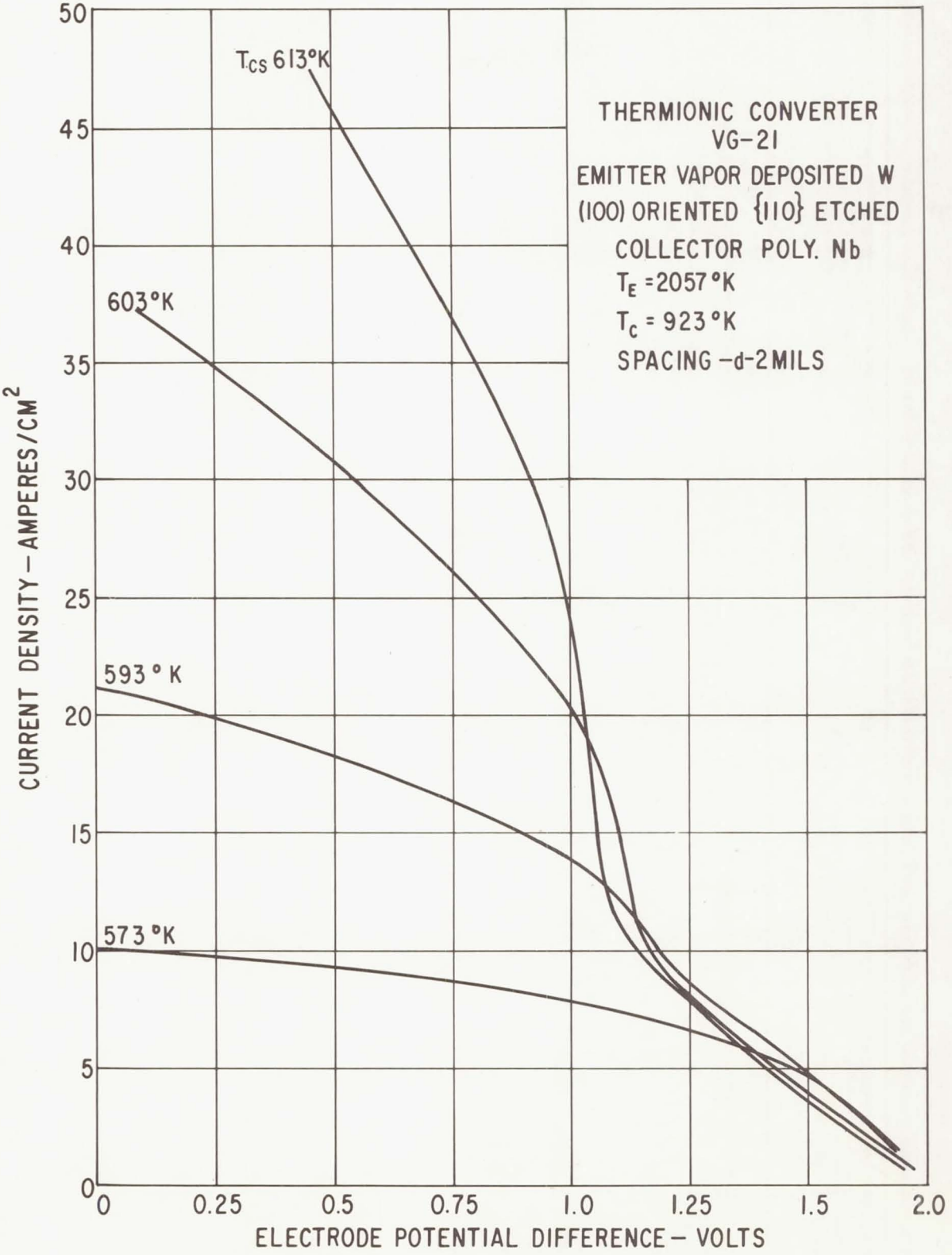

Figure 72. - Load lines for $T_E = 2057^O$ K, $T_C = 923^O$ K, and spacing d = 2 mils.

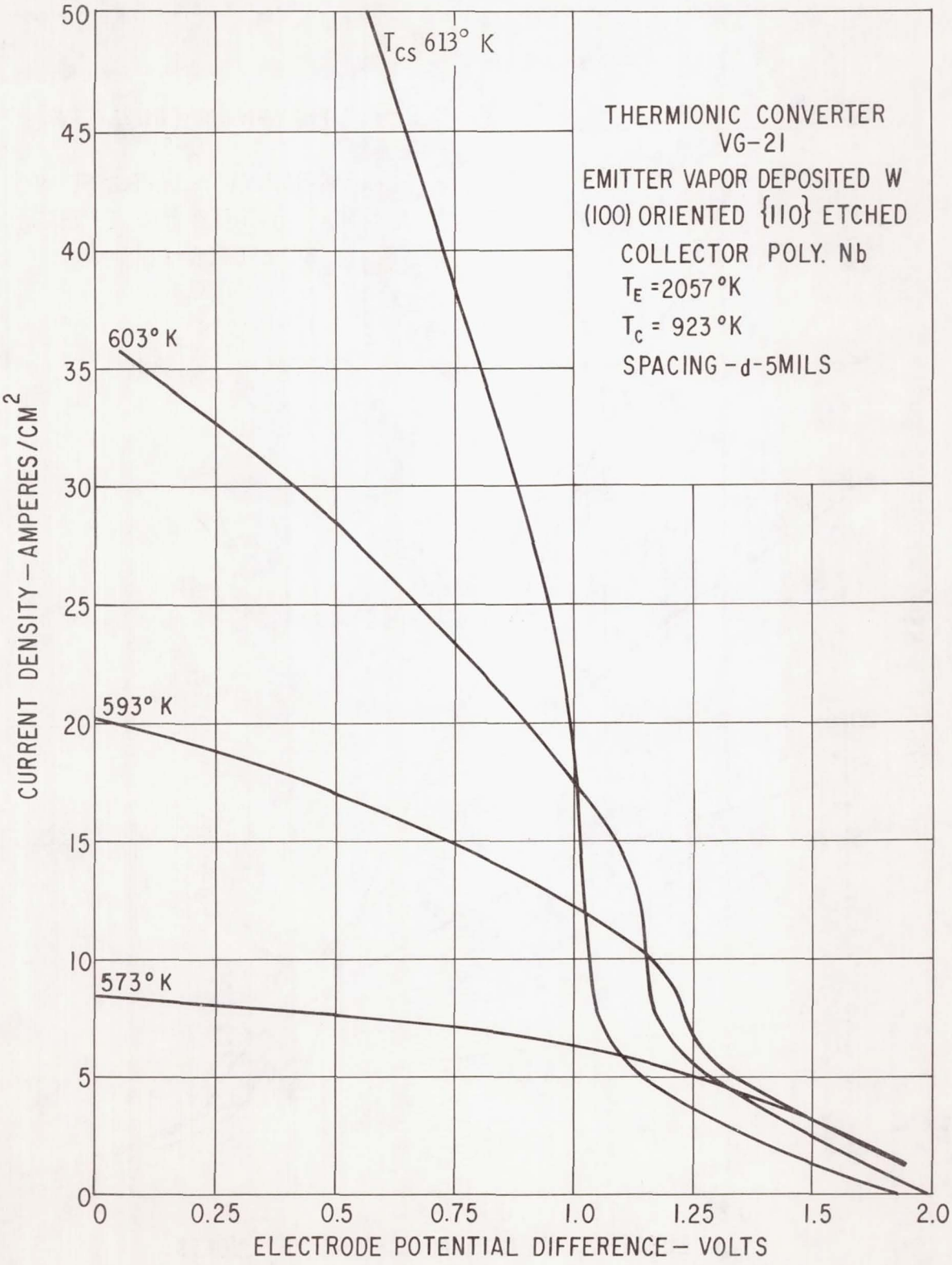

Figure 73. - Load lines for T_E = 2057° K, T_C = 923° K, and spacing d = 5 mils.

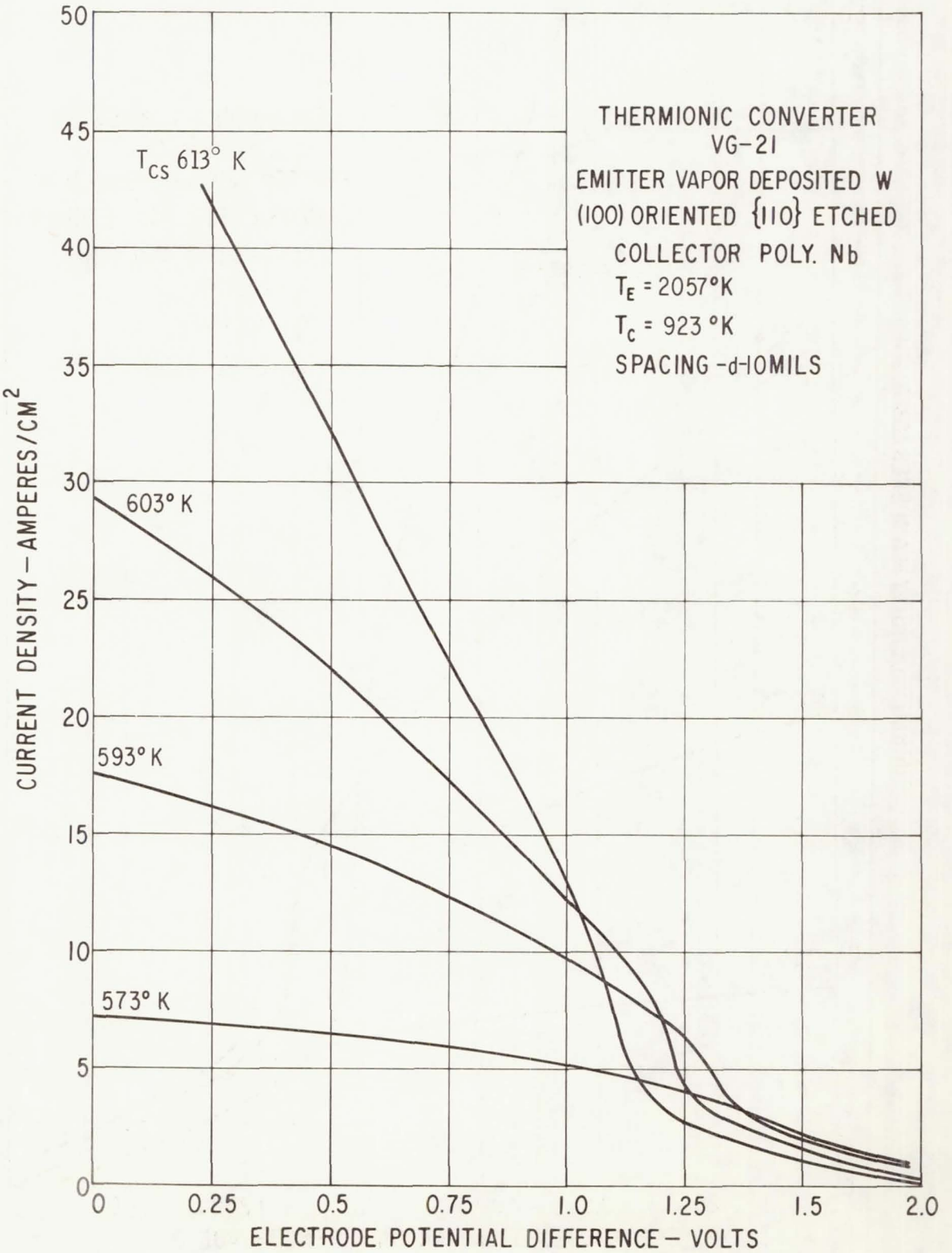

Figure 74. - Load lines for $T_E = 2057^O$ K, $T_C = 923^O$ K, and spacing d = 10 mils.

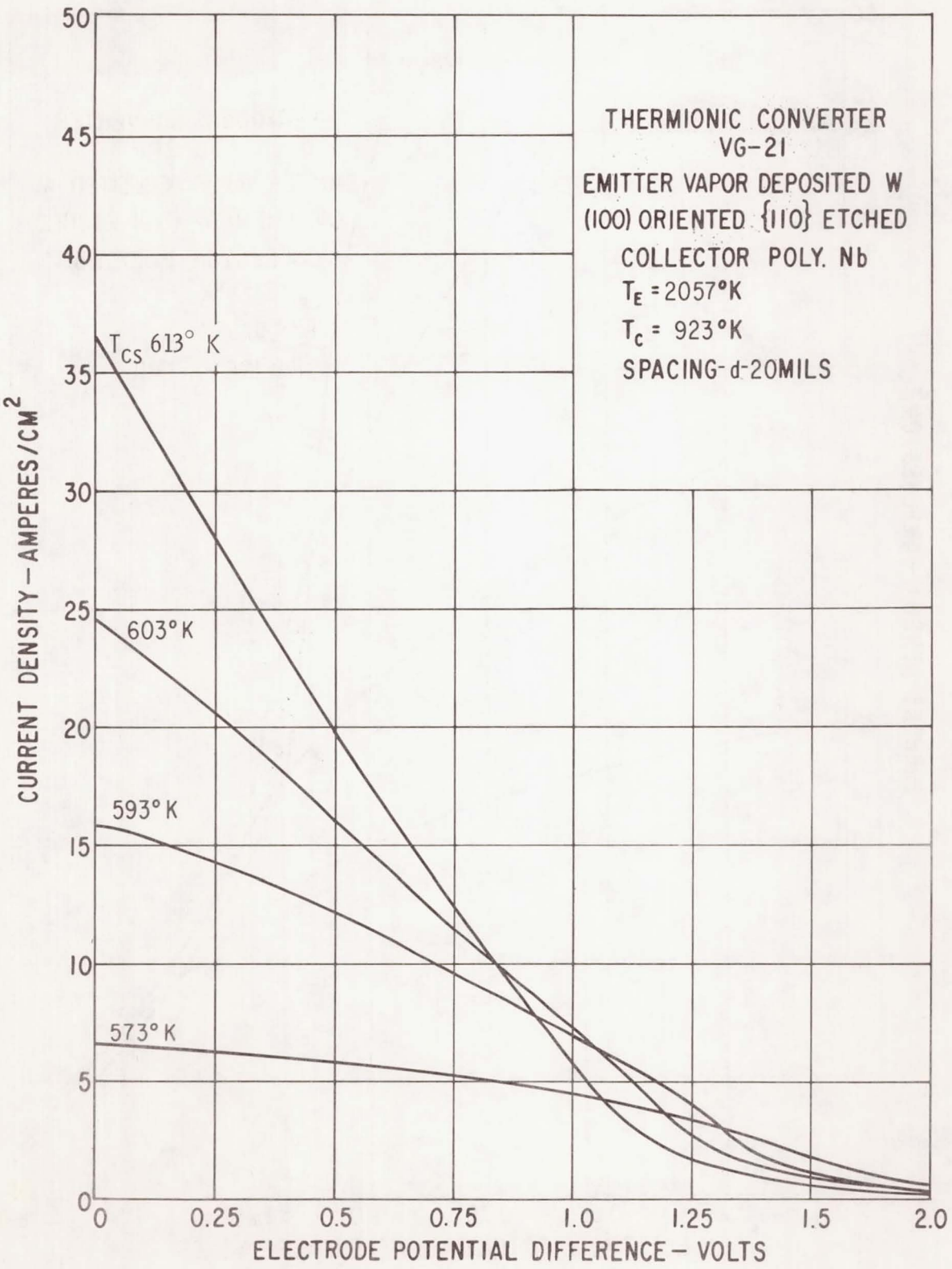

Figure 75. - Load lines for $T_E = 2057^O$ K, $T_C = 923^O$ K, and spacing d = 20 mils.

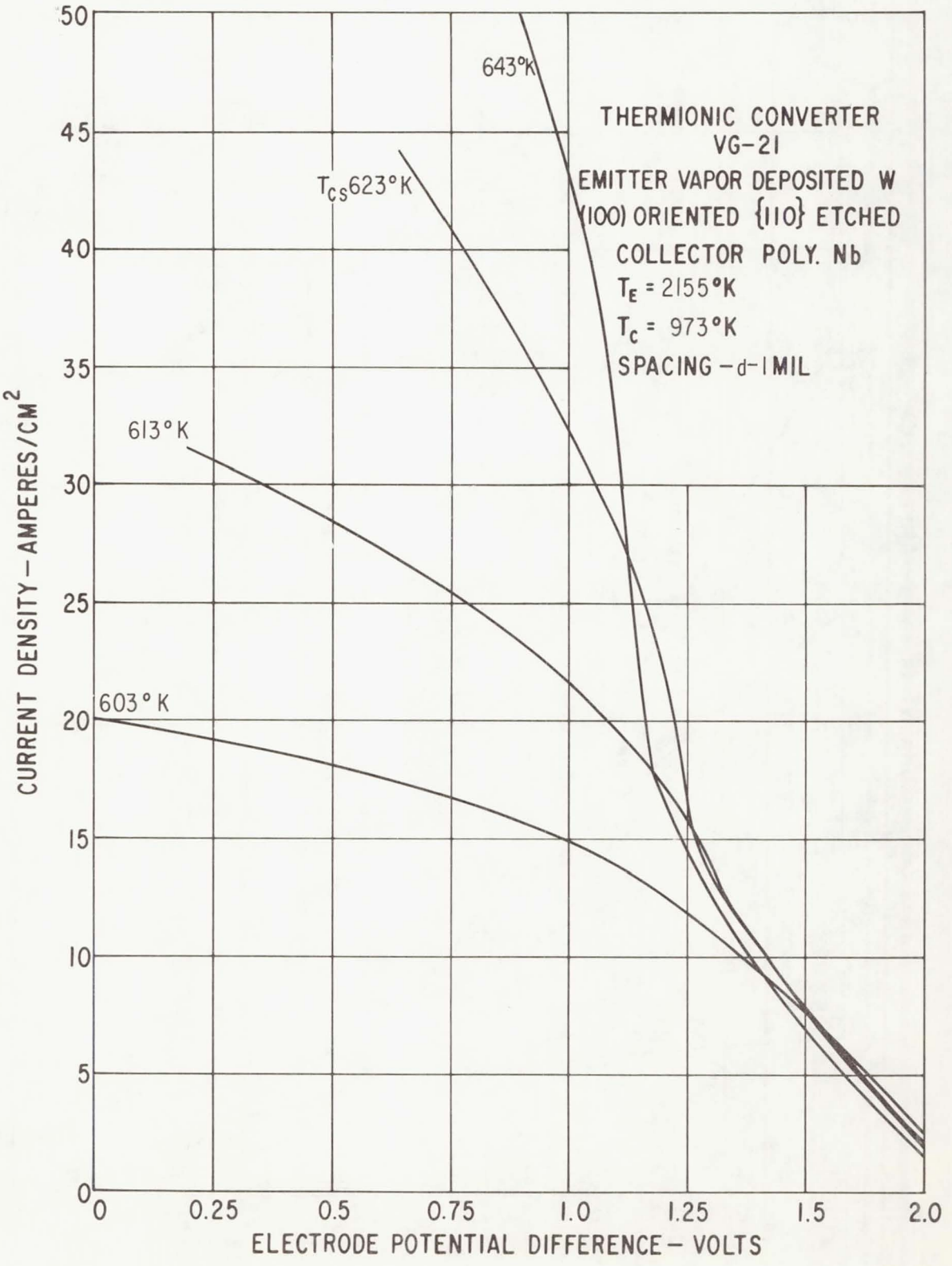

Figure 76. - Load lines for $T_E = 2155^{\circ}$ K, $T_C = 973^{\circ}$ K, and spacing d = 1 mil.

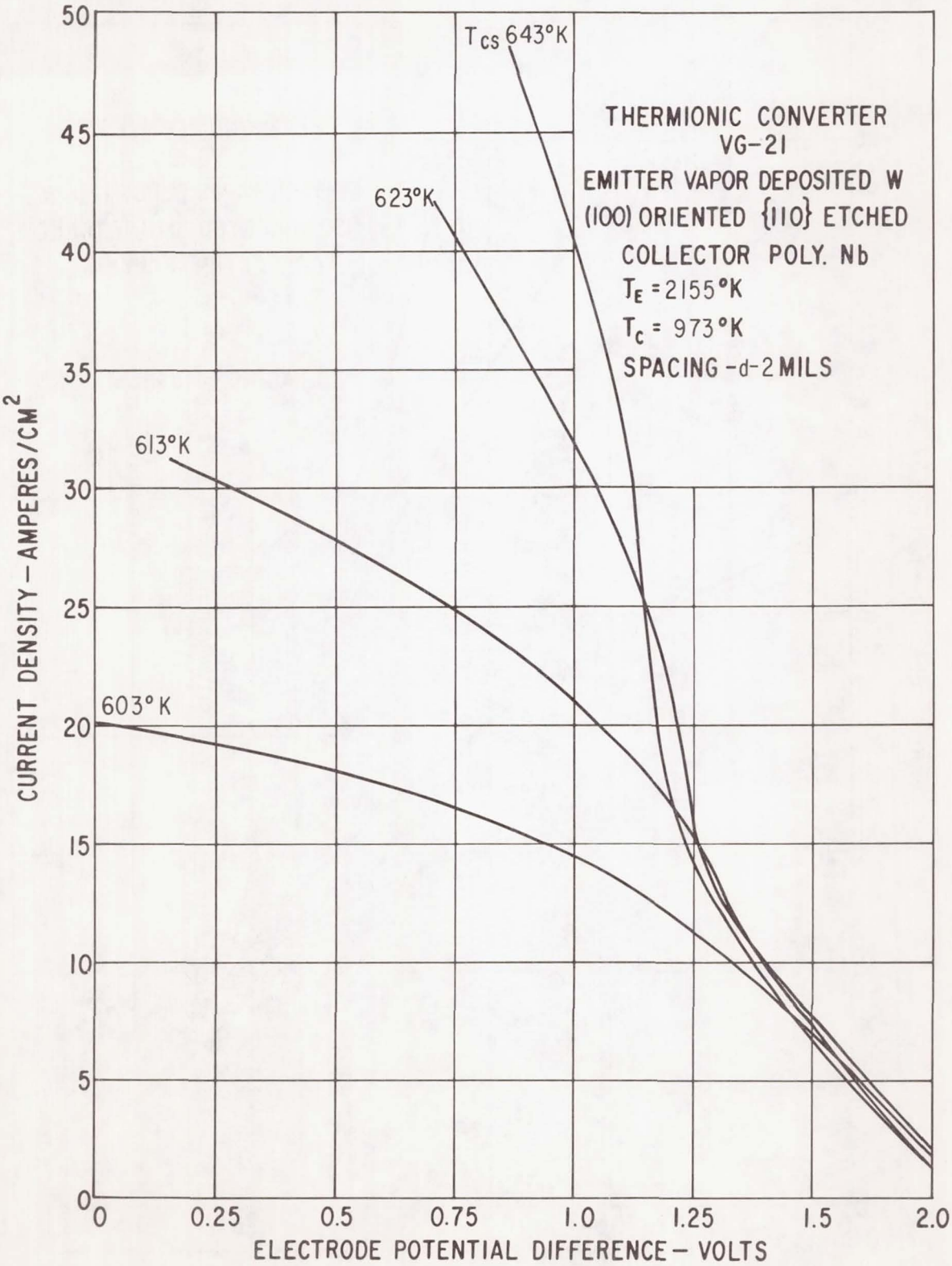

Figure 77. - Load lines for $T_E = 2155^{\circ}$ K, $T_C = 973^{\circ}$ K, and spacing d = 2 mils.

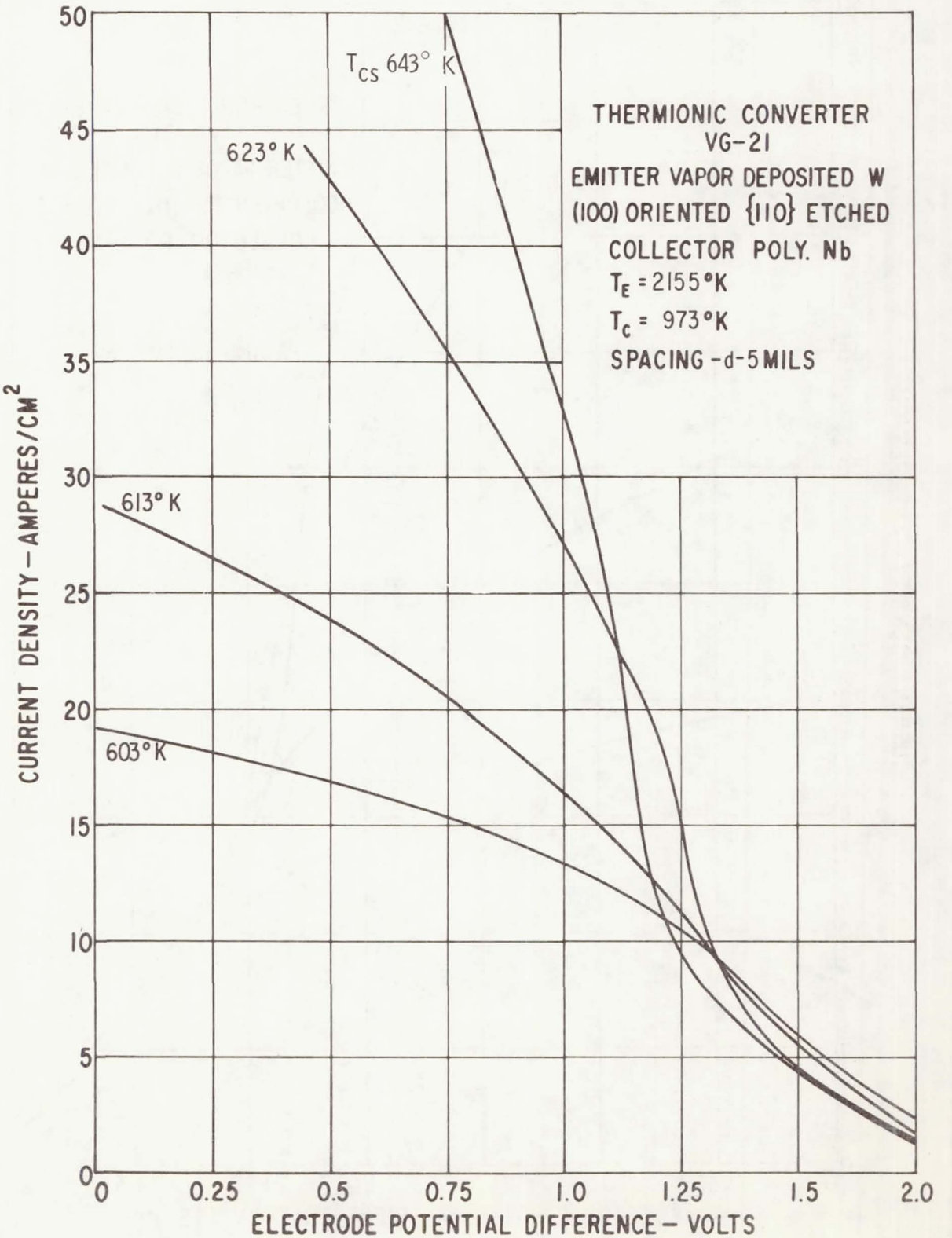

Figure 78. - Load lines for $T_E = 2155^O$ K, $T_C = 973^O$ K, and spacing d = 5 mils.

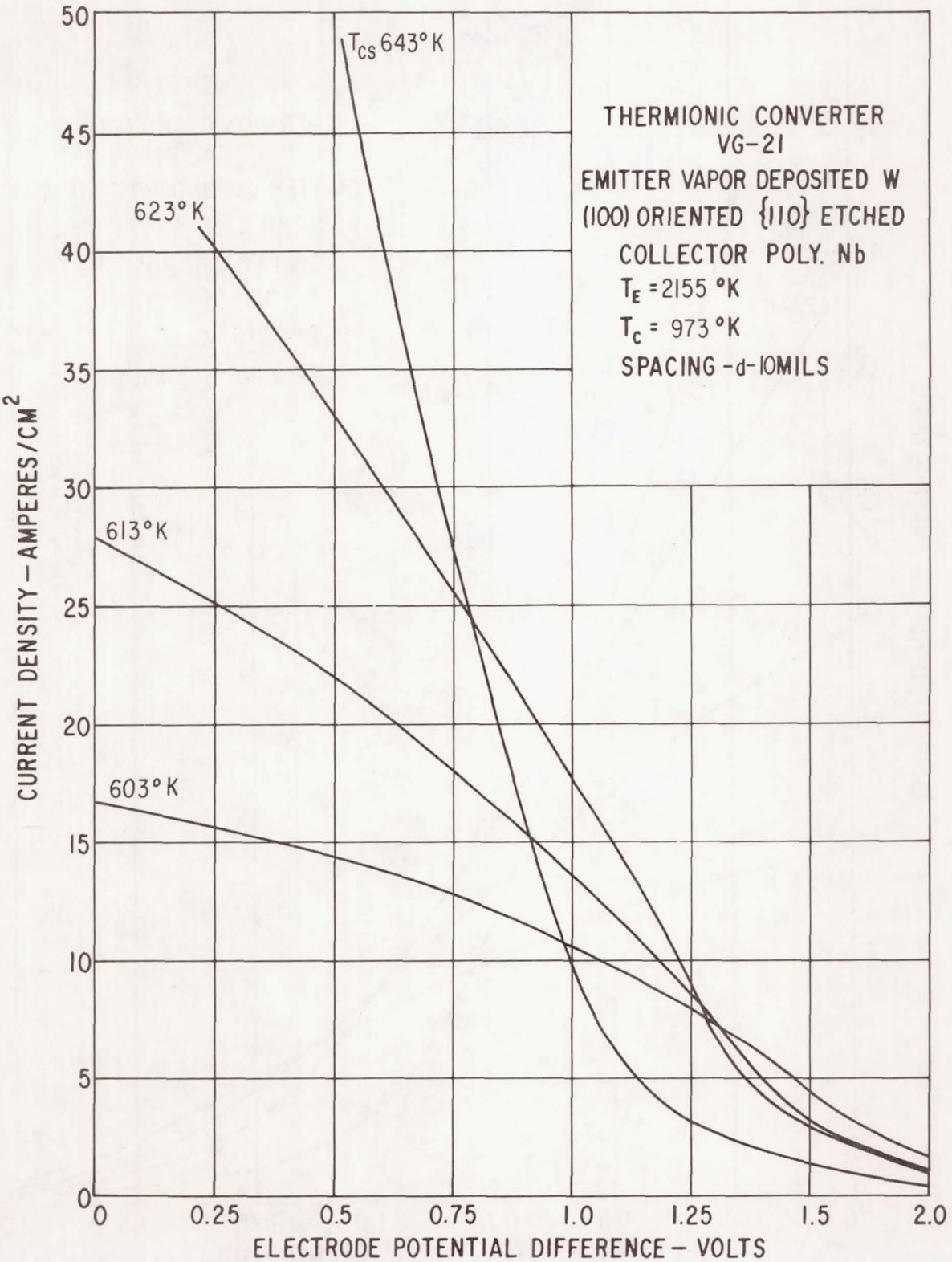

Figure 79. - Load lines for $T_E = 2155^{\circ}$ K, $T_C = 973^{\circ}$ K, and spacing d = 10 mils.

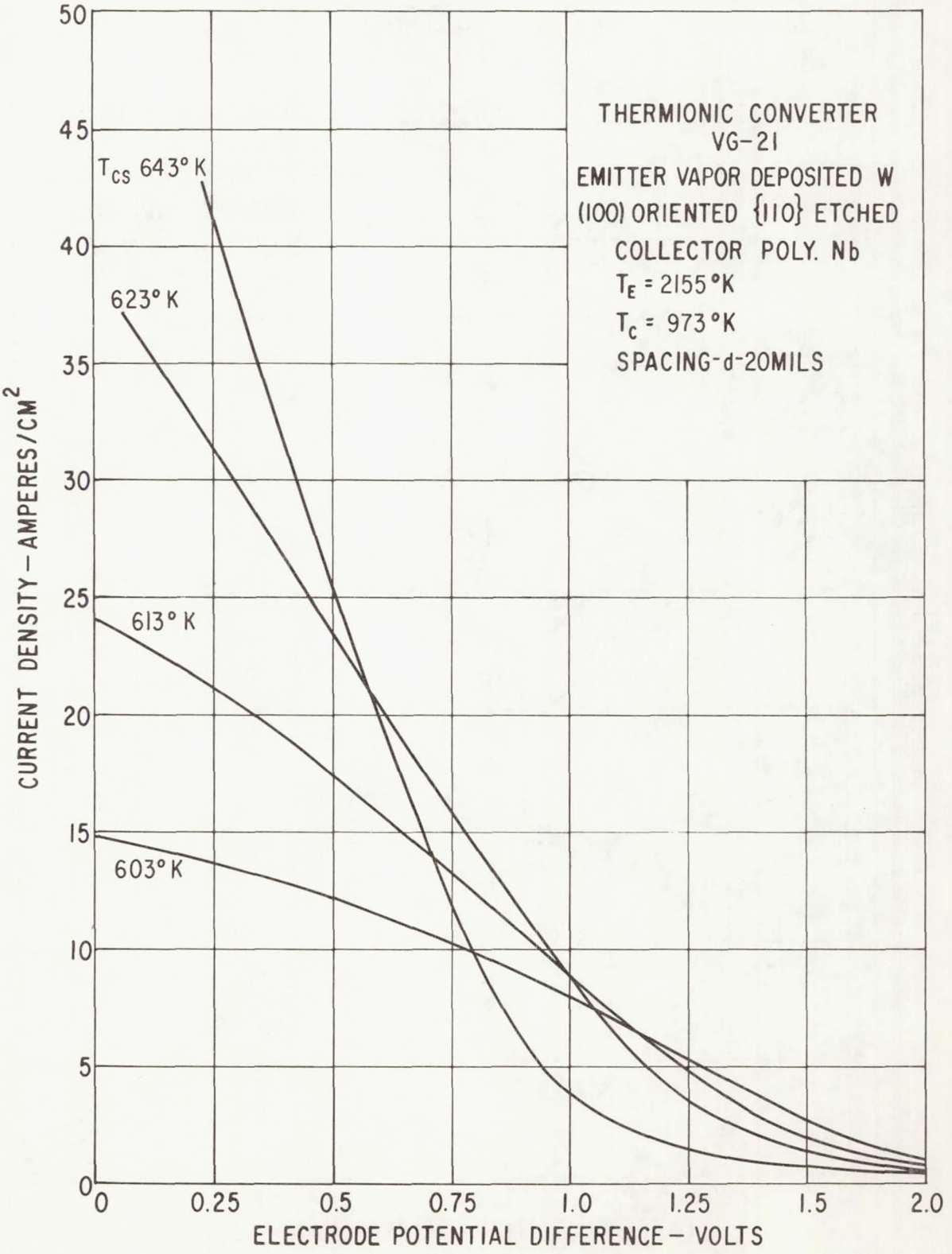

Figure 80. - Load lines for $T_E = 2155^O$ K, $T_C = 973^O$ K, and spacing d = 20 mils.

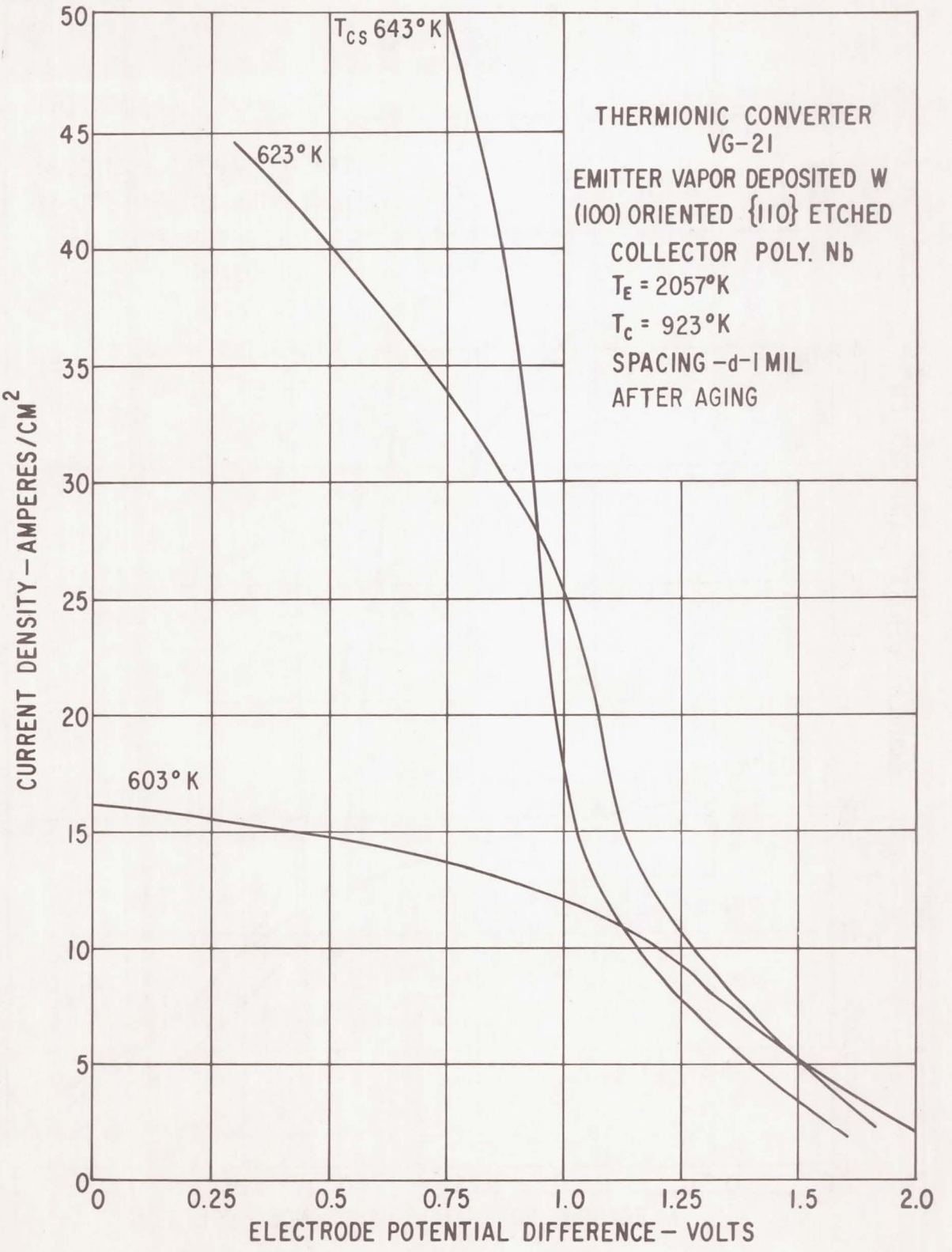

Figure 81. - Load lines for $T_E = 2057^O$ K, $T_C = 923^O$ K, and spacing d = 1 mil; after aging.

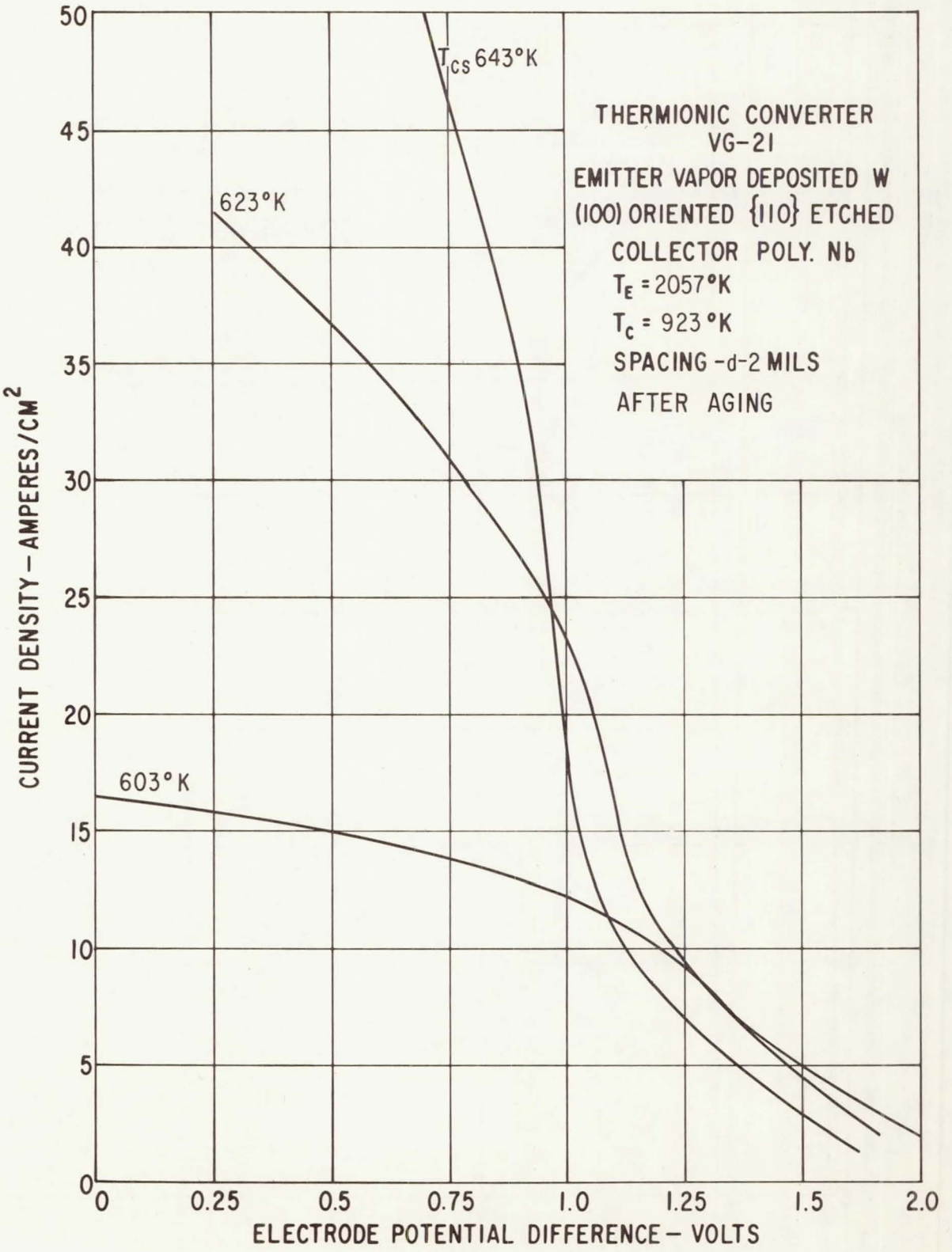

Figure 82. - Load lines for $T_E = 2057^O$ K, $T_C = 923^O$ K, and spacing d = 2 mils; after aging.

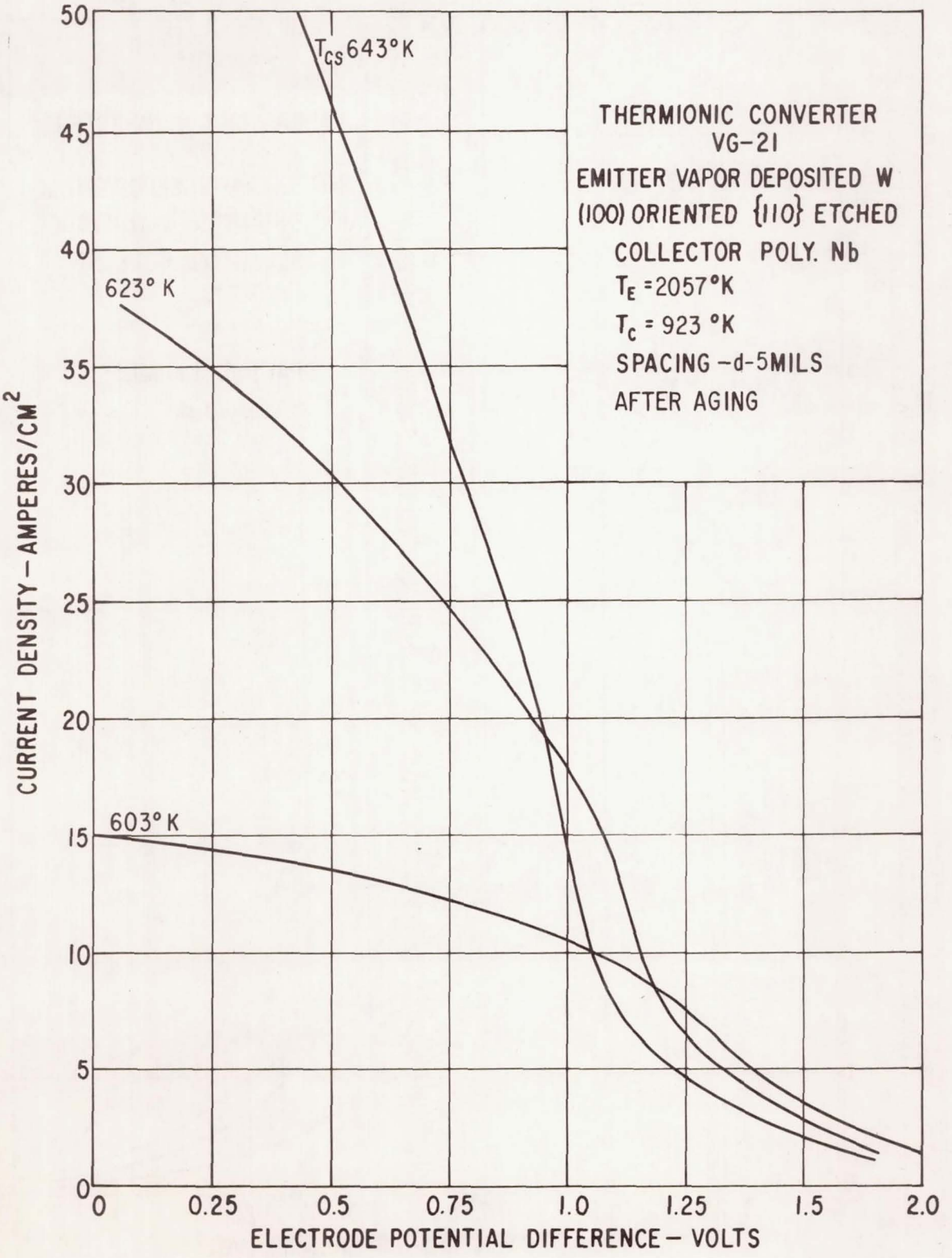

Figure 83. - Load lines for $T_E = 2057^O$ K, $T_C = 923^O$ K, and spacing d = 5 mils; after aging.

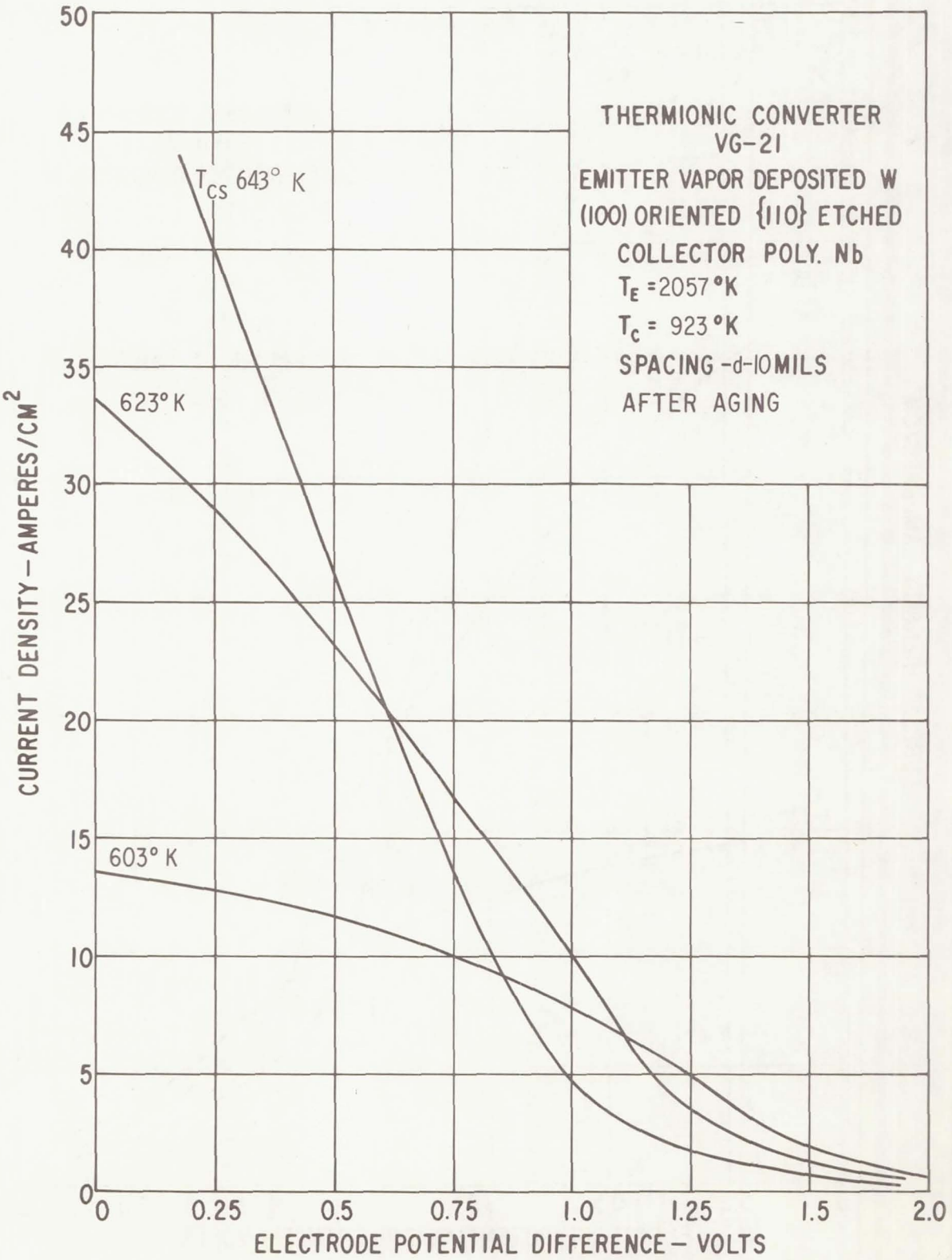

Figure 84. - Load lines for $T_E = 2057^O$ K, $T_C = 923^O$ K, and spacing d = 10 mils; after aging.

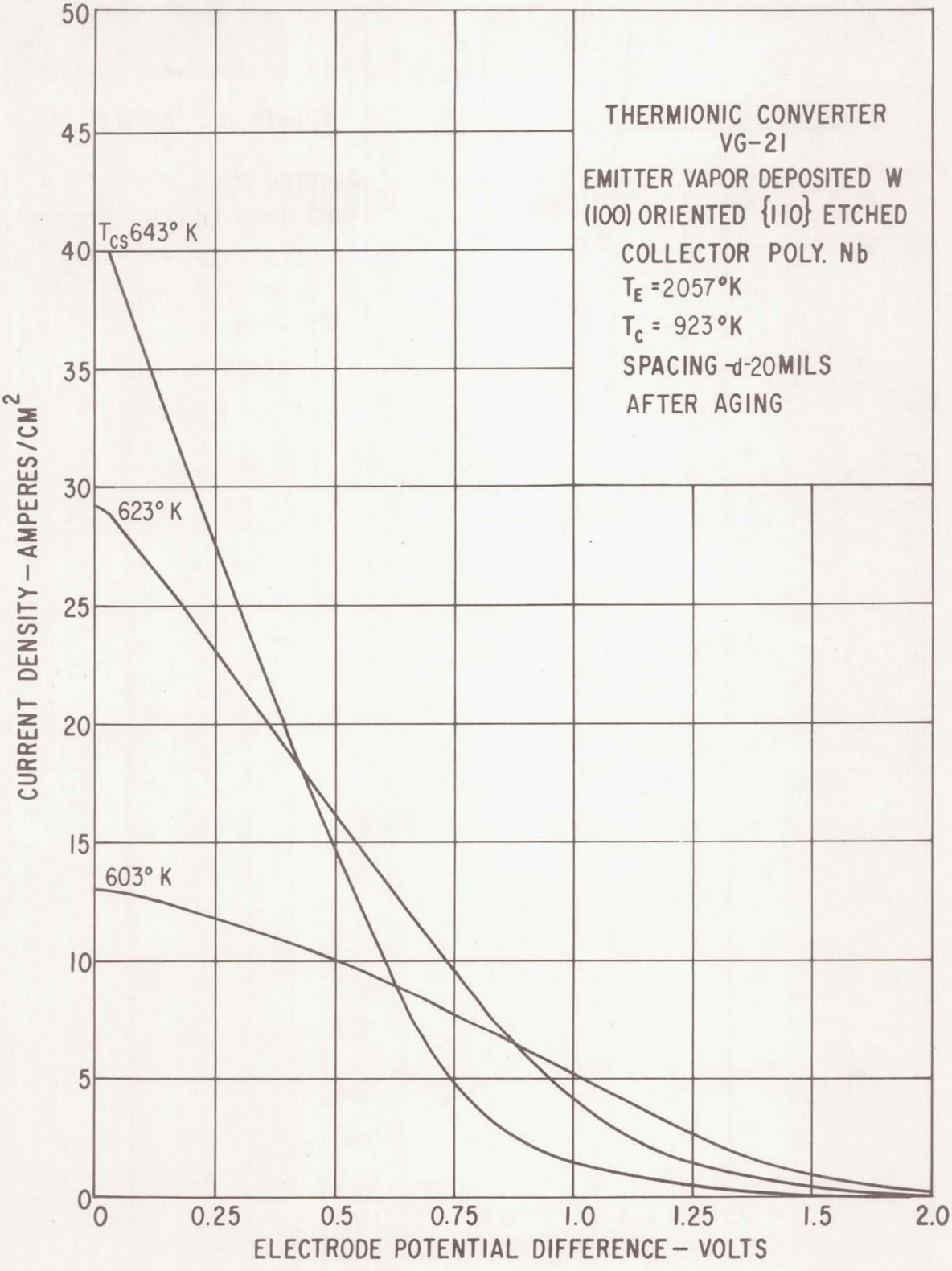

Figure 85. - Load lines for $T_E = 2057^O$ K, $T_C = 923^O$ K, and spacing d = 20 mils; after aging.

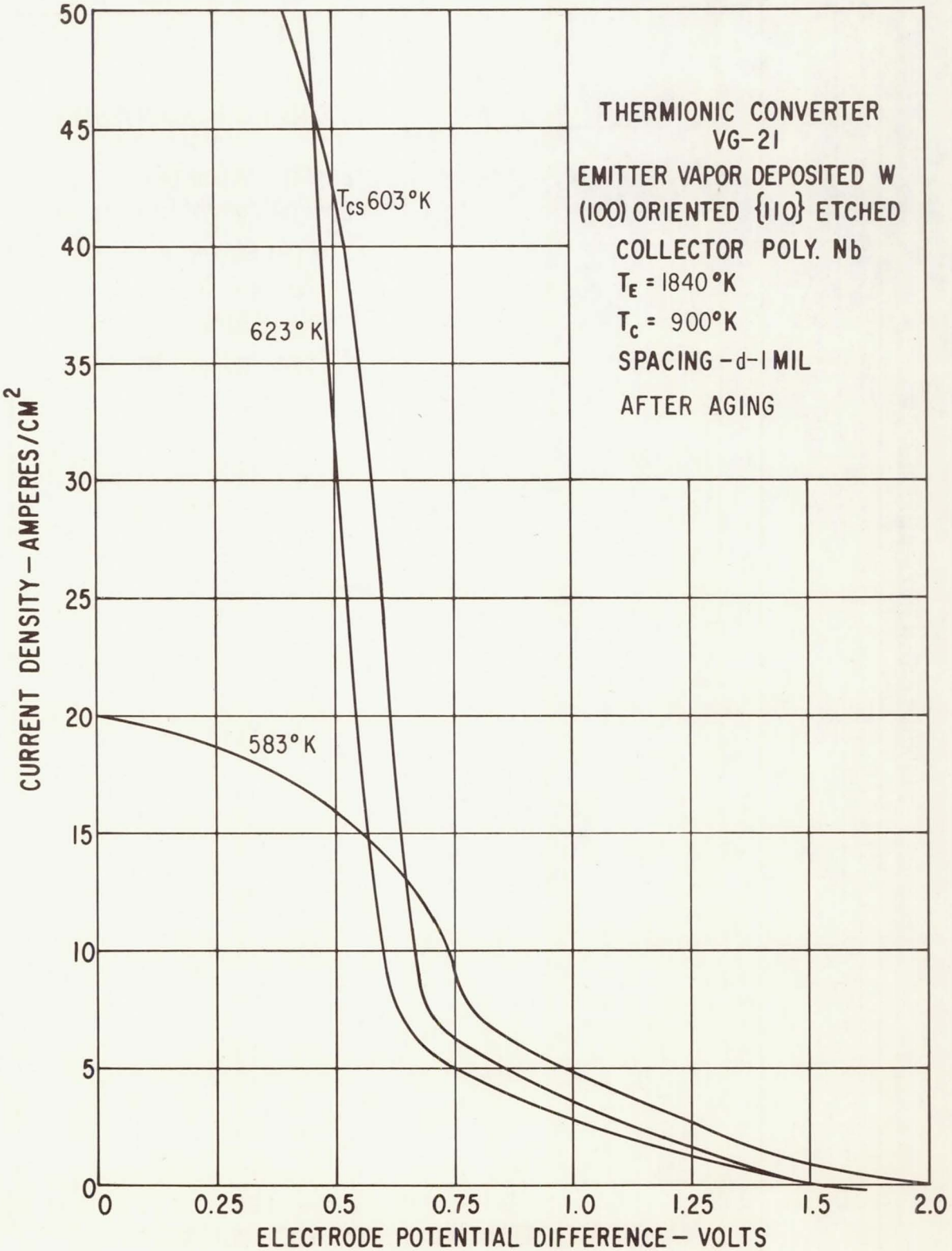

Figure 86. - Load lines for $T_E = 1840^O$ K, $T_C = 900^O$ K, and spacing d = 1 mil; after aging.

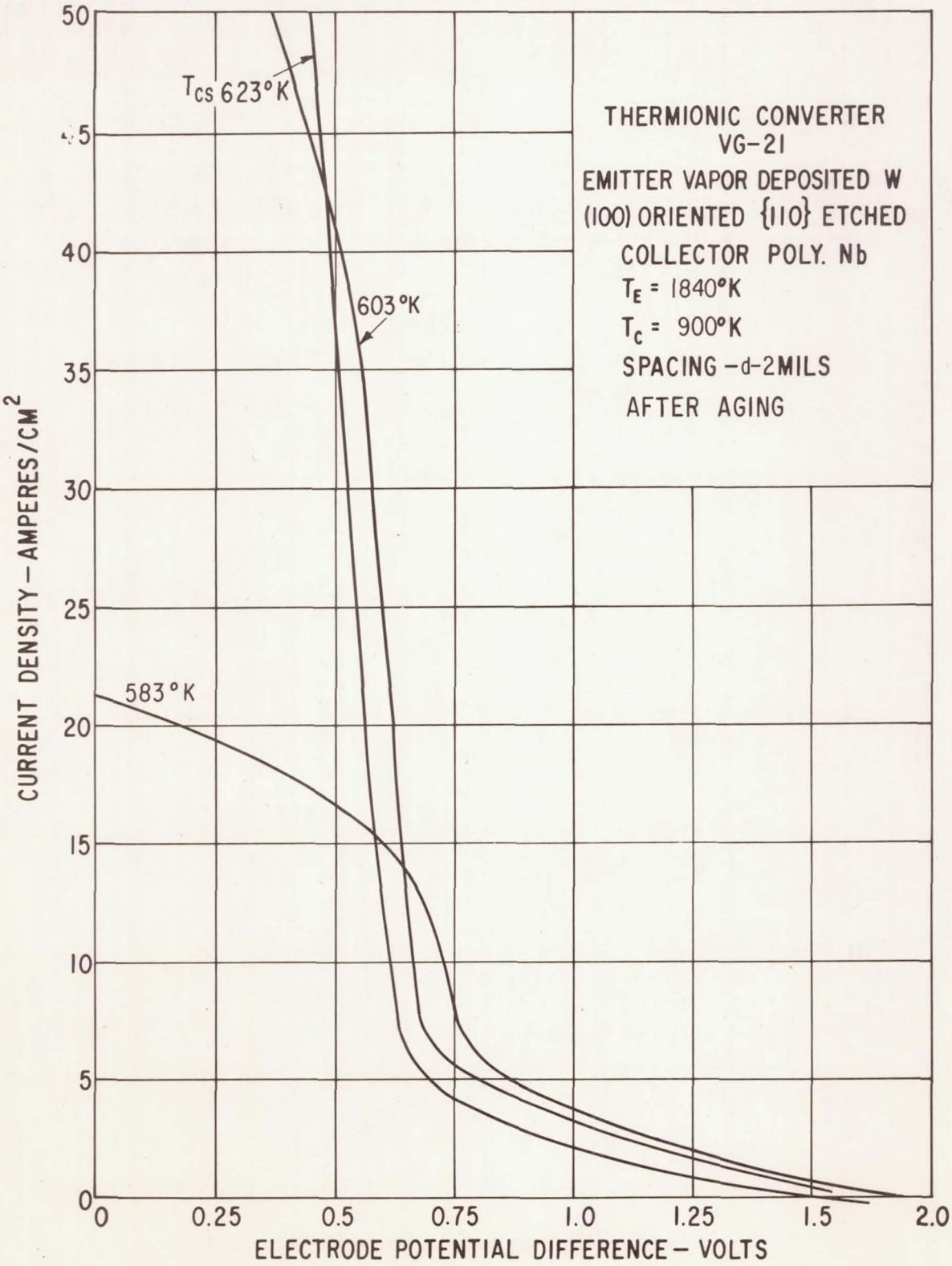

Figure 87. - Load lines for $T_E = 1840^{\circ}$ K, $T_C = 900^{\circ}$ K, and spacing d = 2 mils; after aging.

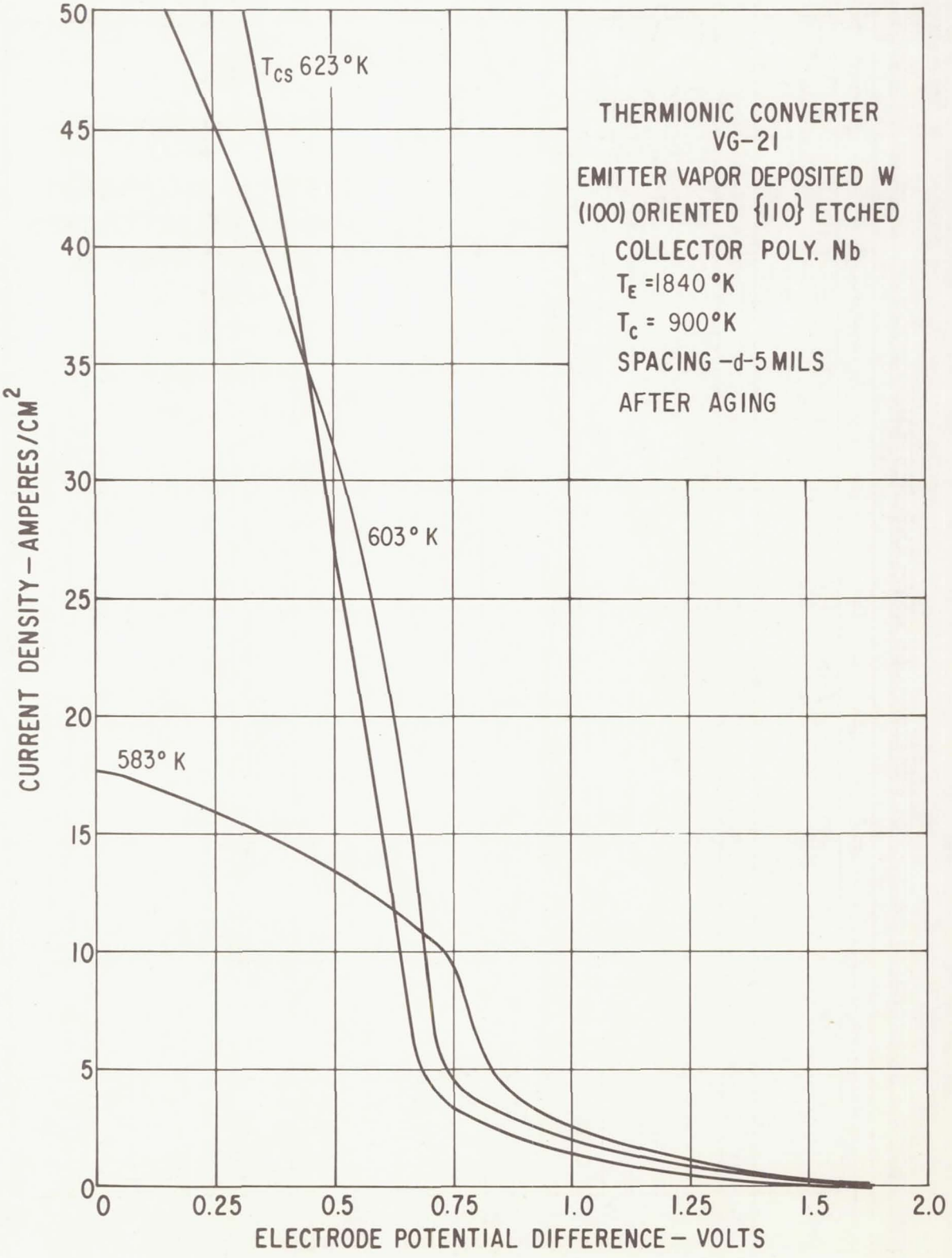

Figure 88. - Load lines for $T_E = 1840^O$ K, $T_C = 900^O$ K, and spacing d = 5 mils; after aging.

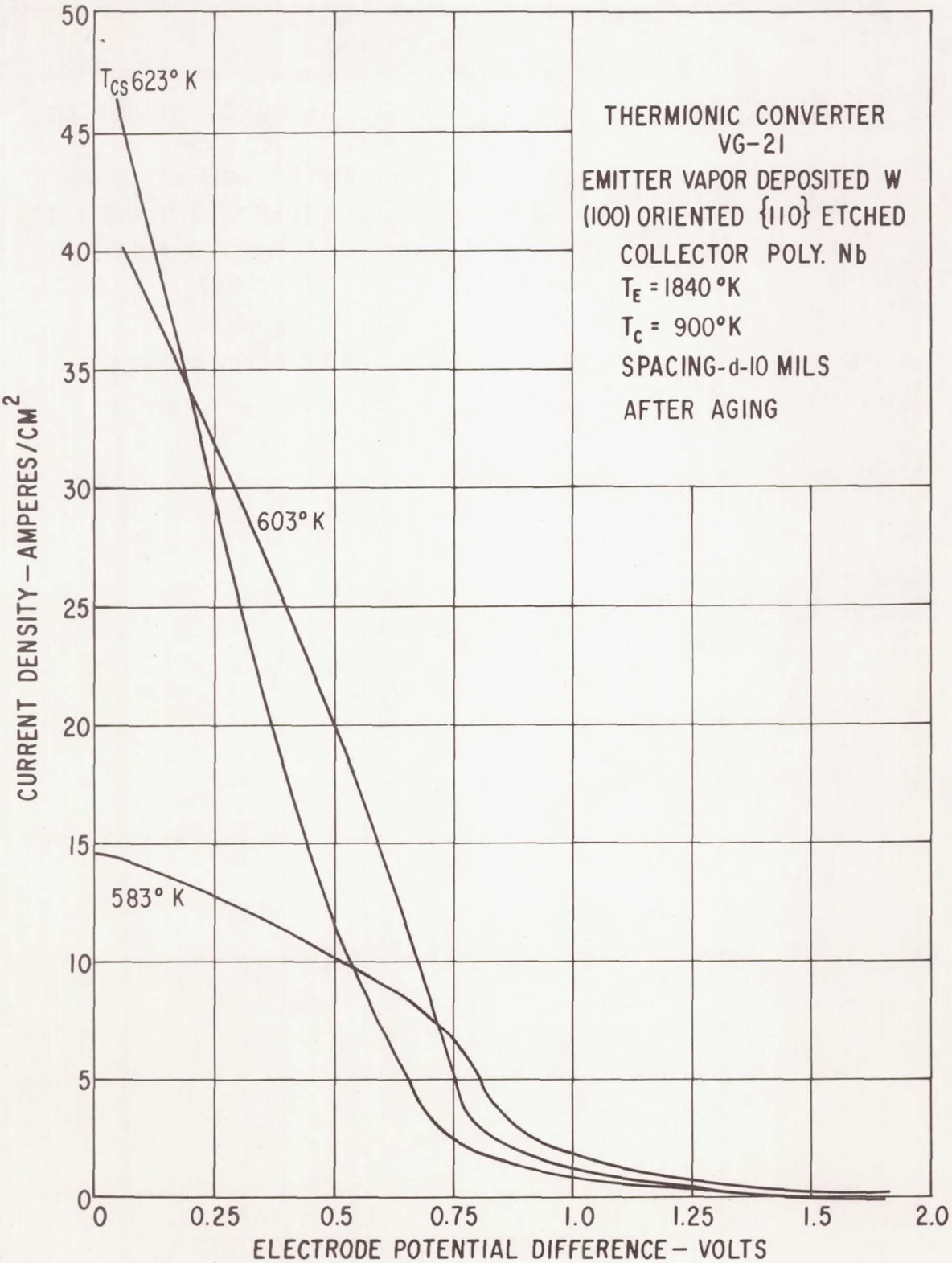

Figure 89. - Load lines for $T_E = 1840^O$ K, $T_C = 900^O$ K, and spacing d = 10 mils; after aging.

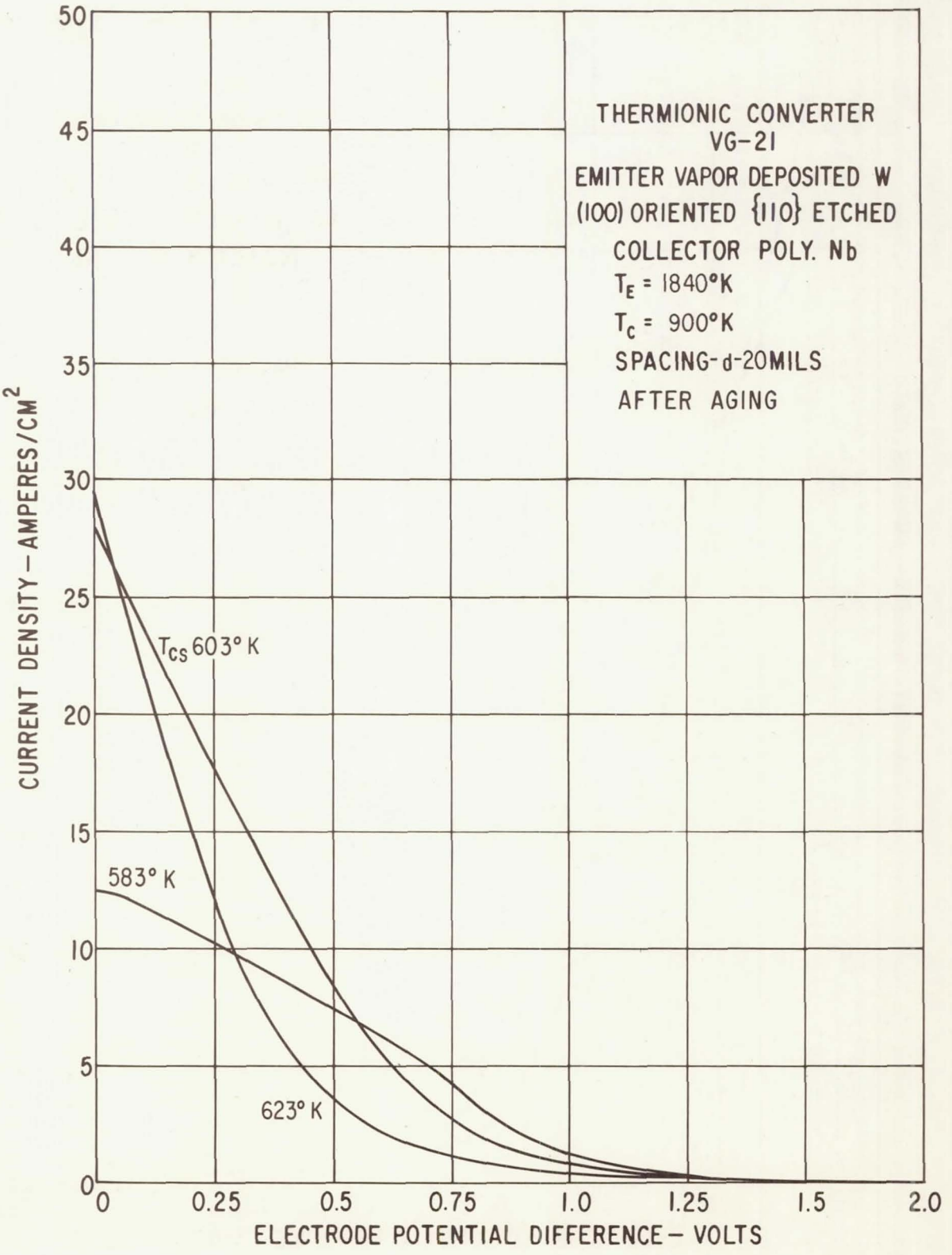

Figure 90. - Load lines for $T_E = 1840^O$ K, $T_C = 900^O$ K, and spacing d = 20 mils; after aging.

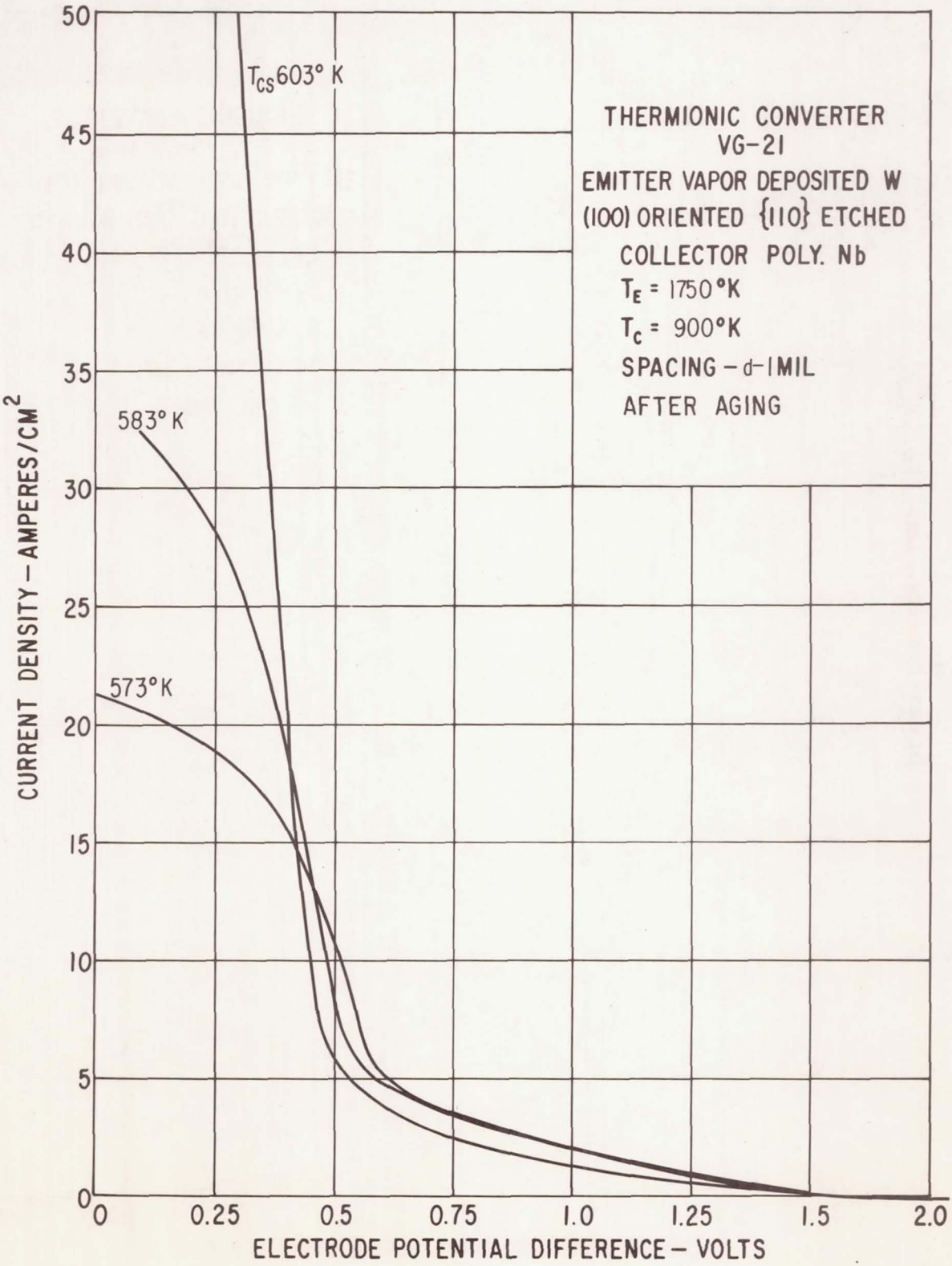

Figure 91. - Load lines for $T_E = 1750^O$ K, $T_C = 900^O$ K, and spacing d = 1 mil; after aging.

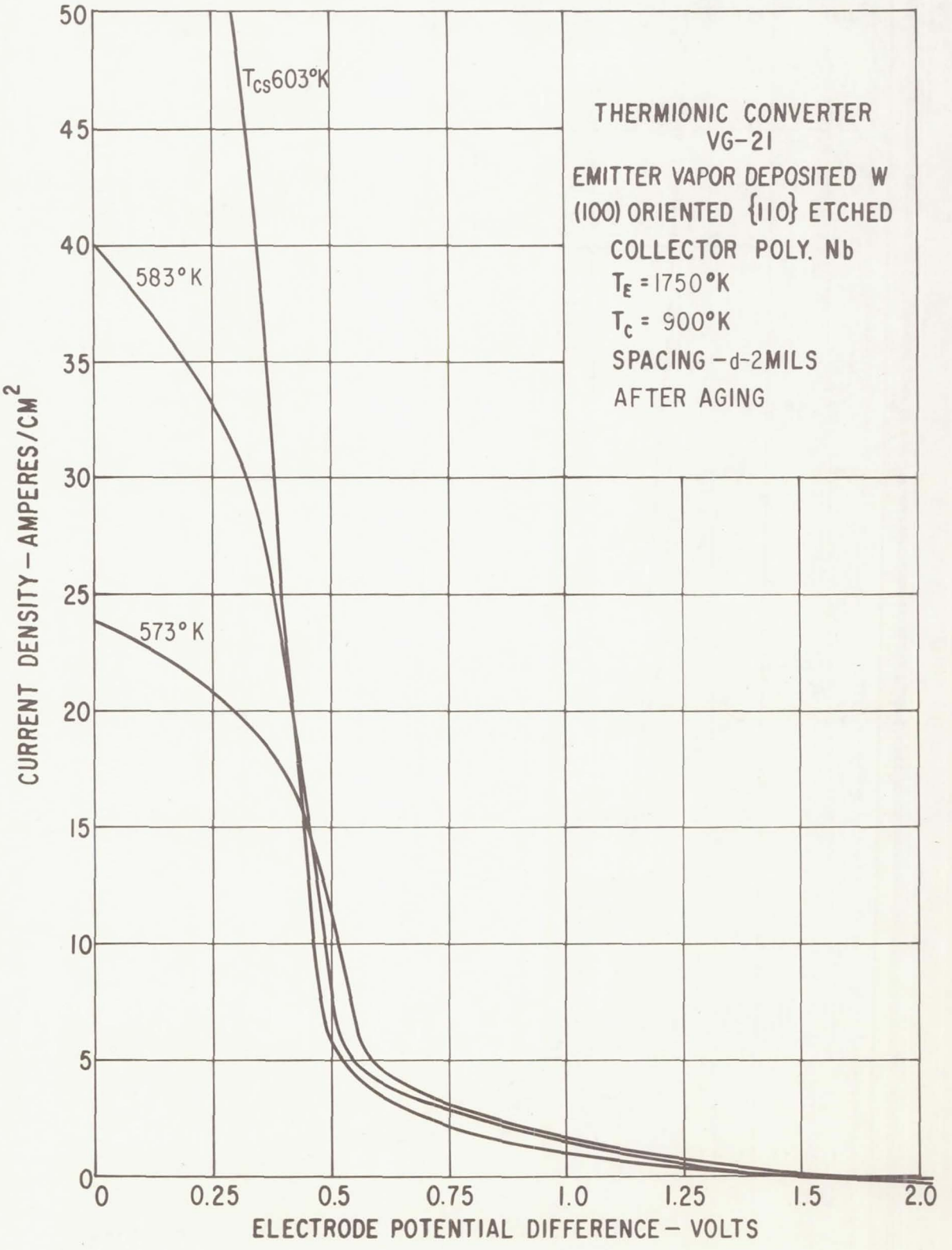

Figure 92. - Load lines for $T_E = 1750^O$ K, $T_C = 900^O$ K, and spacing d = 2 mils; after aging.

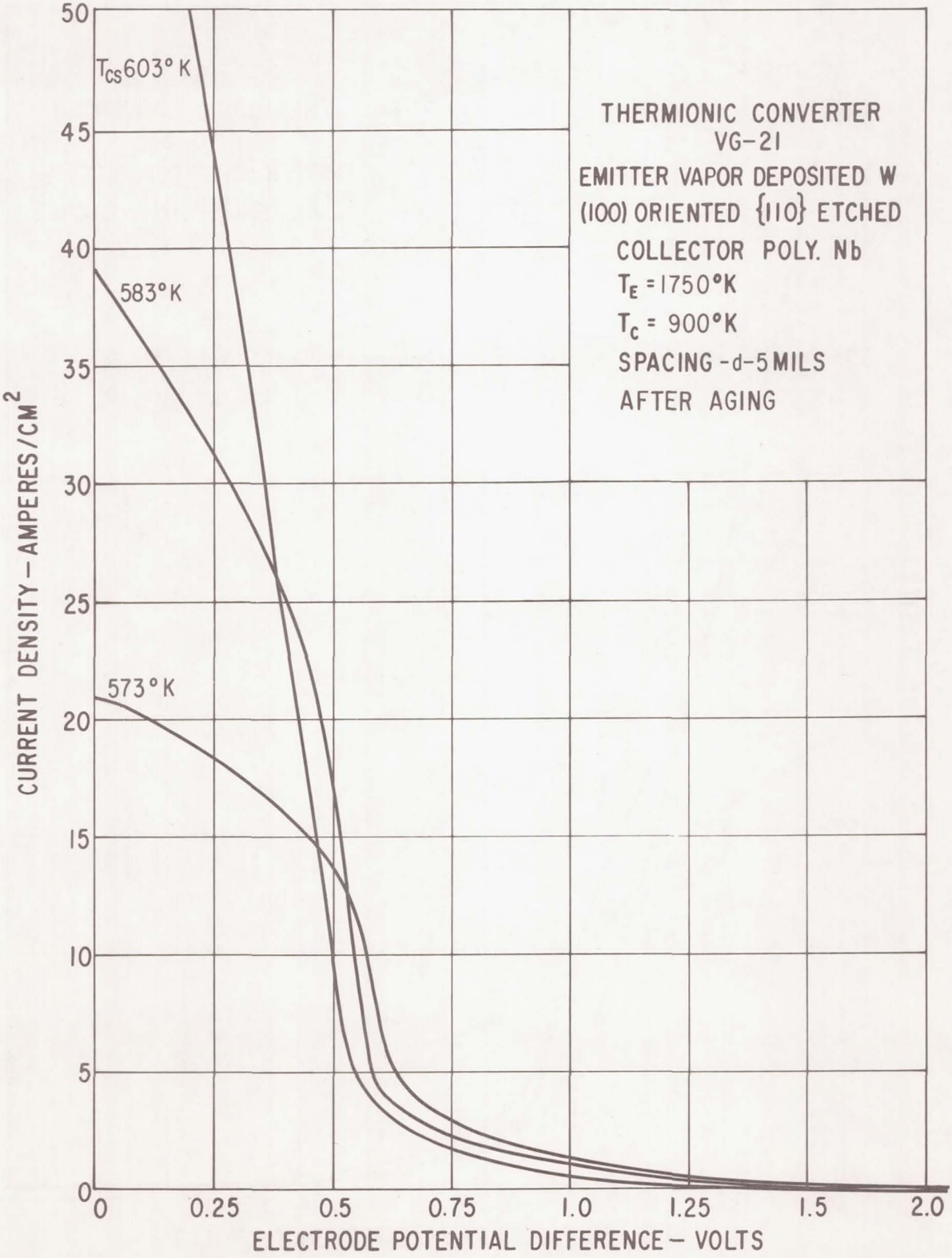

Figure 93. - Load lines for $T_E = 1750^O$ K, $T_C = 900^O$ K, and spacing d = 5 mils; after aging.

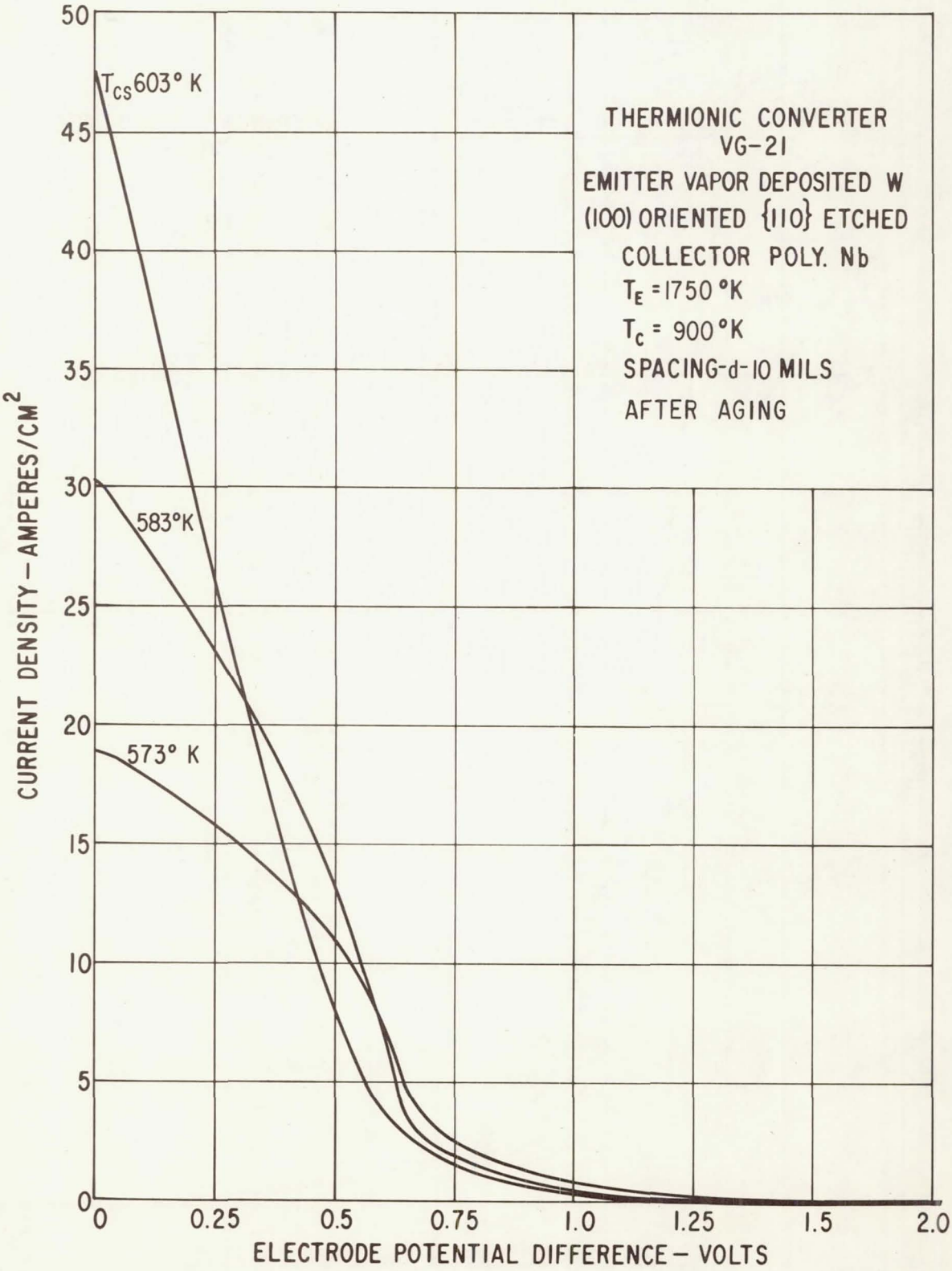

Figure 94. - Load lines for $T_E = 1750^O$ K, $T_C = 900^O$ K, and spacing d = 10 mils; after aging.

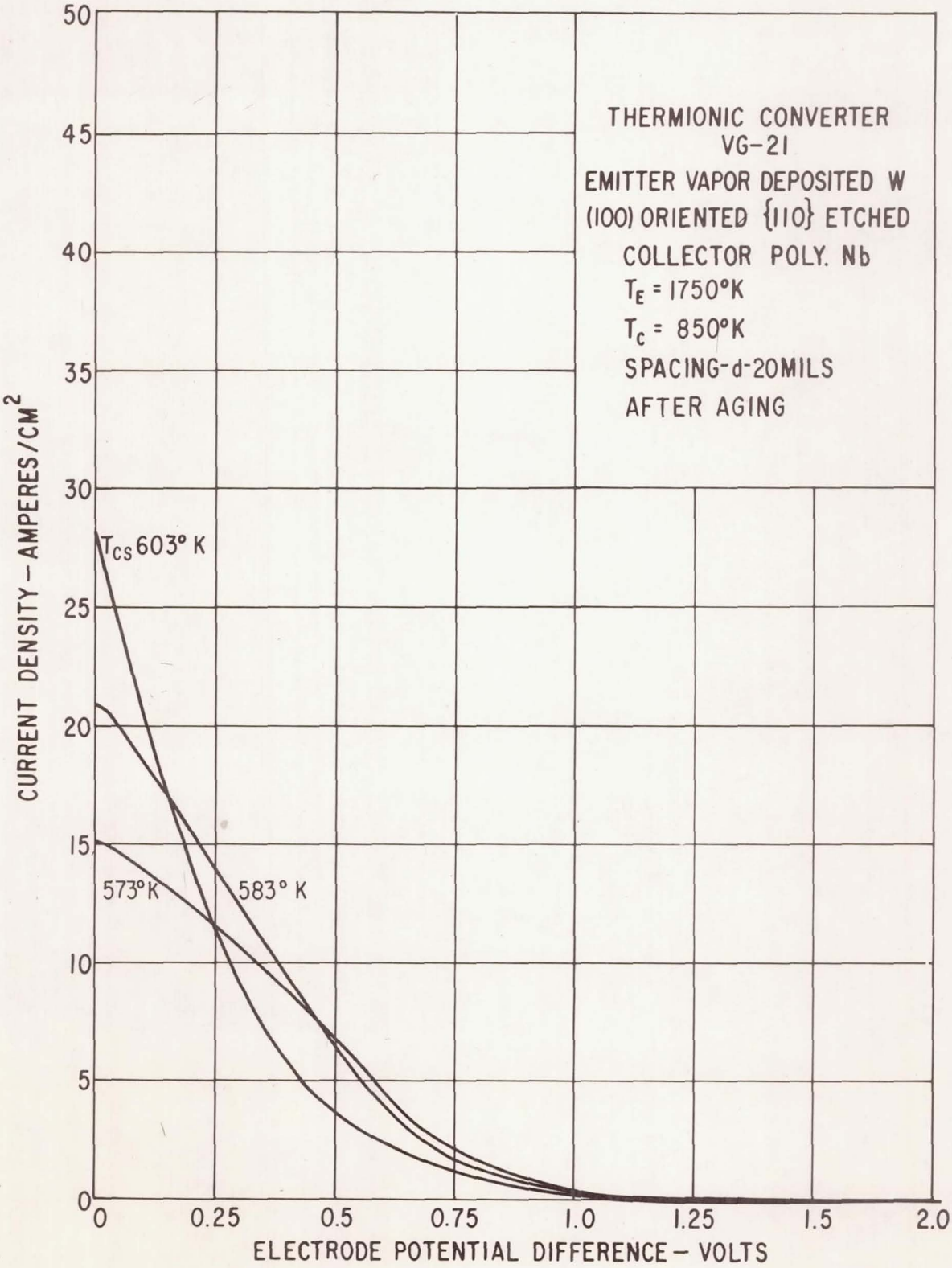

Figure 95. - Load lines for $T_E = 1750^O$ K, $T_C = 850^O$ K, and spacing d = 20 mils; after aging.